Ana Luísa Garcias Mestre

Ultra-sensitive bioelectronic transducers to monitor electrical activity in cell populations

Doctor of Philosophy

Electronics and Telecommunications Engineering

2023

Ana Luísa Garcias Mestre

Ultra-sensitive bioelectronic transducers to monitor electrical activity in cell populations

Doctor of Philosophy

Electronics and Telecommunications Engineering

Supervisor:
Prof. Henrique Leonel Gomes

Co-Supervisor:
Prof. Deborah Mary Power

UAlg FCT
UNIVERSIDADE DO ALGARVE
FACULDADE DE CIÊNCIAS E TECNOLOGIA

2023

This work would not have been possible without funding provided by the Portuguese Foundation for Science and Technology (FCT/MCTES), through national funds and when applicable co-funded EU funds by FEDER under the PT 2020 Partnership Agreement, namely, by the project “Implantable organic devices for advanced therapies” under the contract number PTDC/EEI-AUT/5442/2014 – INNOVATE; by the Instituto de Telecomunicações (IT) under the contract numbers UID/Multi/04326/2013, UID/EEA/50008/2019 and UIDB/EEA/50008/ 2020; by the Centro de Ciências do Mar (CCMar) under the contract numbers UID/Multi/04326/2019.

Ultra-sensitive bioelectronic transducers to monitor electrical activity in cell populations

Declaração de autoria de trabalho:

Declaro ser a autora deste trabalho, que é original e inédito. Autores e trabalhos consultados estão devidamente citados no texto e constam na listagem de referências incluídas.

(Ana Luísa Garcias Mestre)

Agradecimentos

Começo a minha secção de agradecimentos de forma atípica e irá para o meu supervisor Professor Henrique Gomes. Estou segura de quem me conhece também conhece o Professor Henrique. E digo isto porque efetivamente nos últimos anos referenciei o professor vezes sem conta e mesmo havendo muita gente que nunca o viu, pelo menos já ouviu falar. Ao professor Henrique estou mesmo profundamente agradecida e seria demasiado extenso enumerar todos os porquês, no entanto sei que a pessoa que sou hoje devo grandemente a ele. O professor viu-me crescer, não só como profissional, mas também como pessoa e se há agradecimentos impagáveis, este é um deles. Curiosamente, talvez seja uma das coisas mais fascinantes no professor, é o fato do professor não se aperceber disso. Quem não o conhece, faça o favor de o conhecer. E posso dizer que, sem dúvida, o término deste capítulo me deixa de certa forma emocionada e triste porque quando abraçamos novos capítulos, mesmo cheios de expectativas, nunca pensamos que têm um fim, nem no que nos vai custar afastarmo-nos deliberadamente de pessoas com quem gostamos de estar e neste caso também trabalhar. Ao professor Henrique o termo "*workaholic*" assenta-lhe perfeitamente, mas também o de líder. Com uma capacidade de trabalho absolutamente incrível e um ritmo que nos dá 10-0. Sei que para além de um chefe encontro no professor um amigo e estou muito agradecida de as nossas vidas se terem cruzado há mais de dez anos atrás. Muito obrigada fundo do meu coração.

O meu segundo agradecimento vai para a grande instituição que escolhi e que há tantos anos me acolhe e na qual me sinto em casa, à Universidade do Algarve. Pelos excelentes profissionais que também acolhe, pelos incentivos criados, pelo apoio fornecido, pelas ótimas instalações e excelente espírito académico envolvente em toda a Universidade. Foram muitos os dias (e muitas as noites também) passados no laboratório para realizar esta dissertação. É de fato uma honra poder fazer parte desta grande família. Também gostaria de agradecer ao Instituto de Telecomunicações do qual fiz parte, com profissionais extremamente competentes e do qual me orgulho muito ter tido a oportunidade de trabalhar. Ao CCMar, que me proporcionou a experiência de estar num centro com tanto reconhecimento científico, preenchido por profissionais tão competentes.

À Professora Deborah o meu profundo agradecimento por me ter acolhido no seu laboratório e ter partilhado tamanho conhecimento. Foi uma honra e um gosto enorme poder ter tido a oportunidade de trabalhar tão de perto com a professora. A professora Deborah é uma força da natureza com conhecimentos sem fim. É uma pessoa irreverente, que nos mostra diariamente que tudo é possível com esforço, sejamos nós homens ou mulheres, jovens ou mais experientes, é um autêntico exemplo de como podemos ser todos iguais. Uma professora que tem a seu cargo tantos alunos e profissionais e dá tudo para mantê-los sempre por perto. Sendo um deles a Rute Félix, que partilhou comigo imensos dias e bastante conhecimento. É também graças a ela que hoje sei tantas técnicas no laboratório em tempo record. Queria também agradecer a todos os membros do laboratório de "Endocrinologia Comparativa e Biologia Integrativa". Gostaria também de agradecer muito à Professora Leonor Cancela que acreditou em mim desde o primeiro dia. Foi uma ponte essencial para eu ter chegado até aqui e nunca se esqueceu de mim.

Gostaria de prestar também o meu agradecimento à Dra Patricia Madureira por nos ter fornecido as células U87 e as culturas primárias de glioblastomas (HOPE). A obtenção

destas células também só foi possível graças à colaboração da Dra. Clara Romero e do Dr Artur Lourenço do Hospital de Faro que permitiram que tivéssemos acesso a amostras de biopsias e purificaram as culturas celulares. À Professora Inês Araújo gostaria de prestar o meu profundo agradecimento por toda a ajuda e colaboração na realização do trabalho referente às culturas primárias de astrócitos.

À "*dream team*" queria também deixar o meu agradecimento. Refiro-me claro aos meus colegas de laboratório de eletrónica dos últimos dez anos. É inevitável começar pelo Pedro Inácio. Entrámos juntos no laboratório e acabamos ao mesmo tempo e da mesma forma, lado a lado. Fomos muito companheiros um do outro ao longo destes anos, nunca deixamos que a competição nos afastasse, nem tão pouco dos rivalizasse. Obrigada Pedro. À minha querida Rita Ferreira, sempre tão doce e tão alegre. A alegria diária era inevitável e de uma competência incrível. Ensinou-nos que o copo está sempre meio cheio. E, por fim, ao Youssef. O Youssef é um ser humano inacreditável. Provavelmente a pessoa com melhor temperamento que já conheci e está sempre disponível. Muito obrigada. Sem vocês então era mesmo impossível. Esta tese também é vossa, espero que vos orgulhe.

Por fim, queria agradecer profundamente à minha família, que assistiu nos bastidores à montanha russa de emoções que vivi nestes últimos anos e que nunca me deixaram cair. À minha mãe, gostaria de prestar o meu profundo agradecimento. Por todo o amor sem limites que me deu e apoio desmesurado. É um exemplo de determinação e persistência e fez muita diferença. Obrigada. Ao meu pai, que é o meu melhor exemplo de perseverança. Mostra-nos que o esforço é sempre compensado. Um exemplo de humanidade e profissionalismo e um apoio incondicional. Obrigada pai. Aos meus irmãos e às minhas cunhadas, o meu mais profundo agradecimento, Mafalda, Miguel, Fatinha e João (por ordem de idades para não terem ciúmes), muito obrigada. Já tinha dois irmãos fantásticos e ter ganho duas irmãs foi uma dádiva que dificilmente conseguirei retribuir. Com vocês, toda esta etapa se tornou bem mais fácil e leve. É também graças a vocês que me levanto todos os dias com força e vontade de continuar. Não posso deixar de agradecer também aos meus sogros, Madalena e Luís, que me têm acompanhado e tanto apoio e amor me têm dado, o meu muito obrigada.

Aos meus amigos gostaria de deixar um agradecimento profundo. Sou uma pessoa extremamente afortunada e também muito grata por ter há tantos anos as mesmas pessoas sempre a servirem de base, de referência e de inspiração. Obrigada por existirem, obrigada por toda a paciência e força desta altura.

Ao meu querido Luís vai um agradecimento sem medida. Se houve alguém que contribuiu muito para que eu nunca desistisse e olhasse sempre em frente, esse alguém é ele. Esteve incondicionalmente ao meu lado, acreditou em mim, apoiou-me e foi uma inspiração emocional para seguir em frente. Fez-me rir tantas vezes em que só me apetecia chorar, fez-me ver tanta coisa boa quando só via más, foi "colo" quando mais precisei e quando nem precisava. O Luís é sempre tão leve que me faz ver quase diariamente que se não posso resolver um problema, também não me posso preocupar, nem sofrer por antecipação. E essa leveza faz toda a diferença na nossa vida. Muito obrigada.

Por fim, quero agradecer todo o suporte financeiro providenciado pela Fundação para a Ciência e a Tecnologia (FCT), através da bolsa de doutoramento SFRH/BD/148688/2019.

Acknowledgments

I would like to start my acknowledgment in an atypical way to my supervisor Professor Henrique Gomes. I'm sure those who know me also know Professor Henrique. And I say this because in the last few years I have referred to the professor countless times and even though there are many people who have never seen him, at least have heard of him. I am really grateful to Professor Henrique and it would be too long to enumerate all the reasons why, however I know that the person I am today I owe a great deal to him. The professor saw me grow, not only as a professional, but also as a person and if there are priceless thanks, this is one of them. Interestingly, perhaps one of the most fascinating things about Professor Henrique is that is not aware of it. If you do not know him, please do it. And I can say that, without a doubt, the end of this chapter makes me somewhat emotional and sad because when we embrace new chapters, even full of expectations, we never think that they have an end, nor what it will cost us to deliberately distance ourselves from people with whom we like to be and, in this case, also work. For Professor Henrique, the term "workaholic" fits him perfectly, but also that of leader. With an absolutely incredible work capacity and a pace that gives us 10-0. I know that in addition to a boss, I find a friend in the Professor and I am very grateful that our lives crossed ten years ago. Thank you so much from the bottom of my heart.

My second thanks go to the great institution that I chose and for so many years has welcomed me and in which I feel at home, the University of Algarve. For the excellent professionals that it also welcomes, for the incentives created, for the support provided, for the excellent facilities and excellent academic spirit surrounding the entire University. There were many days (and many nights too) spent in the laboratory to carry out this dissertation. It is indeed an honour to be part of this great family. I would also like to thank the Telecommunications Institute of which I was a part, with extremely competent professionals and for which I am very proud to have had the opportunity to work. To CCMar, who gave me the experience of being in a centre with so much scientific recognition, filled with such competent professionals.

To Professor Deborah my deep gratitude for having welcomed me in her laboratory and for sharing such knowledge. It was an honour and a great pleasure to have the opportunity to work so closely with the Professor. Professor Deborah is a force of nature with endless knowledge. She is an irreverent person, who shows us daily that everything is possible with effort, whether we are men or women, young or more experienced, she is an authentic example of how we can all be equal. A Professor who is in charge of so many students and professionals and gives everything to keep them close at all times. One of them being Rute Félix, who shared many days with me and a lot of knowledge. It is also thanks to her that I now know so many techniques in the laboratory in record time. I would also like to thank all the members of the "Comparative Endocrinology and Integrative Biology" laboratory. I would also like to thank Professor Leonor Cancela who believed in me from day one. It was an essential bridge for me to get here and she never forgot me.

I would also like to thank Dr Patricia Madureira for providing us the U87 cells and the primary glioblastoma cultures (HOPE). Obtaining these cells was only possible thanks to the collaboration of Dr. Clara Romero and Dr Artur Lourenço from Hospital de Faro who allowed us to have access to biopsy samples and purified cell cultures. I would like to

thank Professor Inês Araújo for all her help and collaboration in carrying out the work on primary astrocyte cultures.

To the “dream team” I would also like to express my deepest gratitude. I am clearly referring to my colleagues in the electronics laboratory of the last ten years. It is inevitable to start with Pedro Inácio. We entered the laboratory together and ended up at the same time and in the same way, side by side. We've been very good friends with each other over these years, we never let the competition push us away, nor did we rival each other. Thank you Pedro. To my dear Rita Ferreira, always so sweet and so cheerful. The daily joy was inevitable and incredibly competent. She taught us that the glass is always half full. And finally, Youssef. Youssef is an unbelievable human being. Probably the best tempered person I've ever met and is always available. Thank you very much. Without you then it was really impossible. This thesis is also yours, I hope it makes you proud.

Finally, I would like to deeply thank my family, who watched, behind the scenes, the roller coaster of emotions that I lived these last years and that never let me down. To my mother, I would like to express my deep gratitude. For all the boundless love you've given me and unmeasured support. It is an example of determination and persistence and made a lot of difference. Thank you. To my father, who is my best example of perseverance. He shows us that effort is always rewarded. He has also shown us that it's okay to make mistakes, it's wrong not to try. An example of humanity and professionalism and unconditional support. Thank you. To my brothers and sisters-in-law, my deepest gratitude, Mafalda, Miguel, Fatinha and João (in order of age so they are not jealous), thank you very much. I already had two fantastic brothers and having two sisters was a gift that I will hardly be able to repay. With you, this whole step became much easier and lighter. It is also thanks to you that I get up every day with strength and the will to continue. I must also thank my parents in law, Madalena e Luís, who have been with me and given me so much support and love, thank you very much.

To my friends I would like to express my deepest gratitude. I am an extremely fortunate person and also very grateful to have the same people for so many years always serving as a base, a reference and inspiration.

To my dear Luís goes an immeasurable thanks. If there was anyone who contributed a lot so that I never gave up and always looked forward, it was him. He was unconditionally by my side, believed in me, supported me and was an emotional inspiration to move forward. He made me laugh so many times that I just wanted to cry, he made me see so many good things when I only saw bad things, he was “lap” when I needed it the most and when I did not need it. Luís is always so light that he makes me see almost daily that if I can't solve a problem, I can't worry or suffer in advance either. And that lightness makes all the difference in our lives. Thank you.

Finally, I would like to thank all the financial support provided by the Foundation for Science and Technology (FCT), through the doctoral grant SFRH/BD/148688/2019.

Resumo

O avanço na área da microeletrónica tem permitido a fabricação de matrizes de microeléctrodos (MEAs) planares, que são elétrodos individuais com dimensões tão pequenas quanto uma célula individual. Estas matrizes são comumente utilizadas para medir sinais extracelulares em neurónios, permitindo entender mecanismos de comunicação entre redes de milhares de neurónios. Os neurónios, os cardiomiócitos e as células nervosas têm a capacidade de despoletar potenciais de ação. Este tipo de células, conhecidas como células eletrogénicas ou excitáveis, passam a informação a alta velocidade e desenvolvem a capacidade de gerar oscilações viajantes, conhecidas como potenciais de ação, que podem deslocar-se a uma velocidade de metros por segundo. Por outro lado, células não eletrogénicas ou não excitáveis, como é o exemplo de células epiteliais, utilizam oscilações químicas que viajam a uma velocidade muito lenta através dos tecidos. Um exemplo típico destas flutuações são as ondas ou oscilações de cálcio. As ondas de cálcio são flutuações internas de cálcio que viajam a micrómetros por segundo numa população de células conectada. A flutuação gerada é frequentemente produzida por muitas células que sincronizaram o seu comportamento. As células são classificadas como células não excitáveis ou não eletrogénicas.

Esta tese está focada nos sinais bioelétricos extracelulares produzidos por células não eletrogénicas. Este estudo coloca a hipótese que oscilações iónicas, como ondas de cálcio e outras flutuações iónicas geradas por células não eletrogénicas possam induzir flutuações iónicas extracelulares. As flutuações iónicas extracelulares podem ser detetadas por elétrodos extracelulares como oscilações em voltagem.

Esta tese examina e discute as propriedades das flutuações elétricas medidas por elétrodos extracelulares em vários tipos de populações de células não eletrogénicas, nomeadamente fibroblastos dérmicos (células da pele) e células C6 gliais. As propriedades destes sinais, como a frequência, duração, forma e sinais com padrões específicos são discutidos em detalhe.

Os sinais gerados por células não eletrogénicas tem propriedades especificas, incluindo encontrarem-se dentro da banda de frequência dos milihertz (f<1 Hz), tendo durações no intervalo de segundos e sendo quase-periódicos quando ocorrem atividades intensas.

Treinos de sinais padronizados quase periódicos frequentemente apresentam padrões de modulação em amplitude e na frequência.

As propriedades dos sinais gerados por populações de células não eletrogénicas estabeleceram dois requisitos no design dos sensores elétricos para medições de eletrofisiologia que são discutidos nesta tese.

Primeiramente, na banda de frequência dos milihertz, o ruído base é imposto pelo ruído rosa, também conhecido como $1/f$ noise. Este tipo de ruído determina o limite de deteção dos sensores elétricos. Estratégias para minimizar este ruído, como a utilização de elétrodos micro-estruturados são discutidas. Em segundo lugar, os sinais de células não eletrogénicas são um resultado de um processo de sincronização celular. A área do elétrodo necessita ser otimizada para medir o número de células envolvidas na sincronização, prevenindo assim medir outros eventos que vão resultar em ruído elétrico.

Os resultados eletrofisiológicos são apenas relevantes se fornecerem informação acerca de processos nos quais as células estão envolvidas. Portanto, esta tese induziu tarefas celulares especificas e mediu alterações correspondentes a resultados eletrofisiológicos. Por exemplo, a migração celular foi monitorizada após uma ferida ser feita numa população de células. Esta tese demonstra que diferentes tipo celulares tem diferentes processos migratórios quando estes são medidos em eletrofisiologia. O padrão de migração de células cancerosas pode estar relacionados com a velocidade de migração, enquanto que nas células da pele, o padrão de migração medido através de sinais eletrofisiológicos revela informação acerca dos sinais bioelétricos utilizados pelas células para coordenarem a reparação de uma ferida.

Por fim, esta tese discute como é que os sensores elétricos utilizados em eletrofisiologia podem ser utilizados em estudos biológicos fundamentais em células não eletrogénicas e em dispositivos terapêuticos.

Palavras-chave: Eletrofisiologia, sinais bioelétricos, células não-eletrogénicas, elétrodos extracelulares.

Abstract

The advancement of microelectronics has enabled the fabrication of microelectrode arrays (MEAs), which are individually addressable electrodes with dimensions as small as a single cell. MEAs are commonly used to measure extracellular signals in electrogenic cells, which have the capability of firing action potentials, such as neurons, cardiomyocytes, and nerve cells, exchanging information at high speed (up to meters per second). In contrast, non-electrogenic cells, such as skin cells, use chemical oscillations, such as calcium waves, to communicate with their neighbouring cells. These chemical oscillations travel very slowly (micrometres per second) through a connected cell population. The fluctuation generated by these cells is often a result of several cells which synchronize their behaviour.

In this thesis different topics are discussed. Primarily, the extracellular bioelectrical signals generated by non-electrogenic cells. This study hypothesizes that ionic oscillations, such as calcium waves and other ionic fluctuations caused by non-electrogenic cells also induce extracellular ionic fluctuations. The electric fluctuations can be detected by extracellular electrodes as voltage oscillations. Secondly, specific properties of the electrical fluctuations measured by extracellular electrodes in several types of populations of non-electrogenic cells. The properties of these signals, such as their frequency (millihertz frequency band (f<1 Hz)), duration (few seconds), shapes, and specific signal patterns (quasi-periodic activity, amplitude and frequency modulated) is discussed. Furthermore, the requirement of the design of sensing electrodes to measure in the millihertz frequency band and also to be able of measuring biosignals, resulting in a cell synchronization process is also discussed. Thirdly, different electrophysiological signal migration patterns generated by cancer cells and skin cells while migrating is discussed. The analysis of electrophysiological data provides information about the processes in which the cells are involved. For instance, cell migration was monitored after a wound was inflicted in a cell population. It is demonstrated that different cell types have different migration processes when electrophysiological activity is recorded. Lastly, how electrophysiological sensing electrodes can be exploited in fundamental biological studies in populations of non-electrogenic cells and in therapeutic devices.

Keywords: Electrophysiology, bioelectrical signals, non-electrogenic cells, extracellular electrodes.

Table of Contents

List of Figures

List of Tables

Abbreviations and Symbols

2D	2 Dimensions
3D	3 Dimensions
AC	Alternative current
AI	Artificial intelligence
AM	Amplitude modulated
ASIC	Acid Sensitive Ion Channels
ATCC	American Type Culture Collection
ATP	Adenosine 5'-triphosphate
C	Capacitance
CNS	Central Nervous System
Cx43	Connexin 43
DC	Direct current
DGAV	*Direção Geral de Alimentação e Veterinária*
DHEA	Dehydroepiandrosterone
DHT	5α-dihydrotestosterone
DME	Dulbecco's Modified Eagle Medium
ECGs	Electrocardiograms
ECIS	Electric cell-substrate Impedance Sensing
EDL	Electrical double layer
EEGs	Electroencephalograms

EGTA	Ethylene glycol-bis (β-aminoethyl ether)- N,N,N’,N’-tetra acetic acid
F-12K	Kaighn's Modification of Ham's F-12 Medium
FM	Frequency modulated
g	Gap
GABA	γ-Aminobutyric acid
GJs	Gap junctions
Glu	Glutamate
HDF	Human Dermal Fibroblasts
HOPE	Biopsy-derived human high-grade glioma cell
ICC	Immunocytochemistry
ICWs	Intercellular Calcium Waves
IF	Immunofluorescent
ISFETs	Ion-sensitive field effect transistors array-based
l	Length
M199	M199 Modified Medium
MATLAB	Matrix Laboratory
MEAs	Microelectrode arrays
MIS	Metal insulator semi-conductor
MMPs	Matrix metalloproteases
NHDF	Normal Human Dermal Fibroblast

NKCC1	Sodium-potassium-chloride co-transporter isoform-1
NPCs	Neuronal progenitor cells (NPCs)
OV	Overnight
PBS	Phosphate Buffer Saline
PDMS	Polydimethyl siloxane
PEDOT	Poly(3,4-ethylenedioxythiophene)
PEDOT:PSS	Poly(3,4-ethylenedioxythiophene): poly(styrene sulfonate)
PET	Polycarbonate
PFA	Paraformaldehyde
Plasma BK	Plasmalemmal Ca^{2+}-activated K^{+} channels
PLGA	Poly-lactic-glycolic acid
PSS	poly(styrene sulfonic acid)
R	Resistance
RC	Resistor-Capacitance
RCL	Resistance-capacitance layer
Rms	Root mean square
RT	Room temperature
SNR	Signal-to-noise-ratio
T	Temperature
TJs	Tight junctions

UV	Ultraviolet
VGCC	Voltage-gate calcium channel
Vm	Voltage membrane
w	Width

.

CHAPTER 1

Introduction and motivation

"Everybody is a genius. But if you judge a fish by its ability to climb a tree, it will live its whole life believing that it is stupid." Albert Einstein

This chapter provides insight into the goals and motivations that have guided the research presented in this thesis. Additionally, the chapter outlines the structure and organization of the thesis, including the publications that have resulted from this thesis.

1.1 The problem to solve and the motivation

Bioelectrical activity is essential for the proper functioning of all animals, and the development of electrophysiological sensing devices has been a critical step in understanding this complex and vital process. Traditional electrophysiological research has primarily focused on excitable or electrogenic cells, such as neurons, cardiomyocytes, and nerve cells, which generate action potentials. However, there are also non-electrogenic or non-excitable cells, such as skin (dermal) cells and certain types of fibroblasts, that do not generate action potentials. Despite this, these cells have a complex set of membrane channels that allow them to generate extracellular ionic fluctuations. These ionic fluctuations serve as a communication tool that enables cells to coordinate their activity and accomplish complex tasks, such as the repair or regeneration of tissues.

It is important to note that the ability of non-electrogenic cells to communicate with each other within tissue using extracellular ionic fluctuations is not yet well understood, and research in this area is still in its early stages.

This thesis is focused on the electrophysiology of non-electrogenic cells and how these cells use slow voltage oscillations to communicate with other cells. The slow signals are used to carry important instructive information, for instance they are used to guide tissue regeneration and cell migration[7,8].

As non-electrogenic cells do not rely on action potentials to communicate with each other, it is important to distinguish the primary difference between an action potential and a voltage oscillation caused by a slow-varying transmembrane potential. Action potentials are brief electrical impulses that travel down the membrane of a neuron. These signals are concise electrical signals that occur in a matter of milliseconds and require a frequency bandwidth of a few kilohertz to be detected. These signals are relatively strong, with amplitudes that can reach millivolts. In contrast, slow transmembrane potentials occur over minutes or even days, resulting in signals that typically fall in the millihertz frequency band. Signals generated by non-electrogenic cells typically have much smaller amplitudes, only reaching a few microvolts. Therefore, measuring the electrophysiological activity of non-electrogenic cells requires specialized devices and methods capable of detecting low-amplitude, low-frequency signals across populations of cells.

The well-known technique to measure the electrical activity of single cells is the patch-clamp technique. The patch clamp method can measure physiological activity, intra and extracellularly, both in voltage and current[9]. However, there are other methods to measure the bioelectrical activity of cells, namely microelectrode arrays (MEAs) and ion-sensitive field-effect transistors array-based (ISFETs) developed to study individual cells or a population of cells[10,11].

In the field of electrophysiology, excitable cells, particularly neurons, have traditionally been the primary focus. This is because neurons are considered the main contributors to neural activity. To measure and record action potentials, small area electrodes and instrumentation operating in the kilo-Hertz (kHz) bandwidth have been developed and it is now commercially available. These electrodes are known as MEAs, which consist of a high density of small, individually addressed electrodes with a sensing area typically the size of a single neuron. MEAs allow for spatial resolution, enabling researchers to study fundamental issues such as how neurons form communication networks. MEAs also have practical applications, such as in drug screening platforms for investigating how neurons and cardiomyocytes respond to external chemical stimuli.

Contrasting with this intense activity in the field of excitable cells, the electrophysiology of non-excitable cells has been relatively neglected, with only a few studies utilizing patch-clamp methods. The limited interest in non-excitable cells among patch-clamp researchers can be attributed to the fact that the method only measures a single cell at a time, whereas non-excitable cells function in concert with one another to coordinate complex activities such as wound healing and organ formation. This cooperative behaviour of non-excitable cells necessitates a more comprehensive approach to studying their electrophysiology beyond the single-cell level. As a result, there is a growing need to develop new techniques that can measure the collective activity of non-excitable cells.

Measuring the electrophysiological activity of non-electrogenic cells presents several challenges that require specific devices and methods. Some of the requirements and challenges associated with measuring the electrophysiological activity of non-excitable cells include:

- The area of the sensing electrode must be sufficiently large to detect synchronization events involving a cell population. However, it must not be so large as to inadvertently capture large numbers of unsynchronized cells or clusters of cells that are

synchronized out of phase. Doing so would result in a plethora of superimposed signals that would resemble noise. The challenge associated with this requirement is that the optimal electrode area for a given cell population is not known a priori. Electrodes that are too large may record mostly noise, whereas those that are too small may not be able to capture the full range of synchronization event characteristics. As a result, determining the optimal electrode size represents an important challenge in the development of effective electrophysiological sensing devices for non-excitable cells.

- Signals generated by non-electrogenic cells typically occur in the millihertz frequency range. This presents a challenge in minimizing external interference, such as vibrations from buildings, which can also occur in the millihertz frequency range. Overcoming this challenge requires the implementation of effective noise reduction, as well as the use of specialized equipment and materials designed to minimize the impact of external vibrations. These measures are necessary to ensure that the signals obtained from non-excitable cells are accurate and reliable, and to avoid the introduction of artifacts that could compromise the validity of the measurements.
- The signals generated by non-excitable cells are weak, with amplitudes on the order of a few microvolts. As a result, designing electronics that can accurately detect and measure these signals presents significant challenges. Specifically, battery operated ultra-low noise amplifiers must be employed to ensure that the weak signals can be amplified and without introducing additional noise or artifacts.
- One key challenge in designing electronic systems for measuring the electrophysiological activity of non-excitable cells is the presence of $1/f$ noise, which dominates in the millihertz frequency range. This noise is primarily generated by the electrical double-layer formed between the sensing electrode and the electrolyte medium. As a result, the signal detection limit of the electronic system is essentially controlled by this noise. To overcome this challenge, researchers must carefully optimize the device geometry and materials to minimize the impact of $1/f$ noise.

In addition to addressing these technical challenges, the thesis also aims to provide a basic framework for understanding the signals generated by non-excitable cells.

An important contribution of this thesis is the development of a platform capable of quantifying the migration of cancer cell populations. This platform has the potential to

facilitate the development of new cancer therapies and to improve our understanding of the fundamental biological processes that drive cancer growth and metastasis.

Overall, this thesis represents an important step forward in our ability to measure and understand the electrophysiological activity of non-excitable cells and has significant implications for a wide range of biomedical and biological research applications.

1.2 Organization of this thesis

This thesis is organized into seven chapters. The present chapter provides an overview about the motivation of the work and organization of the thesis. Additionally, it provides a brief summary of the published work.

Chapter 2 presents the state-of-the-art related with devices and methods to measure extracellular electrical fluctuations in non-excitable cells. It also includes a discussion about the communication mechanism used by non-excitable cells.

Chapter 3 covers the fundamental aspects of electrophysiological and electrochemical impedance measurements to measure a population of cells using extracellular electrodes.

Chapter 4 provides a detailed account of the devices, cells, and protocols used to perform the electrophysiological measurements. The chapter also covers the biological set-up used in the experiments.

Chapter 5 explores the electrophysiological activity of a primary culture of astrocyte cells using two distinct types of extracellular electrodes: a microstructured electrode array featuring an array of micro mushrooms, and a planar interdigitated electrode. We present evidence that suggests that populations of astrocytes synchronize their bioelectrical activity to generate discrete signals.

Moreover, bioelectrical signal patterns modulated in amplitude and frequency are tentatively explained through the exitance of subpopulations of cells, or cell clusters, that have the ability to change the number of cells involved or contributing to a particular signal.

Chapter 6 presents an electrophysiological sensing device together with a methodology to quantify the migration of cells. Two case studies were carried out. The migration of

C6 cell and the migration of skin fibroblast cells. These studies were complemented through cytotoxicity assay, proliferation, scratch assay, immunocytochemistry and Electrical Cell Impedance Sensing (ECIS).

Finally, the Chapter 7 summarizes and all the major achievements of this thesis. This chapter also presents a critical review of the major findings together with some suggestions for further work.

1.3 Peer Reviewed Published Work and Conference Presentation

Journal Publications

- Pedro M. C. inácio, Maria C.R. Medeiros, Tiago Carvalho, Rute C. Félix, **Ana Mestre**, Peter C. Hubbard, Quirina Ferreira, Jorge Morgado, Ana Charas, Carmen S.R. Freire, Fabio Biscarini, Deborah M. Power, Henrique L. Gomes (2020), "Ultra-low noise PEDOT:PSS electrodes on bacterial celulose: A sensor to access bioelectrical signaals in non-electrogenic cells", *Organic Electronics*, Doi: 10.1016/j.orgel.2020.105882.

- Sophia Letsiou, Rute C. Félix, João C.R. Cardoso, Liliana Anjos, **Ana L. Mestre**, Henrique L. Gomes, Deborah M. Power (2020), "Cartilage acidic protein 1 promotes increased cell viability, cell proliferation and energy metabolism in primary human dermal fibroblasts"*, Biochemie*. Doi:10.1016/j.biochi.2020.02.008.

- Sanaz Asgarifar, **Ana L. G. Mestre**, Rute C. Felix, Pedro M.C. Inácio, Maria L. S. Cristiano, Maria C. R. Medeiros, Inês M. Araújo, Deborah M. Power and Henrique L. Gomes (2019)," Extracellular electrophysiological based sensor to monitor cancer cell cooperative migration and cell-cell connections", *Biosensors and Bioelectronics*. Doi: 10.1016/j.bios.2019.111708.

- S. Asgarifar, P. M. C. Inácio, **A. L. G. Mestre**, and H. L. Gomes (2018), "Ultrasensitive bioelectronic devices based on conducting polymers for electrophysiology studies," *Chem. Pap.*. Doi: 10.1007/s11696-018-0481-z.

- **Ana L. G. Mestre**, Pedro M. C. Inácio, Sanaz Asgarifar, Monica Cerquido, Ana S. Lourenço, Maria L. S. Cristiano, Paulo Aguiar, Maria C. R. Medeiros, Inês M. Araújo, João Ventura and

Henrique L. Gomes (2017), "Ultrasensitive gold micro-structured electrodes enable the detection of extra-cellular long-lasting potentials in astrocytes populations", Scientific Reports. Doi: 10.1038/s41598-017-14697-y.

- **Ana L. Mestre**, Pedro M. Inácio, Youssef Elamine, Sanaz Asgarifar, Ana S. Lourenço, Maria D. Cristiano, Paulo D. Aguiar, Maria d. de Medeiros, Inês M. Araújo, Joao Ventura, Henrique L. Gomes (2017), "Extracellular electrophysiological measurements of cooperative signals in astrocytes populations", Frontiers, Doi: 10.3389/fncir.2017.00080.

- Pedro M. C. Inácio, **Ana L. G. Mestre**, Maria C. R. Medeiros Member, IEEE, Sanaz Asgarifar, Youssef Elamine, Joana Canudo, João M. A. Santos, José Bragança, Jorge Morgado, Fabio Biscarini, H. L. G. (2017), 'Bioelectrical signal detection using conducting polymer electrodes and the displacement current method', *IEEE Sensors Jounal*, Doi: 10.1109/JSEN.2017.2703834.

Oral communications

- **Ana G. Mestre**, Electrical Detection of Extracellular Long-Lasting Potentials in Astrocytes, II Symposium Portuguese Glial Network, 25 May 2017, Braga, Portugal.
- **Ana G. Mestre** et al., Extracellular Electrical Recording using poly (L-lactic) acid coated electrodes, Materials 2017, April 2017, Aveiro, Portugal.

Poster presentations

- **Ana G. Mestre**, Pedro C. Inácio, Sanaz Asgarifar, Inês M. Araújo, Henrique L. Gomes, "Electrical detecting of extracellular long-lasting potentials in astrocytes", XV SPN Meeting, 26-27 May2017, Braga, Portugal.
- **Ana G. Mestre**, Pedro C. Inácio, Sanaz Asgarifar, Joana Canudo, Luís Alcácer, and Henrique L. Gomes, Ink-Jet Printed Polymer Electrodes on Nano Fibrous Bacterial-Cellulose Substrates for Extracellular Signal Recording Industry Day on Printed Electronics and Solar Cells – DaySol2017.

Seminars and lectures

- Lecture in Immunoneurophysiology course, May 23rd-24th 2019, Faculty of Health, Copenhagen, Denmark;
- Seminar "Percurso de vida: Como passar de uma atividade na área de investigação académica para uma atividade na área empresarial e (ou qual a importância de uma

experiência em empresa", in the workshop "A importância da colaboração com empresas – Empresas e Área Bio & Med: novas perspetivas de desenvolvimento de carreira para jovens licenciados", University of Algarve, 12th April, 2019;

- Seminar *"Técnicas de cultura celular animal - TCCA*", 2019, University of Algarve, Campus de Gambelas, Faro, Portugal;
- Seminar at "IX Jornadas Nacionais de Ciências Biomédicas", 20th April 2018, University of Algarve;
- Seminar *"Técnicas de cultura celular animal - TCCA*", 2018, University of Algarve, Campus de Gambelas, Faro, Portugal;
- Seminar *"Técnicas de cultura celular animal - TCCA*", 2017, University of Algarve, Campus de Gambelas, Faro, Portugal.

CHAPTER 2

State-of-the-art

Extracellular bioelectrical signals on non-excitable cells

"If you can't explain it simply, you don't understand it well enough." Albert Einstein

This chapter provides a state-of-the-art view of the technology used to measure excitable and non-excitable cells, as well as basic concepts of bioelectrical activity produced by electrogenic, e.g., neurons, and non-electrogenic cells. Field effect transistors (BioFETs) and MEAS technologies together with impedance-based methods are reviewed. Optical fluorescence which is the gold standard technique for studying ion channels in biology is also presented. The advantages and limitations when compared with the electrical-based technologies are briefly reviewed.

2.1 Introduction

Cells use various chemical species, including ions and small molecules, to communicate with each other. These chemical messengers are produced and released into the extracellular space, where they elicit a response in nearby cells. The response can only occur if the recipient cell possesses specific receptors for the given signal transmitter. Upon binding to the receptors, downstream intracellular signaling cascades are initiated, leading to the release and propagation of signals to other surrounding cells and across the tissue. This mode of cellular communication is referred to as intercellular communication.

Conversely, intracellular signaling involves communication within the cytoplasm of an individual cell. This thesis focuses on intercellular cell signaling because it can be conveniently measured using extracellular electrodes and electrical-based methods.

This chapter is organized as follows; it begins by introducing the basic concepts about ion channels in cells and how cells use the ion channels to perform a number of tasks, namely, migrate, repair wounds, and even construct organs, etc. Subsequently, the chapter reviews how extracellular changes in ion concentration can be recorded by using extracellular devices is reviewed. Specifically, the discussion is centred around two types of devices: transistor-like devices and microelectrodes arrays also known as MEAs. Additionally, the chapter reviews the electrochemical impedance technique used to monitor cell adhesion and migration. The optical fluorescence method is comparatively analysed with the electrical based methods. Finally, the chapter comparatively analyses the optical fluorescence method with the electrical-based methods.

2.2 Ion channels in cells and extracellular signals

Cells usually contain a high ion intracellular concentration of K^+, low Na^+ concentration and a neutral Cl ion concentration balanced with the membrane potential, so low levels of chloride ions inside and outside are kept[12]. The essential ion transporter that sustained the resting membrane potential (RMP) is Na^+/ K^+-ATPase transporter, which requires ATP to pump Na^+ against the concentration gradient and out of the cell, in exchange for the import of K^+. This mechanism keeps the cell alive and it is involved in other processes as cell volume regulation and signal transduction[12]. It has also been

suggested that the Na^+/ K^+-ATPase transporter can be upregulated in malignant cancers, including gliomas[12,13]. The expression of Ca^{2+}, K^+, and Cl^- channels differs between cancer cells and malignant glioma cells. These cells express an inward Na^+ current that is not detected in normal astrocytes or in low grade gliomas[14].

Non-excitable cells communicate via calcium signalling and intracellular calcium oscillations are related to cellular migration of glioma cells, without interfering with their volume[15]. Calcium ions (Ca^{2+}) are a second messenger that is involved in cell growth and proliferation, migration and apoptosis through its influx via voltage-gate calcium channel (VGCC) in glioma cells[16]. Ca^{2+} signaling regulates tumour cells proliferation derived from cytosolic Ca^{2+} activity[16]. The entrance of Ca^{2+} from extracellular space is a skilled process responsible for long lasting intracellular Ca^{2+} elevations[17]. Chloride ion channels are involved in multiple cell procedures, such as, osmoregulation, salt secretion, migration and proliferation[18] and Cl^- ions are responsible for changes in cell volume during migration. The main transporter of Cl^- ions is sodium-potassium-chloride co-transporter isoform-1 (NKCC1), which maintains the electrochemical gradient. This balance is dependent of intracellular potassium concentrations and thus, potassium pumps are also needed and important during cell invasion[15]. In glioma cells, Cl^- channels contribute to the depolarization of voltage membrane (V_m). This enables cell migration and invasion, and also allows the release of K^+ and the decrease of water levels and cellular volume to promote their infiltration into extracellular spaces[19]. Cl^- channels blockers reduce transmembrane Cl^- fluxes and consequently the osmolarity, resulting in cell volume changes. In glioma cells, chloride channels are involved in tumour invasiveness, affecting cell shape and cell volume changes to promote cell migration and invasion[20]. Another process involved in cell migration is the depolarized membrane resting potential V_m that supports cell proliferation in many cancer types as shown by electrophysiological analyses. V_m is influenced by its permeability to distinct ions, Na^+, K^+, Ca^{2+}, and Cl^- as well as by intercellular communications, such as gap junctions. There are studies that showed V_m were able to control wound healing and migration in an indirect manner [19].

The resting potential of the majority of living cells are kept by K^+ channels. However, Ca^{2+}-activated potassium (K_{Ca}) channels are also expressed by many cells and are not

only able to directly communicate calcium signals for changes in cell membrane potential, but also to allow cells to promote changes in intracellular second messenger – Ca^{2+} to membrane K^+ conductance, and thus, are able to modify resting membrane potential[21]. In glioma cells, the resting membrane potential is approximately -40 mV, which might be direct cause of the accumulation of chloride ions intracellularly, comparing to most other healthy cells in the brain, where the resting membrane potential is approximately -70mV. Thus, NKCC1 transporters may be strongly involved in the accumulation of Cl^- ions in glioma cells, causing volume changes. Furthermore, NKCC1 is expressed on the leading edge of glioma tumours where populations of migratory glioma cells are present, and can influence the speed of migration via its interactions with the actin cytoskeleton; plus the inhibition of NKCC1 reduces glioma cells invasion[12]. In order to avoid cell invasion, one therapeutic approach could possibility be to block ion chloride channels[18], as it was shown that the inhibition of NKCC1 reduced glioma invasion[13]. Calcium ion channels also play a key role in cells invasion and when inhibited it reduces the immune activity of anticancer T cells within the tumour[15], thus blocking ion chloride channels could also be a novel strategy for reducing cell invasion, yet not for all cell populations.

Cell-to-cell connections englobes specific junctions as shown in Figure 2.1. These junctions allow intercellular communication through the ions referred above, being the main five: tight junctions, adherents junctions, desmosome junctions, gap junction and hemidesmosome junction. Gap junction channels contain two hemichannels formed by connexins. These channels contribute for the uptake of ions and metabolites as well as the release of neuroactive molecules[22]. Gap junctional connexions are responsible for the synchronization and rhythmic oscillation of neuronal activity in some parts of the brain[23] and play a role in development, maturation as well as cell migration and differentiation[24]. However, not functional gap junctions also play a role a diversity of diseases, such as brain ischemia, Alzheimer's disease and epilepsy[25], and others. The major connexins of gap junctions in astrocytes are Cx43 and Cx30[26], which are also present in glioma cells[27]. C6 glioma cells do not express a significant level of Cx43, which confers them with a more aggressive migratory ability than human gliomas[28]. There are strong associations between gap junctions and migration. *In vitro*, glioma cells increased their motility when gap junction channels are blocked and the decrease of the gap junction protein Cx43

levels increases the cell migration[28]. It was also reported that protein Cx43 expression strongly associates with cell to cell adhesion properties[29]. Following disruption of cell adhesions, astrocytes from the cortex recovered the coupling of gap junctions approximately in ≅ 475 seconds [30].

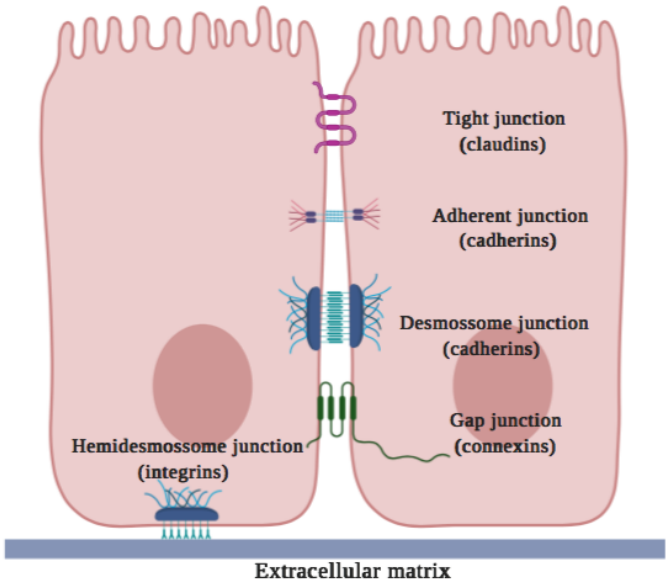

Figure 2.1 Schematic representation of intercellular connections between two cells. This figure was created by Biorender.com.

2.3 Electrophysiological techniques and devices

One efficient way to measure extracellular electrical fluctuations caused by the ion channel activity described in the previous section is through electrophysiological techniques. Electrophysiology is the study of electrical properties of living cells and tissues, aiming to decode the molecular and cellular processes mediated through electrical signals. Electrophysiology measures membrane potentials before, during and after the transactions of chemical compounds. Nobel prize winners in Physiology, Erwin Neher and Bert Sakmann[9], showed in 1991 the opening and closing of ion channels in nerve membranes for the first time through a patch clamp technique.

Electrophysiology has often been used for several purposes, namely, to study brain and heart activity, e.g., electroencephalogram and electrocardiogram, respectively, meaning that cells such as neurons and cardiac are indeed excitable and can be measured *in vitro*, *ex-vivo*, *in vivo* or *in situ*. Electrophysiology can be used for all types of cells. So, non-

excitable cells can also be measured once they also have membrane potential and their electrical potential in the cytoplasm differs from the extracellular environment, when the current is zero[31]. Overall, cells (excitable or non-excitable cells) can be measured by electrophysiological based methods relying on extracellular electrodes because all cells have ion channels, which are the responsible for creating oscillating potentials in the cell membrane through the release of ions into the extracellular space. Figure 2.2 shows two schematic diagrams representing the two approaches to study electrophysiology of cells, patch clamp and extracellular recordings. The patch clamp technique allows the measurement of ion channels conductance (cell membrane). Extracellular electrodes allow the study of extracellular space dynamics between cells. All categories grant knowledge on membrane potentials (inside, in the membrane or outside of the cell). In this thesis, only extracellular recordings were performed.

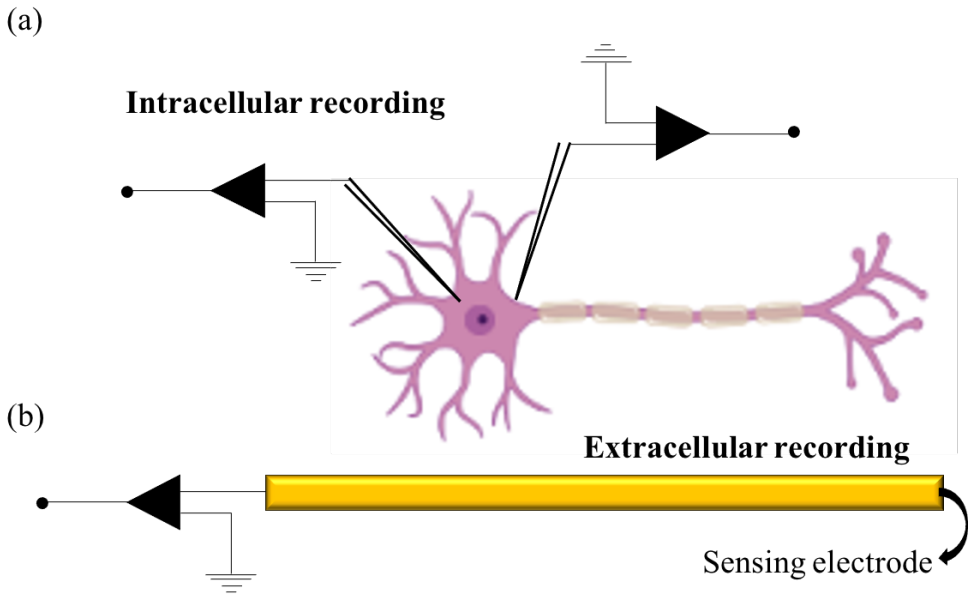

Figure 2.2 The two basic types of electrophysiology measurements (a) The patch clamp method that uses micropipettes in intimate contact with the membrane or even penetrating the cell membrane to record electrical fluctuations inside the membrane. (b) Extracellular electrodes which are sensitive to electrical fluctuation outside of the cell.

An excitable cell is capable of promoting active electrical responses by changes in current or voltage across a cell membrane, resulting in the generation of action potentials, e.g., neurons, muscle cells (skeletal, cardiac and smooth) and some endocrine cells. An action potential is a sudden, fast, transitory and propagating change of the resting membrane potential through the cell, then diffused across the neighbouring cells. This event is

caused by a stimulation strong enough to reduce negativity up until the threshold potential, usually between -50 to -55 mV. This event results in a change of membrane permeability causing ion channels to open and close. An action potential has more than one phase: resting potential, depolarization, increase of sodium ions inside of the cell, increment of cellular positive charges, repolarization, closure of sodium channels and opening of potassium channels (caused by the efflux of potassium ions leading to cells to become more electronegative), reestablishment of the membrane potential, hyperpolarization (when membrane potential is more negative than the default membrane potential), and finally the restoration of the resting potential. These steps culminate in the typical shape known as action potential, as shown in Figure 2.3, which firstly shows (above) the opening of sodium channels and bellow the closing of sodium channels and the opening of potassium channels. The result, including all phases of an action potential is shown in Figure 2.3 on the right, where the signal is shown in voltage in function of time will all phases represented.

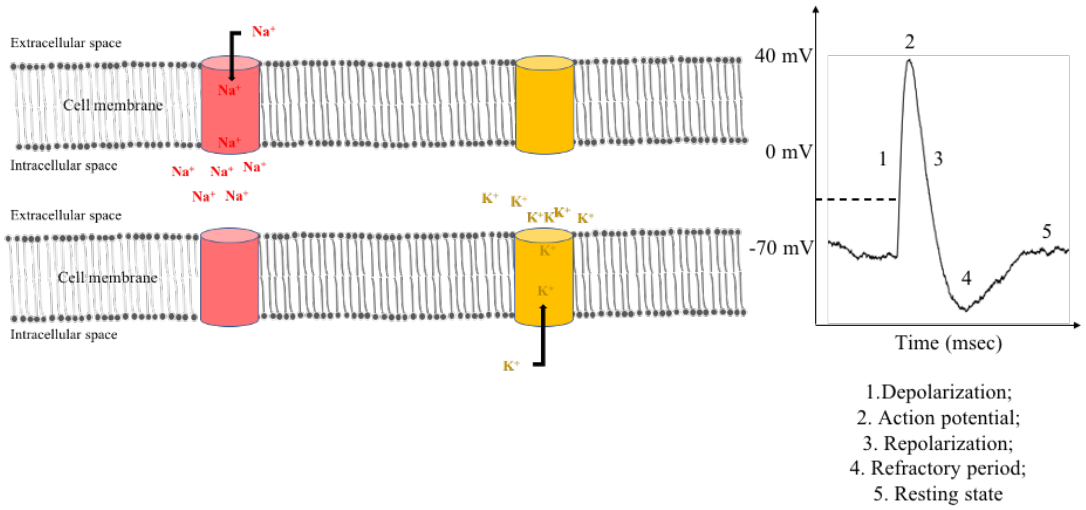

Figure 2.3 Action potential along the cell body. On the left, proceed from a relatively negative to a positive charge inside of a cell. On the right, all phases of the action potentials are shown, from resting stage, passing through depolarization, repolarization and returning to resting stage. Adapted from [1].

A non-excitable cell is a cell that does not produce an action potentials[32]. However, the process of depolarization, repolarization and hyperpolarization also occurs in non-excitable cells. As mentioned before, all cells communicate through travelling waves. Non-excitable cells usually communicate using traveling waves of calcium whereas excitable ones generate their excitability through the plasma membrane. Non-excitable

cells, e.g. fibroblasts, show chemical fluctuations in the cytoplasm[33]. So calcium signalling plays an important role in communication, since non excitable cells are not able to produce an action potential, despite the presence of voltage-gated ion channels, and their excitability is shown through the calcium signalling system[34]. Calcium signalling acts as a second messenger of intra and intercellular communication[35]. This type of communication has a completely different time window. For an excitable cell, e.g. neuron, neurotransmission occurs in milliseconds, while for a non-excitable cell, e.g. astrocyte, the regulation of the synaptic transmission last seconds or tens of seconds[33, 36]. The communication through calcium transients between non-excitable cells demands the presence of a second messenger. The IP_3-induced Ca^{2+} release is indispensable for initiation and maintenance of glial intercellular Ca^{2+} waves that provide for long-range signaling[34]. Stimulation of non-excitable cells through metabotropic receptors triggers cytosolic Ca^{2+} signals and propagating intercellular Ca^{2+} waves. Receptor activation is coupled to a membrane-associated G protein, which stimulates the release of Ca^{2+} from the endoplasmic reticulum via the activation of phospholipase C and consequent production of inositol (1,4,5)-trisphosphate [36,33].

2.4 Sensing technologies devices to measure extracellular cell activity

Three types of devices have been used to sense cells and their extracellular activity. Transistor like devices, named here BioFets, microelectrode arrays also know in the literature as MEAs, and devices based on the measurement of the impedance of the cell sitting on top of sensing electrodes. This last method is known as electric cell-substrate impedance sensing (ECIS). While MEAs and BioFETs can measure electrical fluctuations in the extracellular medium, ECIS is not sensitive to electrical fluctuations, but instead to changes in impedance caused by the presence of the cell or by their activity. Below we outline the major research work carried using these three different devices.

To measure the bioelectrical activity of cells, two type of devices have been used. (i) BioFETs and (ii) MEAs. The major difference between BioFETs and MEAs is that transistors are active devices, they need to be polarized to operate properly as a transistor. MEAs are passive electrodes, therefore no direct bias is applied to these structures unless

they are used to electrically stimulate the cells. The use of transistors has followed two different approaches depending on the transistor architecture. In the early days, the transistor was a solid-state device with a solid dielectric layer interposed between the gate terminal and the transistor channel. The gate was made floating, and the cells usually sit on the top of the floating gate terminal. In recent approaches, the transistor does not have a solid dielectric. The dielectric layer is in reality an electrical-double layer established by electrolyte of the cell culture medium at the surface of a gate terminal. The cells to be measured are adherent to the gate terminal. The gate is made co-planar with the drain and source terminals. This device architecture is known as electrolyte-gated field-effect-transistors[37]. This section presents the major developments using BioFets and MEAs as cell-based sensing technologies.

2.4.1 Field effect Transistors

In the past decades, advances in materials and in nanotechnology allowed the discovery and development of several different materials specially for BioFet devices. BioFETs may be divided in subclasses depending on their material, substrate, or function. In the context of this thesis the relevant ones are, (i) graphene field-effect transistor (GFETs), (ii) organic field-effect transistors (OFETs) and (iii) silicon nanowire field-effect transistor (SiNW-FETs). A field-effect transistor (FET) has three terminals: source, drain and gate. The gate voltage regulates the current between source and drain terminal.

GFETs are highly sensitivity to the detection of biomolecular components at its surface due to its monoatomic thinness, allowing the quantitative analysis of biological relevant molecules such as DNA, proteins, ions and small molecules[38]. GFETs are also able to detect extracellular cell signals. The performance of the GFETs was evaluated using cardiomyocytes cells[39]. GFETs have the advantage of chemical stability, flexibility and biocompatibility[5].

Organic materials are also gaining a significance position with a great potential in electrophysiological and biochemical cell signals recording. OFETS use small organic molecules or polymers as sensing layer[40]. These transistors have been recently used for pulse oximeters, temperature/pressure signals, electrocardiographic recordings and electrophysiology arrays[41]. Additionally, these transistors can detect glucose, protein, ion concentration and DNA molecules[40]. Comparing to inorganic transistors, OFETs presents

several advantages, namely, low-cost solution processing. Additionally, OFETs present high compatibility with flexible substrates and good biocompatibility with biological tissues[40]. Furthermore, it has an easy fabrication, tuneable morphology and surface chemistry[5]. A typical example is the use of organic electrodes Poly(3,4-ethylenedioxythiophene): poly (styrene sulfonate) (PEDOT:PSS). Due to their biocompatibility, flexibility, high stability and low redox potentials, PEDOT:PSS offers a great solution for electrophysiological measurements and also offers several applications, namely in drug delivery, tissue engineering, wearable electronics, etc[42].

Silicon nanowire field-effect transistor (SiNW-FETs) uses nanowires in the sensing channel. A nanowire has a uniform 1D structure with diameters typically from 3 to 500 nm and lengths from several hundreds of nanometers to millimeters. SiNW-FETs present several advantages, such as the capability to use well-developed surface chemistry to functionalize the surface silicon oxide layer and also the potential of interfacing with standard silicon technology. SiNW-FETs allows the analysis of kinetics of biomolecule interactions, cancer detection, signal amplification and detection in high ionic strength solutions. It also allows the monitoring of cell electrophysiology, intra and extracellularly, as well as monitoring of cell metabolic activity[43]. Table 2.1 summarizes the main types of cell-based field-effect devices.

Table 2.1 Main types of BioFETs and their biomedical applications[5]

Device	Main biomedical application
Ion-sensitive Field-effect Transistor (ISFETs)	To detect ion in biological environments – pH detector[44]
Graphene Field-effect Transistor (GFETs)	Electrophysiological measurements – to monitor the dynamics of cell clusters[45]
Organic Field-effect Transistor (OFETs)	Electrophysiological measurements – to measure action potentials[46]
Silicon Nanowire Field-effect Transistor (SiNW-FETs)	To detect biomolecular changes[47]

2.4.2 Microelectrode arrays (MEAs)

Despite neurons being able to communicate between them, an individual action potential travels intracellularly through the axon and can be measured using microelectrode arrays (MEAs). In general, MEAs are used for extracellular recordings, however recent progress allows measurements into intracellular space, and can be divided into three groups: planar electrodes, vertical electrodes or nanowires and geometric electrodes, such as gold-mushroom microelectrodes arrays[5]. Conventional MEAs technology can detect action potentials produced by neurons, providing a high temporal resolution and multi-unit electrode recording. However, these MEAs present some limitations concerning to transmembrane potential in the form of slow ionic fluctuations because this technology was optimized to measure fast (in the range of milliseconds) electrical fluctuations. To measure the bioelectrical activity of a non-excitable cells (e.g., astrocyte, or dermal cells), classical MEAs are inadequate because the thermal noise (typically about 5-20 μV) is too high to detect the weak signal generated by non-electrogenic cells.

In order to improve the electrical coupling between cells and the sensing surfaces, several laboratories have started to develop new sensing electrodes for MEA technologies. These emergent MEAs make use of vertical micro or nano-electrodes[48,49] coated of metal electrodes with carbon nanotubes[50–52] and conducting polymers[53–62], which provide a softer and more roughened surface. The strategy behind these approaches aims to enhance electrical performance by promoting a more intimate interaction with cells. Between them, gold-mushroom microelectrode arrays (GMμEAs)[63,64], which is a large electrode array (>1000μm^2) and can be used to measure the cooperative activity produced by non-electrogenic cells. Table 2.2 summaries the main type of MEAs available and their use.

Table 2.2 Different kinds of MicroElectrode Arrays (MEAs)[6]

MEAS	Application
Rigid MEAs	
2D microelectrodes fabricated on glass	Electrophysiological recording of neurons[65]
3D microelectrodes printed on a biocompatible resin	Electrophysiological recording of neurons[66]
Mushroom-shaped gold microelectrodes fabricated on a glass wafer	Electrophysiological recording of cardiomyocytes[64]
Flexible MEAs	
Parylene-based flexible microelectrode array	Brain signals after implanting MEA on cortical surface in rats[67]
Plateau-shaped microelectrode array on a PDMS substrate	Long-term *in vivo* recordings from the MEA implanted on somatosensory cortex of rats[68]
3D flexible microelectrodes fabricated on polyimide	Electrophysiological characterization of 3D networks of electroactive cells[69]

2.5 Electric Cell-substrate Impedance Sensing (ECIS)

The ECIS technique is an easy method to detect cellular behaviour in a non-invasive, real-time and label-free way[70]. When the electrodes are immersed in an electrolyte solution the system physically behaves as a two-layer system. One of the layers is comprised of a charged interfacial region established on both electrode surfaces known as Helmholtz or Stern layer[71,72]. The other layer is comprised of the bulk

electrolyte. Changes in the cell have an effect on the impedance of the electrical double-layer, providing important information about the cell viability, motility, and cell physiology. For example, the electrical-double-layer impedance (at the sensing electrode) depends on activity of the cells and their adhesion to electrodes, offering evidences about cell attachment, spreading and cell motility[73]. Impedance also gives information about morphology, cell proliferation, migration upon pharmaceutical screening, environmental monitoring and toxin detection[74–76]. It is also possible to motorize cell membrane conductivity, cell monolayer permeability, morphological migration and micromotions[77].

The major advantage of impedance, is the detection at low power consumption and flexibility in the sensor size and sensitivity parameters, as cellular electrical properties have an important function in the physiology in living cells[78]. Furthermore, this method has many advantages such as: swiftness, enhanced sensitivity, bio-recognition on-the-spot and early-stage detection, and targeting[2]. Electric Cell-Substrate Impedance Sensing (ECIS) has successfully being used to study cellular behaviours, like wound healing, cancer, inflammation, cell growth and differentiation in different cell lines[74], as well as cellular responses to toxicity of chemicals and biological origins[76]. Biotechnology, tissue engineering, characterization of biological cells, disease diagnosis and cell culture monitoring are focused by this method since it is non-invasive and label-free[70].

2.6 Techniques-based on optical fluorescence

Optical fluorescence (OF) allows the detection and localization of single molecules with high spatial precision and a resolution in the range of nanometres on both fixed and living cells[79]. This permits the understanding of some biological processes and the basic mechanisms from single cells to an entire body, reason why it is used in so many research fields. Optical imaging uses non-ionizing radiation ranging from ultraviolet to infrared light. One major advantage of optical imaging is the use on biomedical research to access to the interactions at molecular level, such as gene expression, proteins, protein-protein interactions and cellular processes. Optical image often used fluorescence optical imaging with a specific wavelength or wavelength range, where there is an interaction between photons and fluorophores, resulting in an excitation of the fluorophores, and so fluorophores release photons. One representative and often used fluorophore is Alexa

Fluor and fluorescent protein also use commonly is green fluorescent protein (GFP) or red fluorescent protein (RFP). Ordinarily used fluorescent microscopy techniques are laser scanning confocal microscopy (MSCM or CLSM), to obtain high-resolution optical images at controllable depths[80]. Another example is the use of fluorescence-lifetime imaging microscopy (FLIM), also used at cellular level, producing images at differences in the exponential decay rate of a fluorescent sample[81]. Regarding to tissues and cells, immunohistochemistry is used to study tissues constituents (antigens) with the employment of specific antibodies that can be seen through staining. If only cells are used, it is called immunocytochemistry[82].

Fluorescence microscopy is also used for materials, namely electron microscopy (EM) or scanning probe microscopy (SPM), revealing a supreme spatial resolution, 3D information noninvasively and can access fast dynamic processes. However, it also presents some limitations, such as the measuring dynamics *in situ* or probing below the outer surface of a material. Curiously, for polymers, to study structural details in the nanometre range, atomic force microscopy (AFM) is often used, however do not allow imaging inside of the polymers. AFM is preferable to use with polymers comparing to EM since the lack of heavy elements with significant electron numbers decrease the contrast. Usually, AFM and EM are combined with super-resolution fluorescence techniques[83]. Additionally, it is also possible to translate membrane potential into an optical signal, through the use of fast voltage-sensitive dyes in neurons. Using light energy in a specific wavelength, the dye molecule get excited and the voltage of the cell can be determined through the monitoring of the emitted fluorescence or absorption[84]. Concluding, fluorescence microscopy presents several advantages, namely being a minimally invasive technique, rapid acquisition data, and target specific molecules. However, in spite of largely use in biology research, fluorescence microscopy also presents some limitations, such as diffraction-limited resolution, which means high-resolution imaging is hard to achieve[81]. And also, these techniques present a low signal-to-noise ratio and may impact in the physiological functions of the cell membrane. Furthermore, the lifetime of fluorescence dyes limits the observation to a few hours. When optical methods are compared to the use of extracellular electrodes it became clear that extracellular electrodes offer the advantage of being totally non-invasive and enable

monitoring cells and tissues for periods of time as long as weeks in a non-invasive way. However, optical methods offer an excellent support to highlight data recorded.

2.7 Summary

This chapter begins by emphasising that all types of cells have a complex machinery of ion channels. Even if the cells are not capable to generate an action potential, it is clear that non-electrogenic cells exchange, with the surrounding medium, ions which cause ionic fluctuations. These ionic fluctuations can be detected by extracellular electrodes as electrical oscillations. BioFETs and MEAs devices can, in principle, detect these ionic fluctuations with low enough detection limit. This chapter reviews the use of MEAS and BioFETs devices to measure bioelectrical activity in cells. In spite of the surface modifications using nanostructured materials, soft and rough conducting polymers, or nanowires are being developed to improve the interface between the cells and the sensing surface. The striking conclusion of this literature review is that the technology has exclusively been used to measured electrogenic cells.

The impedance technique known as ECIS does not provide information about bioelectrical signalling, but instead ECIS provides very relevant information about the cell properties, namely shape, morphology adhesion and motility. Therefore, is an ideal complementary technique to be used simultaneously with MEAs to construct an overall vision of the behaviour of cell populations.

Finally, the gold standard in the biological community are the optical based methods. These can be made very specific and target specific molecules. However, they can only follow biological process that last for a couple of hours. It is well-known that are ultra-slow biological phenomena that involves biological signalling in a time scale of hours and even days. These time scales are inaccessible by optical fluorescent methods, however optical methods represent an important information carrier to settle electrophysiological data.

CHAPTER 3

Fundamental aspects of electrophysiological and electrochemical impedance measurements in cell populations

"The good thing about science is that it's true whether or not you believe in it." Neil deGrasse Tyson

This chapter presents and discusses the equivalent circuit used to describe the electrical coupling between cells and the sensing electrode. The small-signal model is used to interpret the impedance date and the difference between measurements in current and in the voltage detection method. The role of each circuit element in the signal-to-noise ratio is discussed.

3.1 Introduction

This chapter presents and discusses the equivalent circuit used to describe the electrical coupling between cells and the sensing device, and it is organized as follows: firstly, the basic concept of the electrical-double layer is presented. Secondly, the equivalent circuit that describes the electrical double-layer is described in detail. The importance of electrode impedance is also exploited and finally, the fundament aspects of noise in electrophysiological systems is also briefly discussed.

3.2 Basic concept of electrical double-layer

When an electrode is immersed in an electrolyte solution, the surface of the metal becomes electrically charged. The ionic surface charges are compensated with negative charges (electrons) located in the bulk metal. A dipole layer is established between the metal and the electrolyte solution. The charge region in the electrolyte is named the electrical-double layer (EDL) or the Helmholtz layer. Figure 3.1 (a) shows a schematic representation of the EDL layer. The electrical properties of the EDL determine the electrical coupling between the cell and the sensing surface[2,85], therefore is crucial to have a proper understanding of this layer. A suitable way to interpret the overall electrical properties of the EDL is to use an equivalent RC circuit network. The schematic diagram represented in Figure 3.1 (b) shows the equivalent circuit that describes the Helmholtz layer arranged in series the bulk electrolyte solution[86]. R_D and C_D represent the resistance and capacitance of the EDL. The bulk electrolyte is described by a low capacitance (C_B) in parallel with a resistance (R_B) that accounts for the bulk conductivity of the electrolyte solution. Often in a real system the sensing electrode and the counter electrode are identical. Therefore, there are two EDLs, but only one RC circuit is required to describe them. The individual RC circuits describing the interface and the bulk layer are effectively in series and provide an electrical equivalent for the two-layer system as schematically shown in Fig. 3.1 (b)[87]. From an experimental point of view, the impedance analyser cannot measure the circuit elements such as C_D and R_D, R_B or C_B. The impedance analyser measures the overall combination of all the circuit elements and this combination is represented as the overall parallel capacitance (C_P) and parallel resistance (R_P). It is also

convenient to represent R_P as a *Loss* parameter. The *Loss* is defined as $1/(\omega R_P)$, where R_p is the resistance and $\omega=2\pi f$, and f the frequency of the test signal. This frequency dependence of the *Cp* and *Loss* is represented in Figure 3.1 (c) for a gold/electrolyte system. Both *Cp* and *Loss* have a dispersion, or a relaxation centred at a particular frequency (f_r), called Maxwell-Wagner relaxation. This relaxation is explained as follows; as the frequency increases the high capacitance C_D is short-circuited giving rise to a transition from a high capacitance to a low capacitance that corresponds to geometrical capacitance *Cg*, which is given by the series sum of the interfacial C_D and bulk capacitance C_B ($Cg=C_D//C_B$).

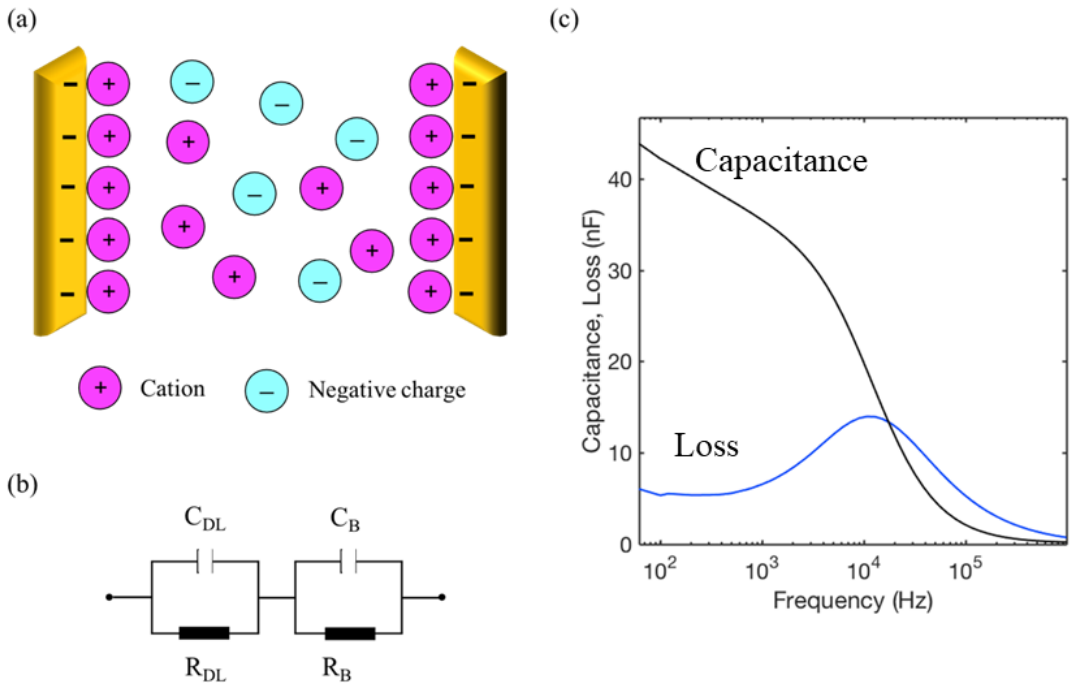

Figure 3.1 (a) Schematic representation of the charge arrangements at the interface between an electrode and an electrolyte solution. (b) Equivalent electrical circuit that describes the frequency response of the EDL layer in series with the electrolyte solution. (c) Typical frequency response of a gold/electrolyte system.

3.3 Characterization of electrical double-layers using impedance-based techniques

Having described the frequency dependence of a sensing electrode immersed in an electrolyte solution, we can now proceed and describe how cells disturb the overall frequency response of the EDL. The goal of this section is to show how measurements of the impedance as function of the frequency can be used to detect the presence of cells adherent on top of sensing electrode.

The cell membranes are high capacitive and also insulating structures. As the cell begins to attach to the sensing electrode the high insulating membrane offers an additional resistance to the high frequency signals. A convenient picture to describe this effect is shown in Figure 3.2 (a). While the high-frequency signal will have easy path through the gaps between cells, the low frequency signals will flow through the cell membrane. The red arrows represent the high frequency signals flowing through the gap junctions. The dashed black arrows represent the low frequency field flowing through the membrane. The uncovered gap between cells is strongly dependent on the cell confluence, cell adhesion, and even cell shape.

The consequence of this "blocking" of the high frequency components, that in overall terms, the electrolyte "looks" more insulating when compared with an electrode free of cells. The frequency dependence of *Cp* and *Loss* keeps the same shape but shifts to lower frequencies as show by the simulation in Fig. 3.2 (b). This is clearly seen by the shift to lower frequencies of the peak in the *Loss* curve. These changes on the impedance are often used to monitor cell adhesion, migration, proliferation, and even changes in cell morphology[77,87–91].

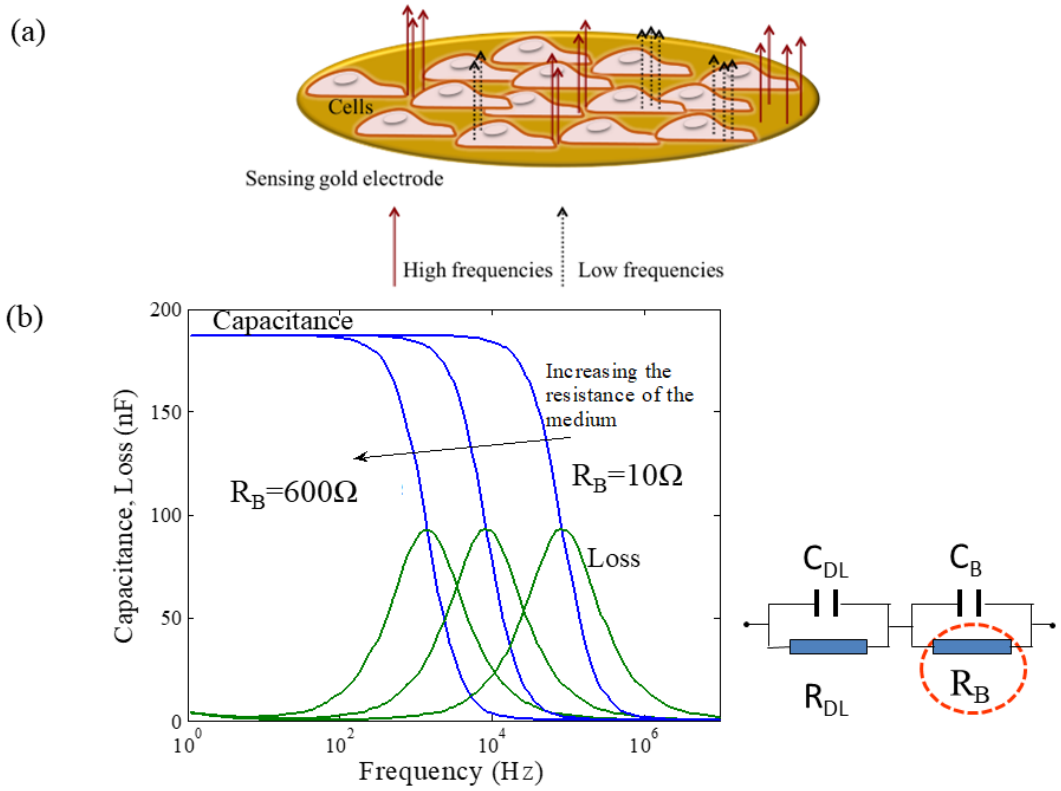

Figure 3.2 (a) Schematic representation to show how electrical fields flows through gap between cells and through cell membrane. Red and continuous arrows represent high frequencies and dashed black arrows represent low frequencies. (b) Simulation of the change in the capacitance and loss curves when R_B increases from 10 Ω to 600 Ω.

3.4 Electrical detection in voltage and in current

In this section we will use the equivalent circuit model described above to interpret now how the voltage or the current signal couples to the sensing electrode. The equivalent circuit network of the electrical double layers in series with the electrolyte resistance is simplified. The simplified circuit network model is shown in the schematic diagram of Figure 3.3 and it has been adapted from a study by Medeiros et al.[2] This circuit is used to understand how the bioelectrical fluctuations near the cell membrane couple to the sensing electrode and finally to the trans-impedance amplifier or alternatively to a voltage amplifier. In Figure 3.3, R_D and C_D are the resistance and the capacitance of the electrical double-layer, respectively. The seal impedance presented in Fig. 3.3 as Z_{Seal} represents

the electrolyte impedance in series with the counter electrode double-layer impedance[2]. Z_{Seal} is assumed to be high. With cells in contact with the measuring electrode, signal loss between cell and the measuring electrode is modelled by the resistance R_C. To ensure extracellular signal is coupled to the measuring electrode, $R_C \ll R_S$. The resistance R_C models the signal loss between cell and the measuring electrode. R_C should be small, to ensure that extracellular signal is coupled into the measuring electrode.

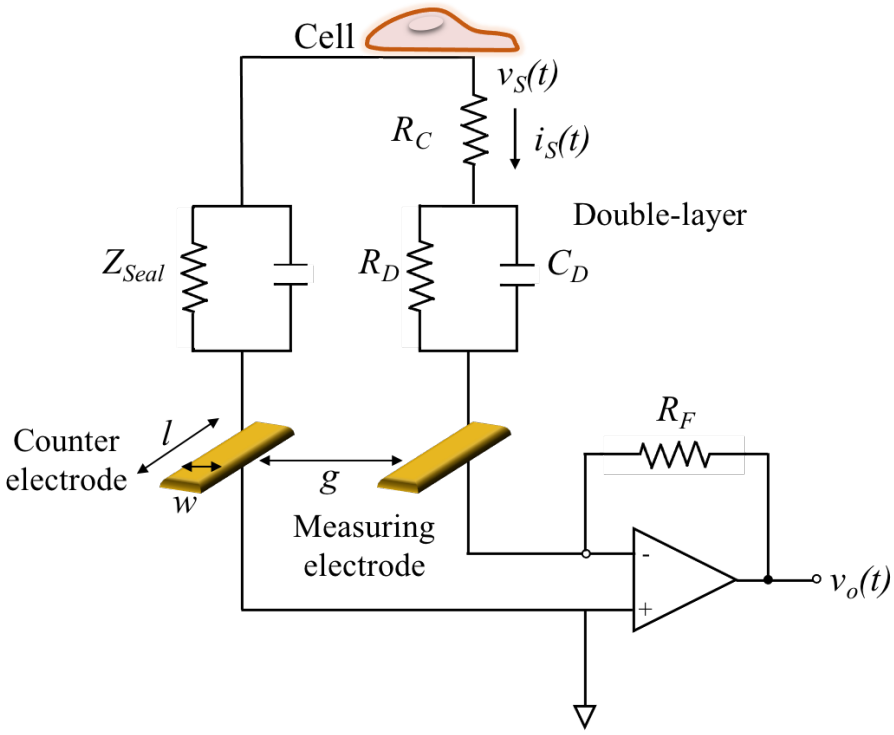

Figure 3.3 Schematic diagram of equivalent circuit model to describe the electrical coupling of a bioelectrical signal to the measuring circuit. The cell signal is $i_s(t)$. Adapted from a study by Medeiros et al.[2]

In order to understand the role of resistance and capacitance in the definition of the signal shape, it is important to analyse the current flowing through the equivalent circuit that describes the electrode/electrolyte interface.

Our measurements set up we use a trans-impedance amplifier, whose output voltage is given by[2]:

$$v_o(t) = -R_F i_s\,(t) \qquad (3.1)$$

where R_F is the feedback resistance an $i_s(t)$ the current flowing through the measuring electrode impedance. When a single square voltage pulse is applied to the device, the current $i_s(t)$ that flows through the system consists of two components, one is the displacement current through C_D, and the other is a steady state current flowing through R_D:

$$i_S(t) = C_D \frac{dv_C(t)}{d_t} + \frac{v_C(t)}{R_D} \qquad (3.2)$$

and then,

$$v_s(t) = \left(\frac{v_C(t)}{R_D} + C_D \frac{dv_C(t)}{dt}\right) R_C + v_C(t) \qquad (3.3)$$

This equation can be rearranged as:

$$\frac{dv_C}{dt} + \frac{(R_D + R_C)v_C(t)}{R_D R_C C_D} = \frac{v_S(t)}{R_C C_D} \qquad (3.4)$$

Considering a particular solution of Equation (3.4), when is a voltage ramp rising at a constant rate m i.e., then the solution of Equation (3.4) yields:

$$v_C(t) = k\left[t - \tau\left(1 - e^{-t/\tau}\right)\right] \qquad (3.5)$$

where,

$$k = \frac{R_D m}{R_D + R_C} \qquad (3.6)$$

and

$$\tau = \frac{R_D R_C C_D}{R_D + R_C} = C_D(R_C // R_D) \qquad (3.7)$$

t is the time constant for the device to be charged or discharged. The electrical current through the circuit can now be readily calculated by replacing Eq. (3.5) into Eq. (3.2) as:

$$i_s(t) = \frac{kt}{R_D} + \frac{k\tau}{R_C}\left(1 - e^{-t/\tau}\right) \qquad (3.8)$$

Since $R_D \gg R_C$, the time constant for the device is $\tau \cong R_C C_D$. In this limit the current is given by,

$$i_s(t) \cong \frac{mt}{R_D} + mC_D\left(1 - e^{-t/t}\right) \qquad (3.9)$$

$i_s(t)$ signal is the sum of two independent terms, a component proportional $v_s(t) = mt$ and a transient term with a peak amplitude proportional to the product mC_D that decays with a time constant $t \cong R_C C_D$. C_D acts as a multiplying factor for the current. If voltage signal changes rapidly (with large m) produce large transient displacement current across the capacitor. Under these conditions, the measured current signal shape is also proportional to m, the derivative of the original signal $v_s(t)$[2].

3.5 The importance of the electrode impedance

The amplitude of the noise generated by electrodes is controlled by the capacitance and resistance of the double-layer region[75]. To measure extracellular signals in the range of a few Hz (f < 1Hz), electrodes must possess certain key characteristics. These include low resistance to minimize thermal noise and improve signal-to-noise ratio, as well as a low impedance path for slow varying signals[92]. The RC circuits that describe the interface and bulk layer of the electrode are effectively in series and provide an electrical equivalent for the two-layer system[87]. The RC model considers the high interfacial capacitance (C_D) and typically also a high interfacial resistance (R_D). The dimensions and design of electrodes play a crucial role in achieving high-performance measurements. The resistance of the electrode depends essentially on the geometrical parameters of the electrodes, such as the active area and the distance between them. By carefully optimizing the design of electrodes, it is possible to achieve a high SNR.

The signals recorded depend on the noise generated by the electrodes and how this noise is coupled to the front-end amplifier. Electrodes impedance (capacitance and resistance)

and their frequency dependence has to be evaluated. Based on schematic representation of double-layer circuit in Figure 3.4 (a) without cells, the high impedance double-layers appear effectively in series with the low impedance electrolyte layer described by the resistance R_S and the capacitance C_S. The parallel circuit RC network is shown in Figure 3.4 (b). This circuit generates input noise, but also changes the overall system performance of the current amplifier.

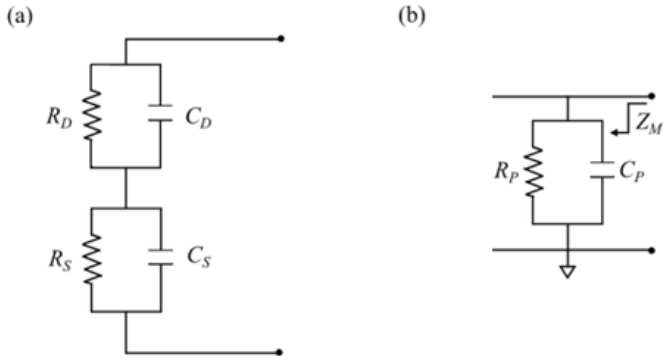

Figure 3.4 Equivalent RC circuit that describes the cell/electrolyte interface. (a) Double-layer circuit without cells; (b) Double-layer circuit showing the interface cell/electrolyte. Adapted from Medeiros et al.[2]

The series of the two double-layer network will have an equivalent resistance (R_P) and capacitance (C_P) that are measured externally using an impedance analyser. The equivalent admittance Y_T of the series-parallel network is given by:

$$Y_T = \frac{1}{R_P} + j\omega C_P \tag{3.10}$$

where R_P (ω) and C_P are the total parallel resistance and capacitance, respectively given by:

$$C_P(\omega) = \frac{R^2{}_D C_D + R^2{}_S C_S + \omega^2 R^2{}_D R^2{}_S C_D C_S (C_D + C_S)}{(R_D + R_S)^2 + \omega^2 R^2{}_D R^2{}_S C_D C_S (C_D + C_S)^2} \tag{3.11}$$

$$R_P(\omega) = \frac{(R_D + R_S)^2 + \omega^2 R^2{}_D R^2{}_S C_D C_S (C_D + C_S)}{R_D + R_S + \omega^2 R_S R_D (R_D C^2{}_D + R_S C^2{}_D)} \tag{3.12}$$

To estimate the frequency response of the capacitance and *loss* (where $loss=1/\omega R$), the above equations can be used. With the following equation, Eq. (3.13), it becomes clear the higher the resistance R_P smaller is the thermal noise when measured in current:

$$S_P(\omega) = 4kTRe\{Y_P(\omega)\} = \frac{4kT}{R_P(\omega)}\left[\frac{A^2}{Hz}\right] \qquad (3.13)$$

where k the Boltzmann constant and T the absolute temperature. From the frequency dependence of the R_P, it is possible to predict that the electrode current noise contribution will be minimized at low frequencies.

3.6 Fundamental aspects of noise in electrophysiological systems

To measure the ultra-weak electrical fluctuations generated by the cells at very low frequencies, it is important to reduce the electrical noise of the sensing electrodes. This noise is controlled by Helmholtz interfacial layer. The noise measured depends on the electrode impedance parameters and the measuring bandwidth.

The noise sources considered are the thermal current noise, generated by the amplifier feedback resistor R_F and by R_P, and the noise, generated by amplifier. For a state of art amplifier with low current and voltage input noises the dominant noise source is the thermal noise, which is inversely proportional to R_P. According to Medeiros et al.[2] thermal noise generated by R_P is low at low frequencies and increases for high frequencies. The input mentioned amplifier noise reflected in the access of the equivalent electrodes circuit is only appropriate for amplifiers with high input voltage noise. The low noise performance at low frequencies in current amplification contrasts with traditional voltage measurements where noise dominates at low frequencies. The electrode contributes to the noise by adding thermal noise proportional to R_P and by shaping and multiplying by a factor of R^2_P at low frequencies the amplifier current noise.

In order to reduce the electrode noise, when using voltage amplifiers, the electrode impedance must be small.

3.7 Conclusions

In this chapter the equivalent circuit model and electrophysiological measurement method to record extracellular signals is explained.

The voltage fluctuations generated by cells induce a large displacement current that can be easily amplified by the capacitance of the double layer, making current detection an effective signal detection mode. Additionally, a high capacitance is also desirable for voltage detection mode because it lowers the impedance seen by the bioelectrical signal. However, considerations regarding the resistance value differ depending on the signal detection mode.

In current detection, the fundamental thermal noise decreases with increasing resistance, making a high interfacial resistance desirable. In contrast, in voltage detection mode, the thermal noise increases with interfacial resistance, so a lower resistance is preferable. Overall, while a high interfacial capacitance is always desirable, the optimal resistance value depends on the signal detection mode used.

CHAPTER 4

Experimental procedures and cell cultures

"Those who can imagine anything can create the impossible." Alan Turing

This chapter describes the instrumentation and the cell cultures used in this thesis. Details about electrode geometries and materials are also provided. Cell handling and characterization procedures are also described together with the main cell lines used.

4.1 Introduction

The purpose of this chapter is to provide the reader basic knowledge about the experimental procedures and methods adopted in this thesis. The methods cover two main areas, (i) electrical measurements and (ii) biological assays. The electrical measurements used were electrophysiology, electrical noise and electrochemical impedance techniques. The electrodes are an important component of all electrical measurements. Therefore, this chapter also describes the types of electrodes used (geometry and materials) as well as the techniques used to characterize the electrode impedance. As referred in Chapter 2, MEA technology is used to measure the bioelectrical activity in the range of kHz, particularly action potentials generated by neurons. Nevertheless, these electrodes present limitations regarding to the measurement of non-electrogenic cells, which activity is at low frequencies. As MEAs are incapable to measure low-frequency signals produced by non-electrogenic cells, here is present a methodology to measure slow and weak signals produced by non-electrogenic cells using extracellular electrodes. These electrodes are suitable to measure at low frequencies the cooperative activity of non-electrogenic cells with an improvement of the signal-to-noise ratio (SNR). Due to the large size of electrodes, it is necessary to measure a population of cells, which is equally exciting because it allows us to measure the intercellular communication and synchronization dynamics. Figure 4.1 shows a schematic representation of the different types of assays carried out in this thesis and explained in this chapter, including methods to handle cell cultures, electrical measurements, and data analysis procedures.

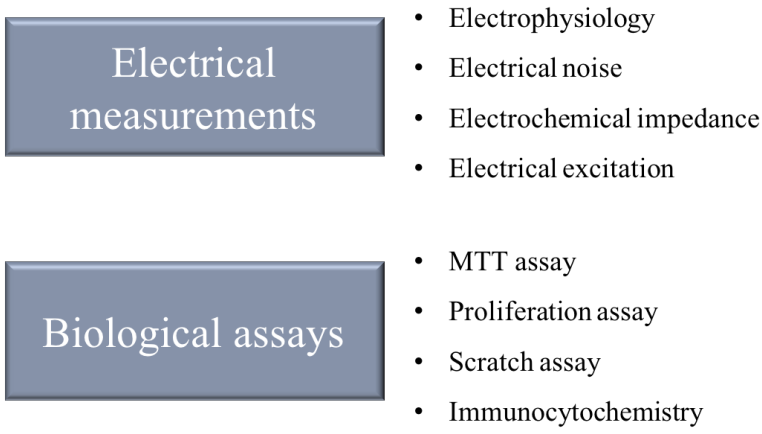

Figure 4.1 Block diagram outlining the two types of measurements used in this thesis to characterize biological cells and the sensing electrodes.

This chapter is organized as follows: it begins by describing the experimental setup for electrophysiological measurements. Particular emphasis is put on the role of the electrodes in the signal quality. Electrophysiological measurements are complemented with information about cell confluence and cell adhesion. This information about cell confluence and adhesion is obtained by impedance measurements. The instrumentation used to perform impedance and how impedance-based measurements are used to monitor cell adhesion and cell attachment are described. The electrical measurements are complemented by a basic description several of biological essays, which provide information about cell viability, proliferation and biological process namely the scratch assay, proliferation assay, and immunocytochemistry. Finally, a list of the basic properties of the cell lines used is also described.

4.2 Electrical measurements and experimental set-up

The sensing electrode can be connected to several electrical instruments. The electrical instrumentation includes low-noise voltage or current amplifiers, an electrical impedance measuring instrument, and a signal generator to excite the cells with well-defined electrical pulses. All instruments are controlled by microcomputer through a dedicated software. Figure 4.2 provides an overall view of all the instrumentation that can be connected to the sensing electrodes to obtain information about the bioelectrical activity and about the adhesion and proliferation of the cells.

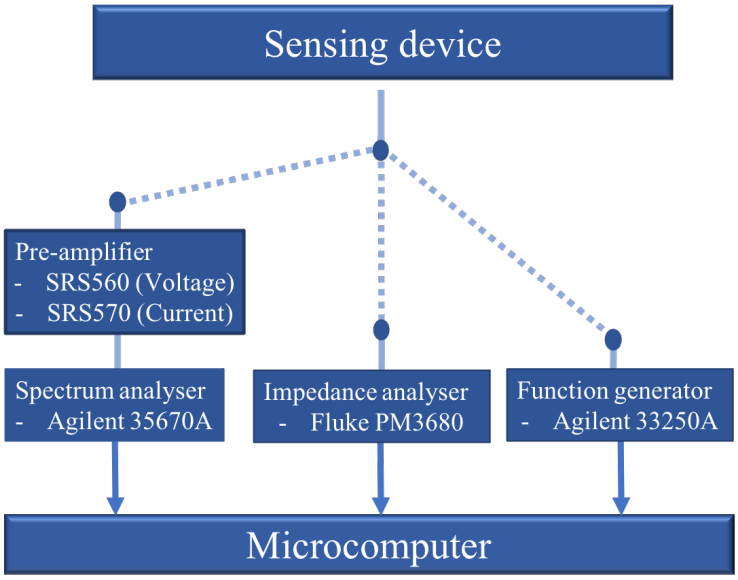

Figure 4.2 Schematic diagram of the electrical instrumentation that can be connected to the sensing device to perform a variety of measurements.

The entire measuring system together with the incubator was kept inside a large iron box (Faraday cage) with an electrical ground to shield external sources of electrical noise and interference. Figure 4.3 shows a photograph of all the experimental setup. A humidified incubator at 37 ºC and 5% CO_2 (ThermoScientific, Midi 40), RCL meter (Fluke PM 6306), signal generator (Agilent), dynamic signal analyser (35670 A, Agilent) and a low-noise voltage amplifier (SR 560, Stanford Research), all equipment is inside of a Faraday cage.

Figure 4.3 Photograph of the experimental set-up used for electrophysiological measurements. The photo shows the view of the instruments placed inside the Faraday cage. The cell incubator, a dynamic signal analyser and a low noise voltage amplifier.

4.2.1 Sensing Electrodes

Several types of electrodes fabricated with different materials and with different geometrical designs were evaluated for electrophysiological sensing. Fig. 4.4 provides schematics of the three major electrode geometries used: (i) square, (ii) round, and (iii) interdigitated type electrodes. In addition, mushroom-like electrodes were also used. Table 4.1 presents the geometry and the physical dimensions of the electrodes used. In the following section, the features of each electrode are described in detail.

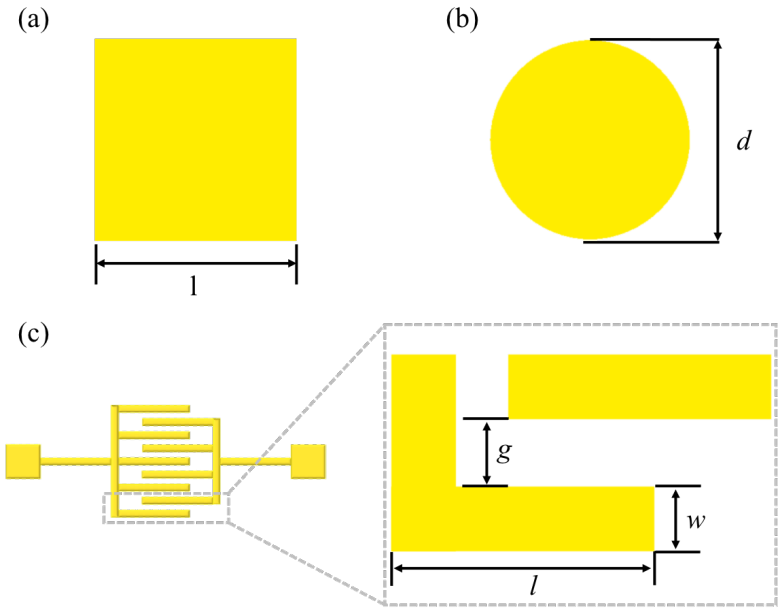

Figure 4.4 Types of electrode geometries used. (a) square geometry; (b) circular electrodes; (c) Interdigitated electrodes; *g* is defined as the gap distance between fingers, *w* the width of an individual finger and *l* the length of an individual finger.

Table 4.1 – Geometry and the area of the sensing electrodes used.

Electrode type	**Geometry**	**Nº of fingers**	**Length *l* (µm)**	**Width *w* (µm)**	**Gap *g* (µm)**	**Diameter *d* (µm)**	**Area (A_{el}) (μm^2)**
Microstructured Gold mushroom	Square	----	2000	2000	----	----	$4x10^6$
Philips	Interdigitated	5	1000	5	10	----	$50x10^3$
IBIDI 8WE1	Circular	1	----	----	----	250	$49.1x10^3$
IBIDI 8W10E+	Circular	40	----	----	----	250	$1\text{-}96x10^6$
IBIDI 8WID	Interdigitated	5	3.3254	100	325	----	$1.6x10^6$
PEDOT:PSS	Planar	2	5000	500	500	----	5×10^6

(a) Microstructured electrodes (gold mushroom-like)

Microstructured electrodes were used to increase the active sensing surface without increasing the device's physical area. These devices were used in Chapter 5 to measure a population of astrocytes. Microstructured electrodes were fabricated at the

University of Porto, Department of Physics and Astronomy, by Mónica Cerquido, a researcher in the group of Prof. João Ventura. For more detailed information about the fabrication methods, the reader should refer to the reference[93]. The total active area of these electrodes is 4 mm^2.

Microstructured gold mushroom-shape connection electrode arrays together with electrical connections are represented in Figure 4.5. Figure 4.5 (b) is a schematic representation of the sensing device with electrical connections, and Figure 4.5 (c) is a photograph of assembled sensing device together in a vessel to support the structured the cell culture medium.

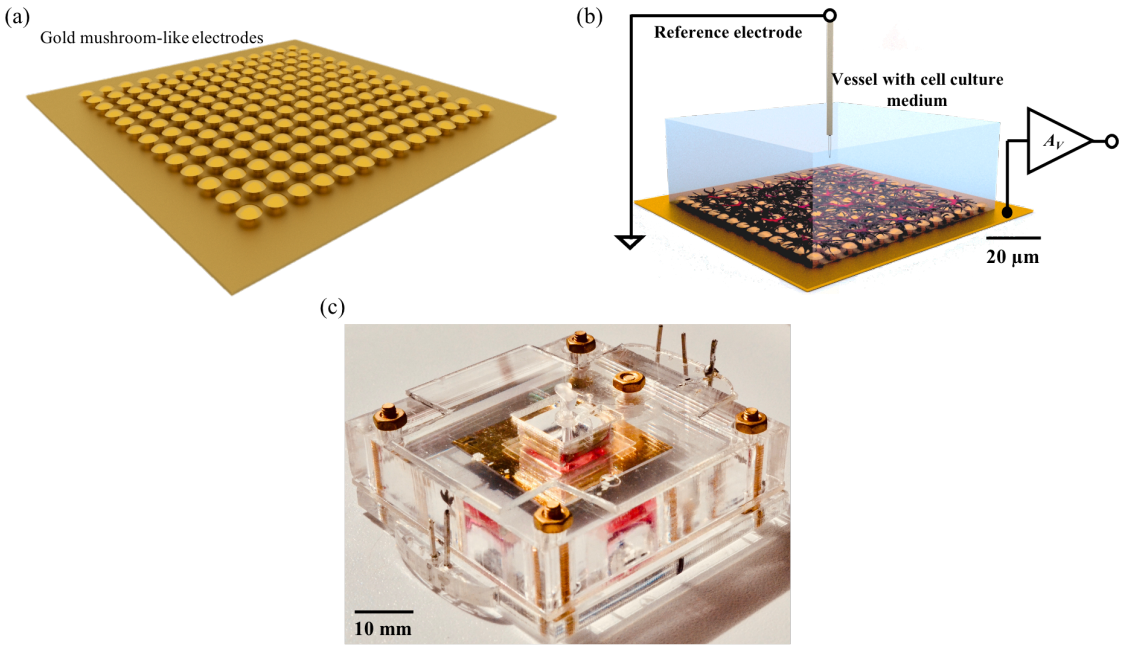

Figure 4.5 Schematic representation of a microstructed electrode surface with an array of gold mushroom-like shapes. (a) Schematic representation of gold mushroom-like electrode; (b) schematic representation of gold mushroom-like electrode with electrical connections; (c) photograph of the electrode assembled in a vessel to support cell culture medium.

(b) Interdigitated planar electrodes

Interdigitated sensing electrodes involve two co-planar, parallel gold tracks on the upper surface of a thermally oxidized silicon wafer. Gold electrodes were deposited by thermal evaporation. The electrode design and the chip holder are represented in Fig. 4.6. Each microelectrode has a total number of 10 interdigitated fingers and each finger has a length (l) of 1000 µm, a 5 µm width (w) separated by 10 µm gap (g). The relation of these parameters with the electrode geometry is shown in Fig. 4.4. The total active sensing area

is 150.000 μm^2. These devices were provided by PHILIPS Research labs in Eindhoven (Netherlands). On top of the interdigitated electrodes, a compartment is attached and can be filled with cells and culture medium. The well is loosely covered with a lid to prevent evaporation of the medium. The system assures the presence of enough cell culture medium to keep the cells viable over more than 24 h without medium change. Figure 4.6 (a) shows a schematic representation of the electrode and Figure 4.6 (b) shows a photograph of the sensing electrode assembled in a container with electrical connections.

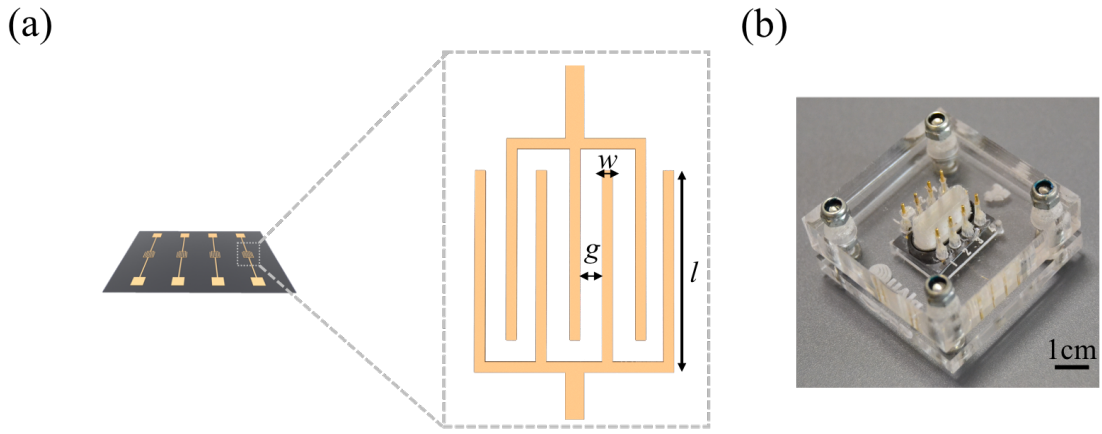

Figure 4.6 Philip device with interdigitated gold electrodes. (a) Schematic representation of gold interdigitated device; (b) Photograph of sensing device complete connected to a device holder for electrical connections.

(c) Planar gold electrodes – Sensing device IBIDI

Sensing electrodes were purchased from Applied Biophysics (NY, USA). The sensing device was comprised of a patterned comprised of eight gold electrodes on a polycarbonate (PET) substrate. The photoresist overlayer insulates the rest of the electrode. The underlying gold layout connects the separated area to the measuring chamber. Each sensing device has eight separated and individual wells to permit multiple individual assays simultaneously, as shown in Figure 4.7 (d). Each chamber has a substrate electrode 0.8, cm^2, and we used a single, centrally located circular 250 μm diameter electrode (Fig.4.7 (a)), ten circular 250 μm diameter electrodes (Fig.4.7 (b)) and finally interdigitated electrodes (Fig.4.7 (c)). In Fig. 4.7 (a), the individual circular electrode is used to detect and record the electrical activity, as the cells migrated from the surrounding area onto the round central sensing electrode. The ten circular electrodes are normally used for attachment and proliferation assays, a schematic representation of these

electrodes is in Fig. 4.7 (b). The device which uses ten electrodes has also a large counter-electrode located at a distance of 75 µm from the sensing electrode.

Impedance measurements were carried out by measuring the capacitance and the electrode between the small sensing electrode and the large counter-electrode. In especially (c), interdigitated devices were used to measure the electrophysiological activity of cells, specially, traveling waves. A photograph of the entire device with the well to support the cell culture medium is shown in Figure 4.7 (d).

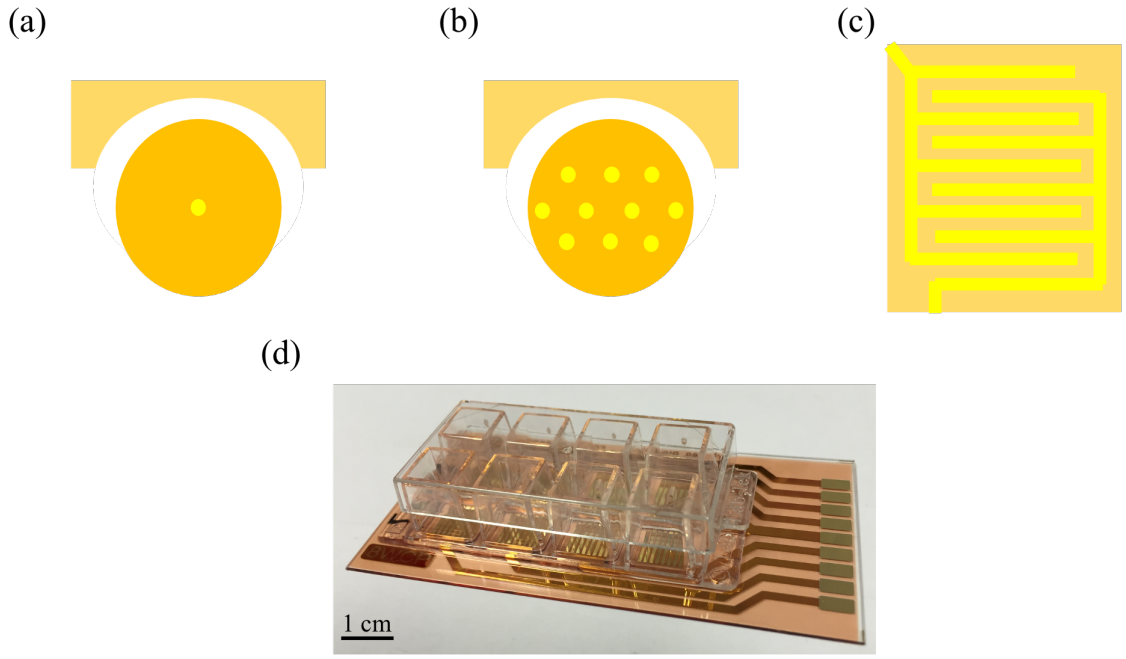

Figure 4.7 IBIDI device with 8 separated wells. (a) Schematic representation of circular electrodes; (b) sensing electrode comprise of 10 small sensing areas; (c) schematic representation of an interdigitated electrode; (d) photograph of device complete.

4.2.2 Electrophysiological instrumentation

Bioelectrical signal detection can be performed in voltage detection mode or in current detection mode. In this thesis, both methods were explored. For voltage detection a low-voltage signal amplifier was used the SRS 560 (Stanford Research Systems, California), and for current detection, a trans-impedance signal analyser the SRS 570 (Stanford Research Systems, California), was used. The amplified bioelectrical signal is converted to a digital signal by an Agilent 35670A Dynamic Signal Analyzer (Agilent, United States). The signal analyser is controlled by dedicated software that visualizes and stores the data. Instruments are connected to a computer with a specific program for data

acquisition. The sensing electrodes were kept inside the incubator and the real measuring system was operating inside a large iron box with an electrical ground to shield external sources of electrical noise and interference.

4.2.3 Electrical stimulation

Electrical stimulation was performed by using a signal generator or by using the internal signal generator of the ECIS Model Z Theta® instrument. Here, we describe the procedures used to make a clean wound in a commercially available electrode designed for studying cell migration.

To induce a wound in the cell population using a voltage sine wave, a specific protocol was followed. A 2 V peak-to-peak sine wave with a frequency of 40 kHz was applied for 5 seconds. This procedure was carefully optimized to be used in a 250 microns diameter round electrode.

Current is the relevant parameter that destroys the cell membrane. When we use an external voltage source from a signal generator, it is important to estimate how much current is applied to the sensing electrode. This current is in reality the displacement current (i_{dis}) defined according to the equation:

$$i_{dis}(t) = C_D \frac{dv_i(t)}{d_t} \tag{4.1}$$

where C_D is the electrical double-layer capacitance and $v_i(t)$ the waveform used, and t is the time.

Therefore, to estimate the current necessary to destroy the cell membranes and kill the cells, we should be taken into account the values of rise time ($\frac{dv_i(t)}{d_t}$), and the value of C_D.

The ECIS Model Z Theta® (Applied Biophysics, USA) instrument was also used to create electrical wounds in cell populations. The procedure to adopted depends on the electrode area and cell type. For an electrode with an area of 250 μm of diameter, Applied Physics company recommends applying a train of current pulses reaching 1.2 mA with a frequency 4 kHz for 10 seconds. The cell membranes were disrupted by the high current

pulses and the cells sitting on top of the electrode die. The protocol was modified for HDF cells. For these cells, the protocol was a train of current pulses with an amplitude of 800 μA at 4 kHz applied for 20 seconds.

4.2.3.1 Minimization of the electrical noise and interferences

Measurement of the weak signals generated by non-electrogenic cells at low frequencies requires a high signal-to-noise ratio. To achieve this, it is crucial to minimize the electrical noise generated by associated instrumentation as well as any interference from external sources. Several strategies were employed to achieve this goal. Firstly, battery-operated amplifiers were utilized to reduce the noise induced by the power line. Secondly, to minimize external noise sources such as electromagnetic radiation and operation of nearby electrical equipment, the entire experimental setup was enclosed within a Faraday cage with a dedicated ground.

To reduce the effects of building vibrations, which are also in the millihertz frequency band, the sensing devices were placed into metallic enclosures (box) that were mechanically decoupled from the Faraday cage. The Faraday cage itself was also situated on top of a soft material that attenuates vibrations originating from the building.

The main sources of electrical noise are thermal noise generated by resistive components of our sensing electrode and $1/f$ or pink noise, originating from electrochemical processes occurring at the electrical double-layer. The noise generated by amplifiers is usually much lower than that of the sensing electrode, therefore, the strategies to lower the intrinsic noise sources should be placed on the sensing device.

4.2.4 Data acquisition

The signal analyser is operated through a custom program developed by a colleague in our group, Pedro Inácio. The program, called Remote Control software (*RC software*), facilitates data transfer between the signal analyser and computer, and allows the user to adjust the electrical settings for signal recording. These settings include bandwidth, number of data points, amplifier gain, and the type of filter used. A photograph of the *RC software*'s user interface is shown in Figure 4.8.

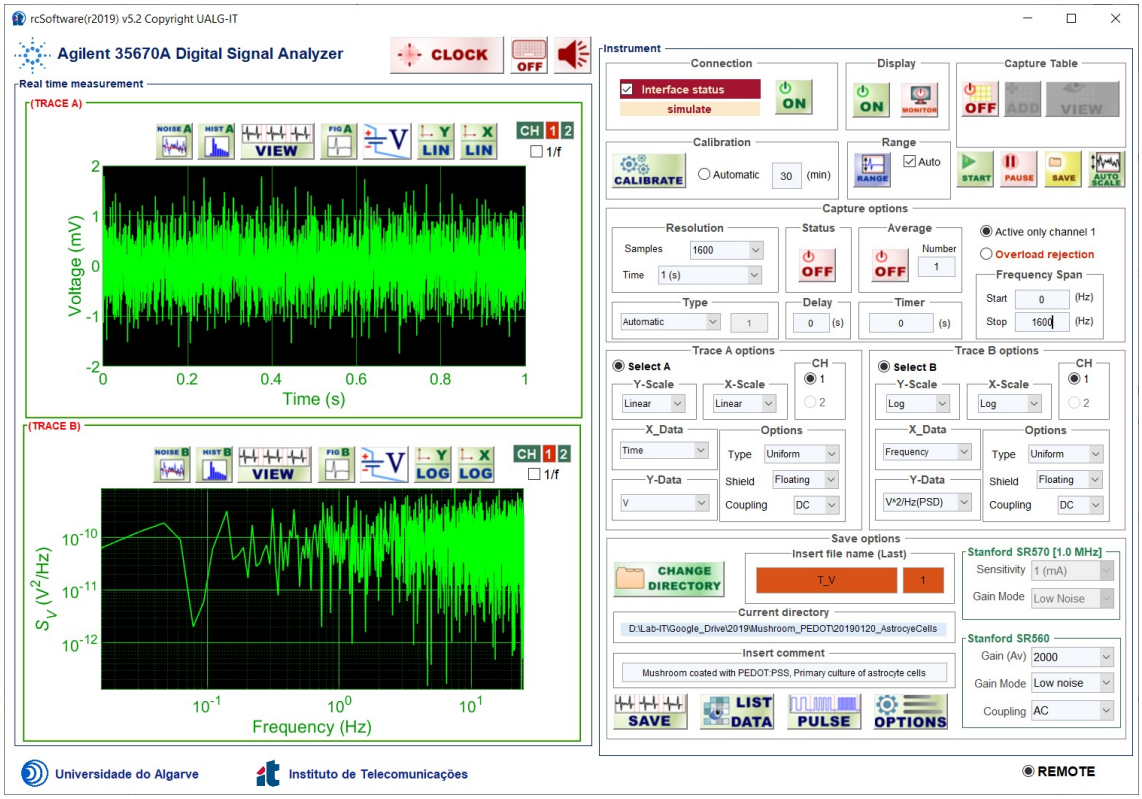

Figure 4.8 User interface of the *RC software* used in this thesis.

We characterized the electrical noise of the electrodes across the full spectral range of our instrumentation, which spans from 0.01 Hz to 1 MHz. To obtain a complete spectrum, we combined various observation windows, as detailed in Table 2. By specifying the number of data points for each window, we set up the instrumentation for the desired resolution. In this thesis we primarily measured non-electrogenic cells, our measurements were largely focused on lower frequencies. We typically used a 64 s or 128 s observation window. Table 4.2 lists all available observation windows and their corresponding bandwidths

Table 4.2 – Frequency range table of data acquisition time window.

Time window	*Frequency range*				
	Number of samples	**200**	**400**	**800**	**1600**
	f_{start}	f_{stop}	f_{stop}	f_{stop}	f_{stop}
1024 s	0.977 mHz	195 mHz	390.6 mHz	781.25 mHz	1.5625 Hz
512 s	1.95 mHz	390.6 mHz	781.25 mHz	1.5625 Hz	3.125 Hz
256 s	3.906 mHz	781.25 mHz	1.5625 Hz	3.125 Hz	6.25 Hz
128 s	7.8125 mHz	1.5625 Hz	3.125 Hz	6.25 Hz	12.5 Hz
64 s	15.625 mHz	3.125 Hz	6.25 Hz	12.5 Hz	25 Hz
32 s	31.25 mHz	6.25 Hz	12.5 Hz	25 Hz	50 Hz
16 s	62.5 mHz	12.5 Hz	25 Hz	50 Hz	100 Hz
8 s	125 mHz	25 Hz	50 Hz	100 Hz	200 Hz
4 s	250 mHz	50 Hz	100 Hz	200 Hz	400 Hz
2 s	500 mHz	100 Hz	200 Hz	400 Hz	800 Hz
1 s	1 Hz	200 Hz	400 Hz	800 Hz	1.6 kHz
500 ms	2 Hz	400 Hz	800 Hz	1.6 kHz	3.2 kHz
250 ms	4 Hz	800 Hz	1.6 kHz	3.2 kHz	6.4 kHz
125 ms	8 Hz	1.6 kHz	3.2 kHz	6.4 kHz	12.8 kHz
62.5 ms	16 Hz	3.2 kHz	6.4 kHz	12.8 kHz	25.6 kHz
31.25 ms	32 Hz	6.4 kHz	12.8 kHz	25.6 kHz	51.2 kHz
15.625 ms	64 Hz	12.8 kHz	25.6 kHz	51.2 kHz	102.4 kHz
7.8125 ms	128 Hz	25.6 kHz	51.2 kHz	102.4 kHz	
3.90625 ms	256 Hz	51.2 kHz	102.4 kHz		

4.2.5 Electric Cell-substrate Impedance Sensing (ECIS)

In this thesis, we utilized two distinct impedance analysers. A resistance-capacitance layer (RCL) meter (Fluke PM 6306) and an ECIS Model Z Theta® (Applied Biophysics, USA). Photographs of both instruments can be found in Figure 4.9. The PM6303 can measure impedance across a frequency range of 50 Hz to 1 MHz, while the ECIS Model Z Theta® has a range of 62.5 Hz to 64 kHz. Both instruments were utilized to record the impedance changes that occurred during our cell migration experiments. The ECIS model can also apply well defined current pulses to make an electrical wound in the cell cultures as described above.

(a) (b)

Figure 4.9 Photograph of both impedance system used. (a) Photo of the RCL impedance analyser Fluke PM3680 with the associated instrumentation. (b) Photo of the ECIS Z-Theta system couplet to ECIS station.

4.3 Biological set-up and protocols

In this thesis, both immortalized cell lines and primary cell cultures were employed. Various companies, such as the American Type Culture Collection (ATCC) and Cell Biology Collection, have developed and adapted different cell types for use in research. Immortalized cell lines are genetically manipulated and enable the study of spontaneous and chemically or electrically evoked activity. These cell lines allow for the development of new therapies, vaccines, and early diagnostics for various diseases, as well as the investigation of gene functions, drug metabolism and cytotoxicity, and antibody production. The use of immortal cell lines provides several advantages, including the avoidance of ethical issues associated with the use of animal tissue and the ability to obtain consistent and reproducible results from pure cell populations. They are also easy to use, cost-effective, and offer an unlimited supply of material.

However, it is important to maintain these immortal cell lines as closely as possible to primary cells, as genetic manipulation can lead to changes in their characteristics over time. Additionally, immortal cell lines can become contaminated with other cell lines or mycoplasma, which can affect the results of experiments [94]. Despite these potential issues, the benefits of utilizing immortalized cell lines in research far outweigh the drawbacks.

4.3.1 Cell lines

In this thesis, commercially available immortal cell lines C6, provided from American Type Culture Collection (ATCC), was used to investigate the electrical cellular behaviour of glioblastoma multiforme tumours. Additionally, BJ-5ta and HDF cells were used to study fibroblast cell migration and their response to steroids. The healthy tissue of the precursor of glioblastoma multiforme tumour was examined through primary cultured astrocytes. Finally, a biopsy-derived human high-grade glioma was cultivated. For a detailed overview of the immortal cell lines and primary cell cultures used in this thesis, please refer to Table 4.3 and Table 4.4, respectively.

The use of immortalized cell lines presents several advantages and between them are the fact that they are well-characterized and intensively used in many laboratories. Their characteristics are well defined and represent genetically identical characteristics of their original tissue, so the results are reproducible. Primary cells cultures are cells that were directly isolated from the original tissue and kept their original characteristics (morphological and functional) and genetic expression. However, primary cultures could have, even in small percentage, the contamination of other cell types from the surrounding tissue. One common feature between all cells chosen is the fact that all of them are non-electrogenic cells.

The mediums used were Kaighn's Modification of Ham's F-12 Medium (F12-K Medium) (Sigma-Aldrich, Germany), Dulbecco's Modified Eagle Medium (DMEM) (Sigma-Aldrich, Germany) and M199 Modified Medium (M199) (Sigma-Aldrich, Germany). All immortal cell lines were provided from American Type Culture Collection (ATCC® CRL-4001™, USA) with exception of HDF cell that are from Evercyte GmbH (Wien, Austria), and were maintained in an incubator at 37°C with a humidified atmosphere of 5% CO_2 (Thermo Scientific, Midi 40).

For electrical measurements, the cells were cultivated in cell culture plates and diluted in cell culture medium to yield cell suspensions with a known cell density, usually 250.000 cells/cm^2, and transferred to the sensing devices. Cells were cultured onto the electrodes for 2 hours before any measurements were performed. Before cell deposition, the devices were exposed to ultraviolet (UV) treatment, and the electrodes were coated with poly-L-lysine to promote cell adhesion.

Table 4.3 – Cell lines used for experimental assays in this thesis.

Cell code	Organism	Tissue	Cell type	Disease	Supplemented medium
C6	Rat	Brain	Glial cells	Glioma	F-12K medium; 15% fetal horse serum; 2.5% fetal bovine serum; 1% penicillin and streptomycin.
BJ-5ta	*Homo sapiens*, male human	Foreskin	Fibroblast immortalized with hTERT	Normal	- 4 parts of DMEM with 4 mM L-glutamine, 4.5 g/L glucose and 1.5 g/L sodium bicarbonate; - 1 part of Medium 199 with 0.01 hygromycin B and 10% fetal bovine serum; 1% penicillin and streptomycin
HDF	*Homo sapiens,* **adult female human,**	Skin	Fibroblast	Normal	DMEM and F12 medium (1:1) 10% fetal bovine serum; antibiotic G418 100 µg/mL
U87	*Homo sapiens,* adult female human	Brain	Epithelial	Glioblastoma	DMEM medium 10% fetal bovine serum; 1% penicillin and streptomycin

Table 4.4 – Primary cell cultures used for experimental assays.

Cell code	Organism	Tissue	Cell type	Supplemented medium
Primary cultured astrocytes	Mice	Cortex, brain	Glial cells	DMEM and F12 medium (1:1) 10% fetal bovine serum; 0.25% gentamicin and 0.25 ng/mL M-CSF
NHDF	*Homo sapiens,* juvenile dermis human	Skin	Fibroblast	DMEM medium 10 % fetal bovine serum; 0.1 % penicillin and streptomycin; 1:100 amphotericin B solution
Primary High-grade glioma HOPE	*Homo sapiens, human*	Brain	High grade glioma	DMEM medium 10% fetal bovine serum; 1% penicillin and streptomycin

Figure 4.10 shows photographs of some immortal cell lines used, cultured on petri dishes. Figure 4.10 (a) is a microphotograph of C6 glioma cells, Figure 4.10 (b) is a microphotograph skin fibroblast, BJ-5ta cell line and on Figure 4.10 (c) fibroblasts HDF cell line is shown. These photographs were taken using the microscope Zeiss Axiovert 200 Microscope (Zeiss, Oberkochen, Germany) with a VisiCam® PRO 20C (VWR, Radnor, Pennsylvania).

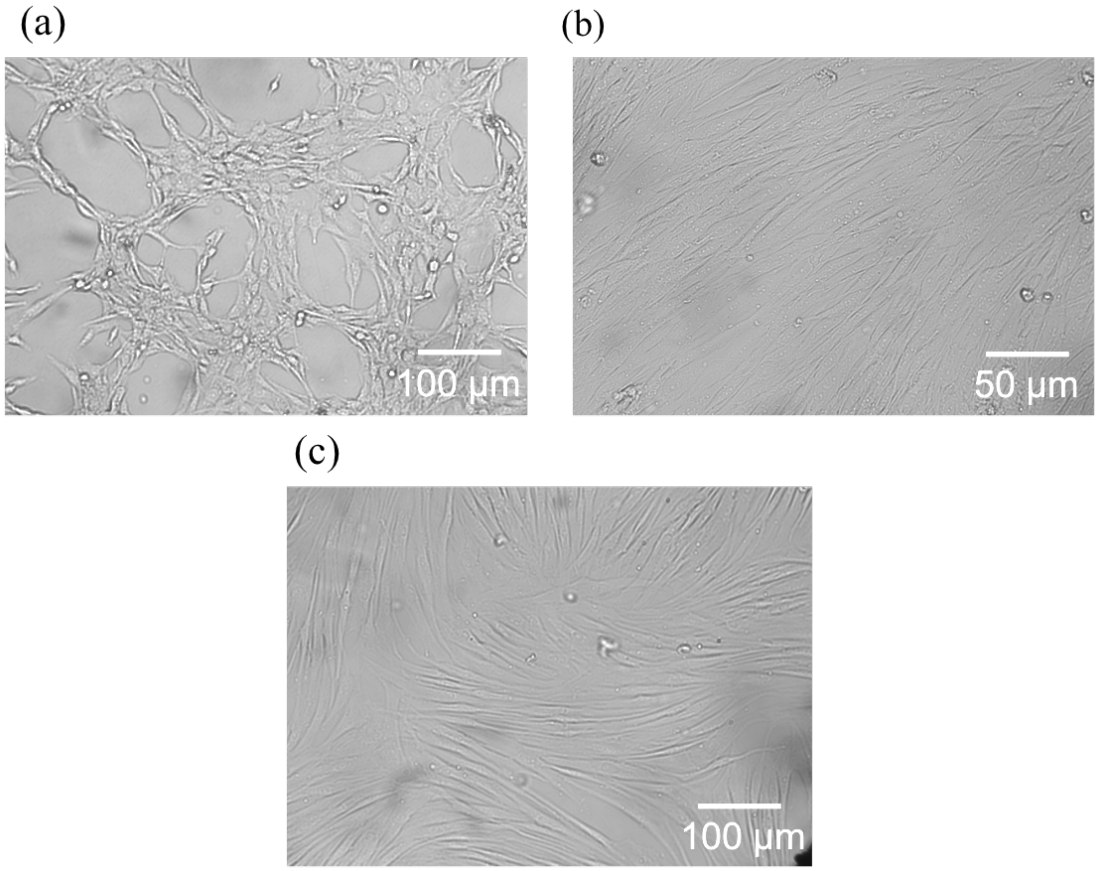

Figure 4.10 a) Photograph of rat C6 glioma population (b) Photograph of a BJ-5ta cell line; (c) Photograph of a HDF cell line. All the photos were taken when the cells populations adherent to a Petri dish.

4.3.2 Biological assays

Several complementary biological techniques were used in this thesis to complement and often to validate the electrical measurements. Well establish techniques were performed and are described in follow.

4.3.2.1 Proliferation assay

Proliferation assay is a method to quantify the cell density on a particular surface. For this assay, the cells were firstly cultured in a 96 well plate with three replicates. For eight days, microphotographs of the wells were taken to count the cells. The cells to be photographed were daily fixed with 70% of Ethanol and dyed with DAPI (300 nM). The microphotographs were taken using the microscope with 4x amplitude and four photographs were acquired of each time to guarantee that all well were present in the microphotograph. The microscope used was Zeiss Axiovert 200 Microscope (Zeiss,

Oberkochen, Germany) with a VisiCam® PRO 20C (VWR, Radnor, Pennsylvania). Regarding microphotographs process, the final image, resulting from the four photographs token, was mounted in Photoshop® program. To count the cells ImageJ® software was used with grid tool. From the entire well, sixteen squares (blue grid in Figure 13) were selected in four different regions (yellow grid in Figure 4.11) and the cells dyed with DAPI were counted using the tool grid in ImageJ® program. After achieved the number of cells in each yellow grid on Figure 4.11, an average number was calculated and the estimative for the entire well calculated. By knowing the total area of the well of 96 well plate, which is 0.32 cm^2, and the total area of the four regions selected, 0.06 cm^2 (16 squares), the average number of cells per well were calculated. This process was repeated daily for seven days. Then, a graphic was built in function of time with the increasing number of cells.

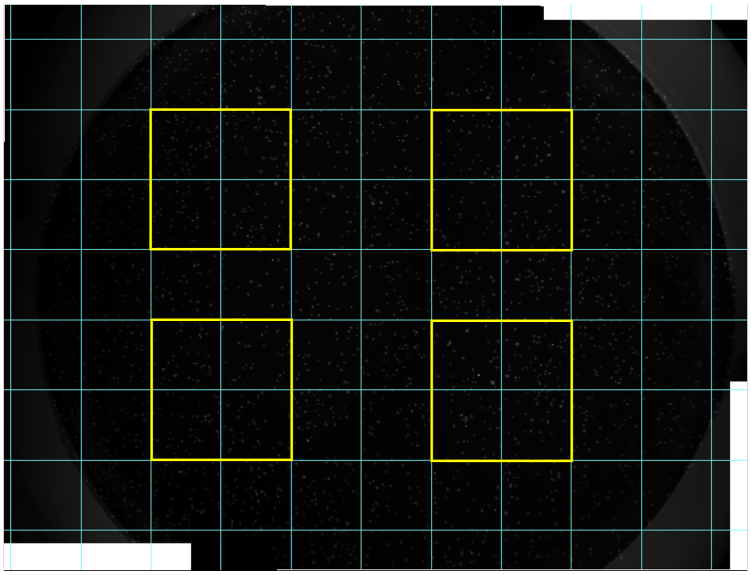

Figure 4.11 Representation of methodology to count the cells on ImageJ software. Four different selected areas, yellow grid, are counted and the total number of cells are calculated.

4.3.2.2 MTT assay

The MTT assay is a colorimetric assay for assessing cell metabolic activity. MTT (3-(4,5-Dimethylthiazol 2-yl)-2,5-diphenyltetrazolium bromide) was firstly developed by Mosmann in the 1980's[95]. This assay is a very powerful tool to measure cell proliferation/viability, drug cytotoxicity, and mitochondrial/metabolic activity of cells [96]. In viable cells, MTT can pass through cell membrane and then through mitochondrial inner membrane and being finally reduced to formazan (purple formazan crystal). Formazan crystals can be measured by absorbance and cell viability can be calculated.

For this thesis, MTT kit was used (Sigma-Aldrich, Taufkirchen, Germany). 7,500 cells were cultured in each well of a 96 well plate (Sarstedt, Nümbrecht, Germany) with four replicates. MTT 12 mM in sterile PBS protected from light was added for 4h at 37 ºC in light absent, and replaced by DMSO (Sigma-Aldrich, Germany), which was resuspended several times and was left for 1h at 37ºC. Absorbance was measured at 540 nm in a plate reader Infinite M200x (Tecan Trading AG, Switzerland). The cell viability was calculated using the following equation:

$$\frac{\text{Sample value} - \text{Average of negative control}}{\text{Average of positive control} - \text{Average of negative control}} * 100 \quad (4.2)$$

4.3.2.3 Wound scratch assay

Wound scratch assay *in vitro* is often used in biology since it is a model of wound repair *in vivo*, so it is a useful, easy, low-cost and well-developed technique. Wound scratch assay can also be used to assess the activity of endocrine factors on skin repair.

In order to create a wound, cells were cultured in a 24 well tissue culture plates (Sarstedt, Nümbrecht, Germany) with specific cell culture medium at a predictable density and after reaching 95%-100% confluency. When confluency was reached, in a gently and a slowly way, several scratches were made in different wells, directly into the monolayer. For that, a 2-200 μL plastic micropipette tip was used. Then, in a gently way, cells were washed twice with fresh cell culture medium to remove the detached cells and fresh medium was added. Fresh medium should be supplement with components that may be involved in migration. Wound healing should be monitored by microscopes and images should be captured. For this thesis the microscope used was Zeiss Axiovert 200 Microscope (Zeiss, Oberkochen, Germany) with a VisiCam® PRO 20C (VWR, Radnor, Pennsylvania). After recorded all images, the area of empty spaces is calculated with ImajeJ® software. Then, the percentage of recovery area in function of time is calculated, as represented in schematics of Figure 4.12. Wound scratch assay was used in Chapter 6.

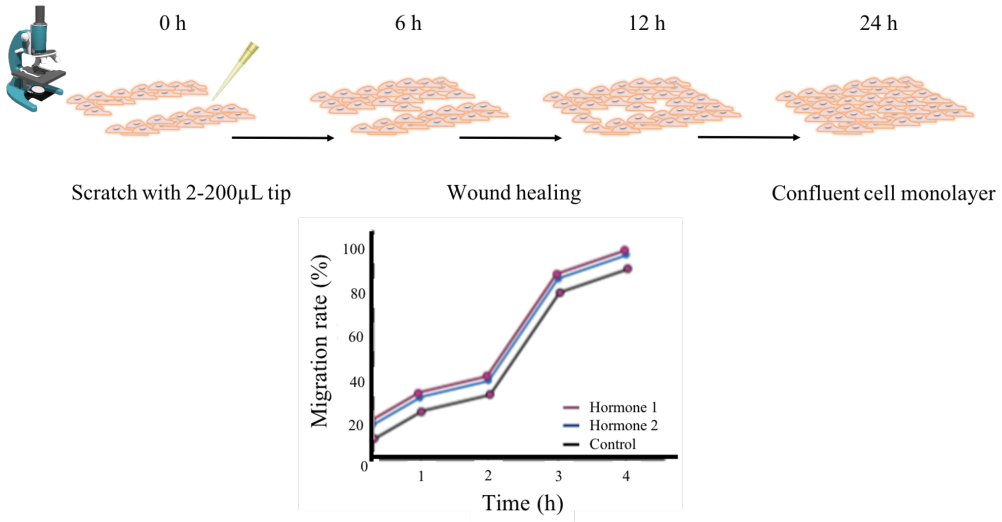

Figure 4.12 Schematic representation of wound scratch assay used to represent wound healing. Different stages separated by hours (0h, 6h, 12 and 24h) from the initial open wound until the wound had fully healed. On bottom is a schematic representation showing the time course of wound recovery, with the x-axis representing the time evolution and the y-axis representing the percentage of wound closure.

4.3.2.4 Immunocytochemistry assay

Immunocytochemistry (ICC) is a technique that uses antibodies for detection and localization of cellular proteins and other antigens within single cells. By using ICC, it is possible to detect the cytoskeleton (actin filaments, tubulins), cell connections (tight junctions (TJs), gap junctions (GJs), adherent junctions), mitochondria, cellular membrane and desmosome[97]. ICC is a very sensitive, low-cost method that has several applications, and it is used in two different fields, scientific research and as a complementary tool for diagnosis. ICC can be used as a diagnosis and prognosis tool of some neoplasias and some subtyping of neoplasias or autoimmune diseases. Further, ICC can be used for the research of prognostic and therapeutics of diseases, helping with the diagnostic[98]. In most cases, cells are fixed and permeabilized, blocked, and incubated with a primary and a fluorescent-labelled second antibody. Nevertheless, fluorescent could limit the quality of samples further than limitation in resolution, noise and optical aberrations, which are the dependency on the deposition of energy into the biological specimen and the use of exogenous fluorescence probes can affect both cellular structure and function[97].

Figure 4.13 shows a schematic representation of an ICC assay. Firstly, a monolayer of cells is cultured in a 24 well plate (Sarstedt, Nümbrecht, Germany) in 250 µm diameter

glass fiber. When 95%-100% confluency is reached, a scratch with a 2-200 µL plastic micropipette tip is made. And then, the cells are washed to removed death cells and fixed with paraformaldehyde (PFA) 4% solution during 15 minutes at room temperature (RT) and washed twice. After that, cells are permeabilized with Triton X-100/PBS (1x) for 15 minutes at RT and then, washed twice with PBS 1x. After, cells were incubated with 3% of BSA/PBS solution for 60 minutes at RT and washed twice with phosphate buffered saline without Ca^{2+} and Mg^{2+}. Forwarding this, primary antibodies or dyes are incubated. Incubation time and temperature of exposure of antibodies and dye are specifically described in Tables 4.5, 4.6 and 4.7. Between incubation, cells should be washed with PBS. Finally, mounting medium is added to a lamina and coverslip is added. Images were captured using Axioimager Z2 microscope and HRm camera (Zeiss, Oberkochen, Germany), as shown in Figure 4.13 C. Specific immunocytochemistry used are described in each chapter.

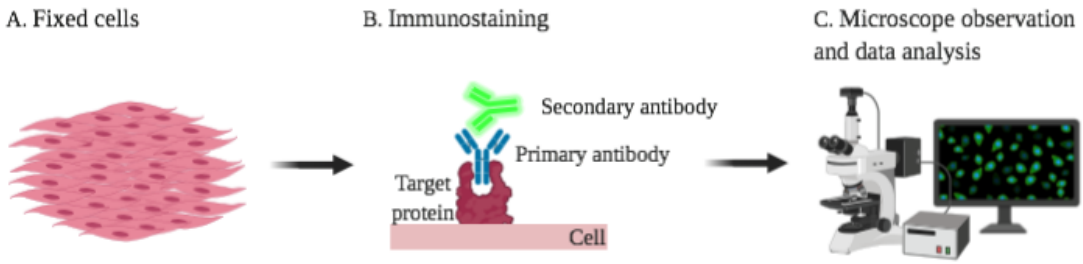

Figure 4.13 Schematic representation of ICC assay. (A) cells are fixed and permeabilized; (B). Immunostaining with primary and secondary antibody; (C). Microscope and data analysis. Schematics were created using BioRender.com.

Table 4.5 – Characteristics of incubation and concentration of primary antibodies.

Primary Antibodies		
Antibody	**Incubation**	**Concentration**
Monoclonal anti-alpha tubulin produced in mouse clone DM1a	1h RT or 4ºC ON	1:500
ZO-1 Monoclonal Antibody (RL90), Host Mouse/IgG2a	1h RT	1:500
Connexin 43 monoclonal antibody (CX-1B1)	4ºC ON	1:200

Table 4.6 – Characteristics of incubation and concentration of secondary antibodies.

Secondary Antibodies		
Antibody	**Incubation**	**Concentration**
Alexa fluor 488 goat anti mouse IgG (H+L)	1h RT	1:1000

Table 4.7 – Characteristics of incubation and concentration of dyes.

Dyes		
Dye	**Incubation**	**Concentration**
Texas Red-X Phalloidin	20 min RT	5μL from 200 μL
MitoTracker™ Deep Red FM – special Packaging	20 min 37ºC	50 nM (conf)
Wheat Germ Agglutinin, Alexa Fluor™ 488 Conjugate	15 min 37ºC	2.5μg/mL (conf)

4.4 Conclusions

This chapter provides a comprehensive overview of the experimental arrangement and procedures utilized to measure the bioelectrical activity of cells, as well as the biological procedures employed. The entire set-up is described in detail, including the specific sensing electrodes used and all electronic equipment employed for electrophysiology measurements. Additionally, the process of creating an electrical wound is explained, as well as the inherent electrical noise and its limitations.

The software used to monitor and record data acquisition, created by my colleague Pedro Inácio, is also described. Finally, this chapter provides a comprehensive description of all cells utilized in this thesis and outlines the biological assays employed to evaluate their properties.

CHAPTER 5

Extracellular devices to measure the electrophysiological activity of astrocytes populations

"Science never solves a problem without creating ten more." George Bernard Shaw

This chapter presents an electrical technique for measuring the electrophysiological activity of primary cultured astrocytes isolated from a rat cerebral cortex with extracellular electrodes. Two distinct types of electrodes were used in this study: a microstructured mushroom-like shaped electrode and a planar electrode. The results demonstrate quasi-periodic signals of electrophysiological behaviour, indicating synchronization of the activity across a population of astrocytes. Both spontaneous and evoked activity were observed.

5.1 Introduction

Substrate integrated planar microelectrode arrays (MEAs)[99–101] are considered the standard electrophysiological methodology for long-term analysis of *in vitro* neuronal cells and networks. MEA technology provides spatial resolution, multi-unit electrical recordings and a mean for the electrical stimulation of neuronal cells. Currently, available MEA electrodes have areas typically below 1,000 μm^2 and generate a thermal noise in the range of 5–20 μV. This intrinsic noise defines the system detection limit. In voltage measurements, the electrode thermal noise is inversely proportional to the surface area. Increasing the area of the electrodes causes an increase in sensitivity due to the reduction in noise and impedance. However, as the area increases the ability to discriminate between individual cell signals is impaired. To circumvent this trade-of between electrode sensitivity and spatial resolution several laboratories have started to develop structured electrodes. These emergent electrodes make use of vertical micro or nano-structures[48,102] coated, namely, with carbon nanotubes[50–52], or conducting polymers[53,55,58–62,103–105], which provide a softer and more roughened surface. The strategy behind these approaches is to increase the effective area and to promote a more intimate interaction of the electrode with cells. A well-known example is the use of micron size gold mushroom-like shapes[64,106]. It has been shown that cells engulf the protruding gold mushroom-like shapes, lowering the impedance and improving the electrical coupling between the cells and the electrode. Such micro-structured electrodes have been optimized to record action potentials. However, there is some less known electrical activity produced by cells and organs with important physiological/functional roles. This activity generates weak and long-lasting electrical perturbations that propagate through the extracellular milieu[106]. They are caused by ions, polar molecules or zwitterions that can pass from cell to cell by gap junctions. These fluctuations are steady or slow changing gradients, and they progress thousands of times more slowly than action potentials. This activity does not show spikes but smooth signals that can change over a period of time, from several seconds to minutes, and often are a result of cell cooperative phenomena. Astrocytes are cells that generate such type of long-lasting signals. Patch clamp recordings and optical fluorescence methods have revealed interesting functional electrical properties in astrocytes but these mechanisms are not yet fully understood[107–111]. Although MEA technology has not been

optimized to record long lasting signals produced by astrocytes, there are few studies reporting astrocyte activity using MEAs. In a study by Wanke E. *et al.*[112], spike trains and glial responses were simultaneously captured from individual sensing electrodes. Also using MEAs Fleischer *et al.*[113] reported that astrocytes can be electrically stimulated and were shown to exhibited extracellular voltage fluctuations in a broad frequency spectrum (100–600Hz). Ultra-weak signals[114] and noisy electrical fluctuations generated by populations of glioma cells were also reported[2,115,116]. The strategy enabling the observation of these weak signals exploits large capacitive electrodes with a low intrinsic thermal noise. In this contribution we demonstrate the potential of this ultra-sensitive electrical method, together with a micro-structured electrode surface, to measure extracellular ionic fluctuations in primary cultures of astrocytes. Comparatively to a typical MEA electrode, our sensing electrodes are few thousand times larger generating a thermal noise of 0.3 μV in the frequency window of 0.1 to 12.5Hz. Although lacking spatial resolution, these electrodes provide unique conditions to capture the signals related to synchronization and cooperative dynamics produced by astrocytes. Herein, we start by presenting the devices, the cells and the electrical methods used. Strategies to achieve an extracellular sensing electrode with a high sensitivity are discussed within the framework of an equivalent circuit of the cell/substrate interface. Then the intrinsic noise spectral characteristics of the electrodes are presented and discussed. The signal detection limit at a particular frequency is determined. The performance of flat bare gold electrodes is also compared with surfaces covered with a matrix of gold mushroom-like micro-structures. The additional increase in capacitance, as well as the corresponding decrease in resistance introduced by the micro-patterned surface, is quantified. Next, the use of micro-structured electrodes to record spontaneous activity generated by a primary culture of astrocytes is reported and the recorded signals are compared and validated with signals measured using optical fluorescence methods, reported by others.

The use of interdigitated electrodes has yielded interesting signal patterns with both amplitude and frequency modulation. These signal modulation patterns are tentatively explained by considering synchronized cell clusters or cell subpopulations. The amplitude modulation can be attributed to an increase in the number of synchronized cells over time, while the frequency modulation can be explained by the simultaneous occurrence of two

or more clusters that are individually synchronized, but out of phase with neighbouring clusters.

Finally, the relevance of the findings and their implications in the development of a tool to study slow and weak electrophysiological events are discussed.

5.2 Methods and materials

5.2.1 Microstructured gold electrodes

To produce the gold mushroom-shaped microelectrode arrays, a thin layer of Cr (3 nm)/Au (40 nm) was first deposited on top of a silicon wafer (Si/SiO_2) using magnetron sputtering. Then, Direct Write lithography (μPG 101 tool, Heidelberg Instruments; UV 400 nm, W=10 mW @ 17%) was used to expose a mask constituted by 2.0 μm dots (in diameter) disposed in a square array (2 mm x 2 mm) with a lattice spacing of 10 μm. The samples were developed in a Microposit 351 solution for 60 s. Gold mushroom arrays were then obtained by electroplating inside the opened holes using a three-electrode configuration where Ag/AgCl was the reference electrode and a gold solution (Orosene E+4gr/lt, for Italgalvano s.p.a.) under −1 V for 70 minutes at room temperature. This procedure led to a stalk height of 1.4 μm, a total mushroom height of 2.4 μm and a cap diameter of 3.8 μm. The stalk of the fabricated gold mushrooms is also seen to vary with the height, due to the profile induced on the photoresist during exposure.

5.2.2 Interdigitated planar gold microelectrode

Interdigitated microelectrodes on the top of oxidized silicon wafers were explored as sensing devices. Each wafer has four devices with different inter-electrode distances. The silicon wafer on the top surface is thermally oxidized (SiO_2). The transducer is an interdigitated microelectrode array (Philips Innovation Services, Eindhoven, The Netherlands) fabricated on thermally oxidized Si wafers 150mm in diameter. The oxide is 200 nm thick and can be used to couple alternative current (AC) signals to the cells. The Au microelectrode arrays have 1000 μm length (l), and separated by a gap (g) of

10 μm and each finger has a width (*w*) of 5 μm. Further details about the device are provided in Chapter 4.

5.2.3 Animals

C57Bl6/J mice were kept in our animal facility, with controlled temperature (21±1 °C) and humidity (55%), with food and water *ad libitum* in a 12 h dark/light cycle. The experiments were performed in accordance with institutional and European guidelines (2010/63/EU) for the care and use of laboratory animals. Both the Portuguese law (DL 113/2013) and the European law (directive 2010/63/EU) state that obtaining tissue for cell cultures without actually performing any procedures in a laboratory animal, as is the case in this paper, does not beg an official approval from the competent authority (Direcção Geral de Alimentação e Veterinária, DGAV), since no procedures are performed (the law understands that a procedure is the equivalent of provoking discomfort in an animal similar to a needle piercing the skin), only that the process of sacrificing animals is performed by a licensed user. Since the cultures are prepared from tissues extracted from animals euthanized by a licensed experimenter and the animals were kept in our licensed animal house facility, we stated that we performed the study according to the instituted guidelines both locally at our institute and by law.

5.2.4 Primary astrocytes cultures

Primary mixed glial cultures were obtained from new-born C57Bl6/J mice with 0–3 days[117]. Briefly, after decapitation the brains were removed, and the meninges and cerebellum were discarded. Brain tissue was then mechanically dissociated and enzymatically digested (0.1% trypsin and 0.001% DNase I, 20 min at 37 °C). Cells were seeded in 25 cm^2 or 75 cm^2 flasks coated with poly-L-lysine, at a density of 0.2x106 cells/cm^2 and cultured in D-MEM/F12 with GlutaMAXTM-I supplemented with 10% fetal bovine serum, 0.25% gentamicin and 0.25 ng/ml M-CSF, at 37 °C and 95% air/ 5% CO_2 in a humidified incubator. Culture medium was replaced every 4 days and confluency was achieved after 15 days *in vitro*. Microglia and oligodendrocyte precursor cells were removed by vigorous shaking resulting in astrocytes culture purity of approximately 98%. After detachment of microglia cells, astrocytes were trypsinized (0.25%, 20 minutes at 37 °C) and seeded on the electronic devices. An aliquot of

200,000 cells per cm^2 was transferred to the well and was placed in an incubator (Termo Scientifc, Midi 40). Prior to cell deposition, the micro-structured electrodes were exposed to UV treatment and the electrodes were coated with poly-L-lysine to promote cell adhesion. The cells were maintained at 37 °C in an incubator with a humidified atmosphere with 5% of CO_2. The system assures the presence of enough cell culture medium to keep the cells viable over more than 24 hours without medium change. Cell numbers and viability were assessed using a Neubauer chamber-based trypan blue live/dead exclusion assay. Cells were incubated with D-MEM/F12 with GlutaMAXTM-I, supplemented with 10.0 mM ethylene glycol-bis(β-aminoethyl ether)-N,N,N',N'-tetraacetic acid (EGTA). After 15 minutes, the EGTA medium was replaced with normal medium.

5.2.5 Device holder

The transducer is based on 4 mm^2 gold mushroom-shaped microelectrode arrays on a glass substrate. An acrylic vessel (see Fig. 5.1(c) and (d)) that could be filled with cells and cell culture medium was attached through an o-ring on top of the sensing gold substrate. A thin silver wire previously bleached to obtain an AgCl layer was used as the reference electrode. The vessel was loosely covered with a lid to prevent evaporation of the medium. After filling, the system was put into an incubator (Termo Scientifc, Midi 40). The total amount of medium supported by the holder is 1mL, although it was used 400 μL, which assures the presence of enough cell culture medium to keep the cells viable over more than 24 hours without medium change.

5.2.6 Electrical measurements

The experimental set-up was designed for ultrasensitive detection. External interference was minimized through the use of a Faraday cage and low noise cables. Extracellular voltage measurements were carried out using a low-noise voltage amplifier (SR 560, Stanford Research) and a dynamic signal analyser (35670A, Agilent). To minimize drift, the current amplifier is calibrated, and the set-up is stabilized for at least two hours before measuring. The current was recorded as a function of time by using zero bias on the electrodes. Small-signal impedance measurements were carried out using a

RCL meter Fluke PM 6306. Quasi-static measurements were carried out using a picometer/voltage source (Keithley 6487).

5.3. Results

In this section, we will first present the results obtained using microstructured electrodes. We will then present a detailed discussion of the signal modulation patterns recorded with a planar interdigitated gold electrode.

5.3.1 Description and characterization of the microstructured sensing electrodes

The basic structure of the microstructured sensing device together with the electrical connections and the cells is represented in Fig. 5.1. A schematic diagram of the gold mushroom-shaped electrode and the electrical connections to the voltage amplifier is represented in Fig. 5.1(a). Figure 5.1(b) shows a scanning electron microscopy photograph of the gold mushroom structured surface. The mushroom density is 4753 mushrooms per mm^2. A schematic diagram of the integration of the sensing electrode in an acrylic vessel is represented in Fig. 5.1(c) and a photograph of a real device is shown in Fig. 5.1(d). Measurements of the electrode impedance and electrical noise were first carried out to provide insight into the sensitivity of the electrodes and the advantages of using a micro-structured surface, in comparison with a fat gold electrode.

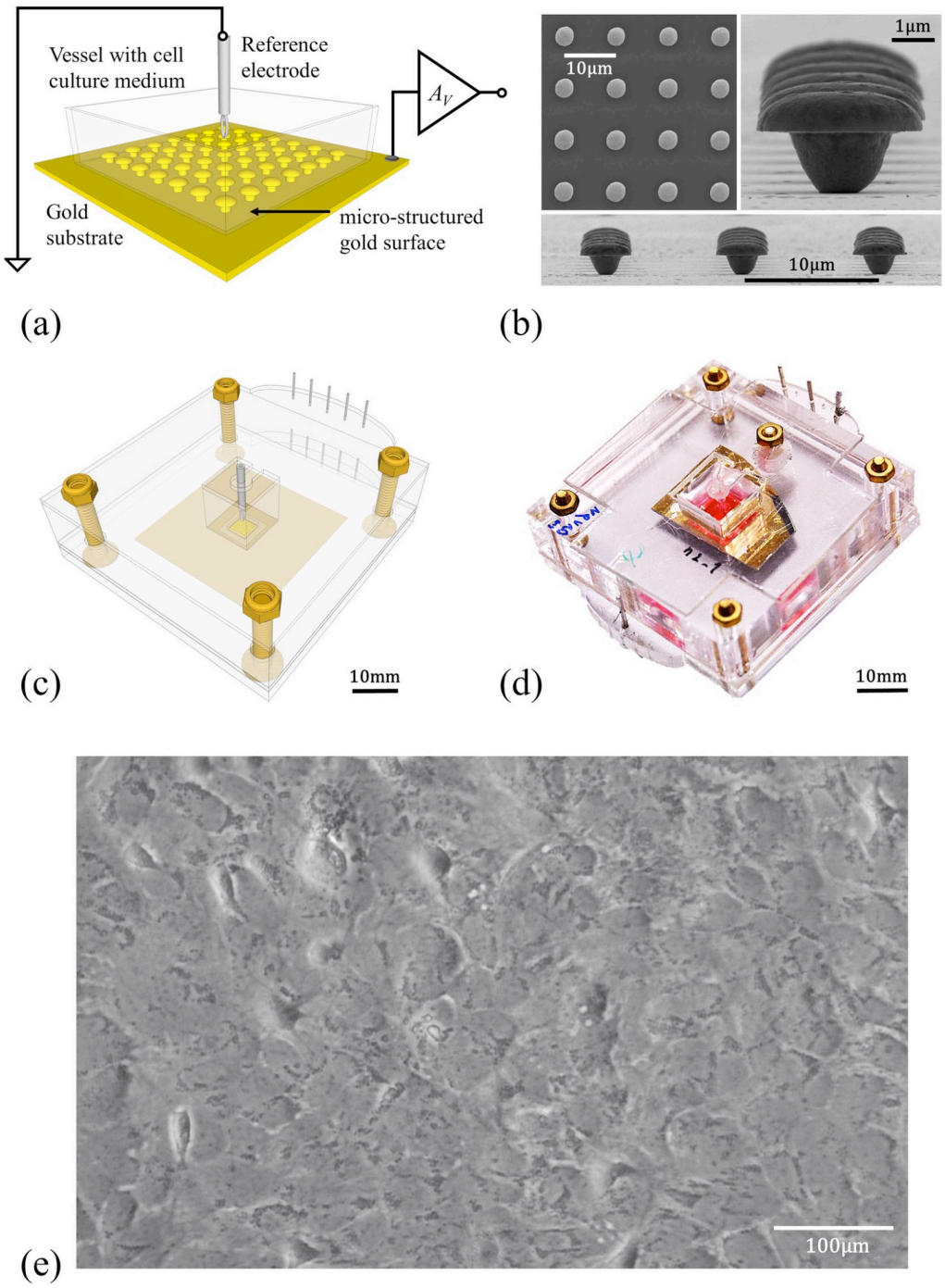

Figure 5.1 Sensing devices and cells used in this study. (a) Schematic diagram of the device, and electrical connections. (b) Scanning electron microscopy photographs of the gold mushroom-like structures. (c) Schematic view of the device holder. (d) Photograph of the complete sensing device. (e) Micrograph of a confluent population of astrocytes[3].

In order to understand how the information about the sensing electrodes is extracted we present and briefly discuss the equivalent circuit model used to represent the electrical coupling between the cells, the sensing electrode, and the amplifier. The equivalent circuit shown in Fig.5.2(a) embodies the electrical coupling between the cells and the electrode. The electrode in contact with an electrolyte is modelled as the parallel between a capacitor (C_D) and a resistor (R_D). This is the electrical double-layer established at metal/electrolyte interface known as Helmholtz-Gouy-Chapman double-layer. C_D models the extent to which the electrode is polarizable, and R_D takes into account the presence of Faradic currents. The parallel network of the double-layer appears in series with a spreading resistance (R_C), which models the signal loss due to the cell-electrode distance. Usually, R_C is very small and can be neglected. The other circuit component is the seal resistance (R_S), which models the cell adhesion to the electrode, the parasitic capacitance of the interface to the ground (C_P) and the amplifier input capacitance (C_{in}). This circuit is a simplified version of the standard model reported in literature[99,101,118]. The equivalent circuit described above allows us to understand how the signal generated by the cell is coupled to the electrode. In particular, it shows which electrode physical parameters have to be optimized to achieve signal detection with maximum SNR ratio. Assuming that the cells are adherent to the sensing electrodes, then R_C is very small, and R_S is high. From a technological point of view the parameters that we can optimize by adjusting the electrode design and materials are C_D and R_D. The signal generated by the cells is an AC signal that couples to the sensing electrode trough C_D. The higher is C_D the lower is the impedance and better is the electrical coupling between the cell and the sensing electrode. In the absence of electrochemical reactions, R_D only contributes to the intrinsic thermal noise. The noise generated by the sensing electrode is usually higher than the noise generated by the amplifier. Therefore, R_D defines the noise floor and determines the signal detection limit.

The design rules for R_D and C_D are dependent on the type of amplification used. Signals can be amplified as current or as voltage signals. The case of current amplification has been addressed in detail in a previous publication[119]. For current amplification the higher the value of R_D the lower is the thermal noise generated. In current amplification methods there is a trade-of between capacitance and resistance. The electrode area should be

increased up to a point where the corresponding decreasing in resistance starts to add thermal noise and counterbalance the benefits of a high capacitance.

In this contribution, we use voltage amplification. For this detection method, C_D should be maximized to lower the impedance and R_D should be low enough to generate a noise level below the noise generated by the voltage amplifier. The gold mushroom micro-structured surface allows us to maximize C_D and minimize R_D for a particular sensing area.

As pointed out by other authors[106], the microstructure also contributes to improve cell adhesion properties because the cells engulf the mushroom shapes and increase the seal resistance.

The power spectral density of the voltage noise, S_V, as a function of frequency, is shown in Fig. 5.2(b). We use 10 times series to obtain the averaged noise. The dashed lines represent the power-law behaviour for reference. The magnitude of the noise decreases with the frequency, and for frequencies higher than 1 kHz the noise becomes frequency-independent (white noise). For frequencies below 100 Hz, the noise follows a $1/f$ law that evolves for the lowest frequencies to a $1/f^2$ frequency dependency (flicker noise). This frequency dependence is typical of electrodes in electrolyte systems[120–122]. The $1/f$ power law agrees with the frequency dependence of the system's total resistance, R_P, (see Fig. 5.2(c)), confirming that the intrinsic thermal noise of the resistive elements dominates the electrical noise of the recording system.

The inset in Fig. 5.2(b) shows a short time trace of the noise measured in the frequency band of 0.1 to 12.5 Hz. The voltage noise is 0.3 μV peak-to-peak and determines the detection limit of our measuring system for signals in the frequency range of a 0.1–12.5 Hz.

In Fig. 5.2(d) we present a comparison of the frequency response of the individual impedance parameters capacitance (C_P) and resistance (R_P) of a bare flat gold electrode with a mushroom-covered surface. For convenience, the resistance (R_P) is represented as Loss ($L_P = 1/(\omega R_P)$). Both C_P and L_P are strongly frequency dependent.

This frequency dependence of the impedance has been extensively studied by us[2] and others[123] and was shown to be characterized by a Maxwell-Wagner dispersion, typical of electrodes immersed in electrolyte solutions.

In Fig. 5.2 (d) this dispersion is located at 10 kHz and corresponds to the frequency position of the peak in the Loss curve. The dispersion occurs because electrodes immersed in electrolyte solutions give rise to electrochemical double-layers with high capacitances (C_D) and high resistances (R_D). This interface layer appears in series with the rest of the electrolyte solution. When compared with the double-layer, the bulk region has a lower capacitance (C_B) as well as a lower bulk resistance (R_B). At low frequencies the high capacitance layer dominates, however, as the frequency increases the interfacial layer is progressively short-circuited and the low capacitive bulk layer starts to dominate the system response. The transition in frequency between the two layers is responsible for two capacitance plateaus shown in Fig. 5.2(d), one at low frequency and the other at high frequency. The values of C_P and L_P below the loss peak are related to the interfacial or double-layer region and the values above the relaxation peak are related to the bulk electrolyte solution. The relaxation frequency is mostly controlled by the bulk electrolyte resistance, R_B[2]. Both flat and micro-structured gold electrodes were immersed in the same electrolyte solution, and therefore, as expected, the relaxation frequency must have the same value for both systems, as confirmed by the data in Fig. 5. 2(d). The difference between the two electrodes is the surface topology; one surface is micro-structured and the other is flat. At 100 Hz, the micro-structured surface has a capacitance 30 nF higher than that of the flat surface. The corresponding double-layer resistance is also lower by 23 kΩ.

As shown in Fig. 5.2(d), neither C_P nor L_P reach steady state values at 100 Hz. Instead, they follow a trend to increasing values for lower frequencies. It is expected that the quasi-static capacitance (for f = 0 Hz) is significantly higher than the values measured at 100 Hz. The quasi-static values for C_D were obtained by measuring the displacement current i_D (t) in response to a slow voltage ramp dv/dt. The inset of Fig. 5.2 (d) shows the displacement current for flat and micro-structured surfaces. The quasi-static capacitance (*Csta*) is estimated to be 0.6 µF for flat gold electrode and 1.1 µF for the micro-structured gold electrode. This represents an increase of 54% in the quasi-static capacitance. As discussed above, the higher the capacitance the higher the electrical coupling of the signal to the electrode. Previously, we have reported that, in voltage detection methods, the SNR increases linearly with the capacitance[119]. Therefore, assuming that the number of cells

synchronized is constant, we would expect an increase in 54% in the SNR in comparison with a flat gold surface.

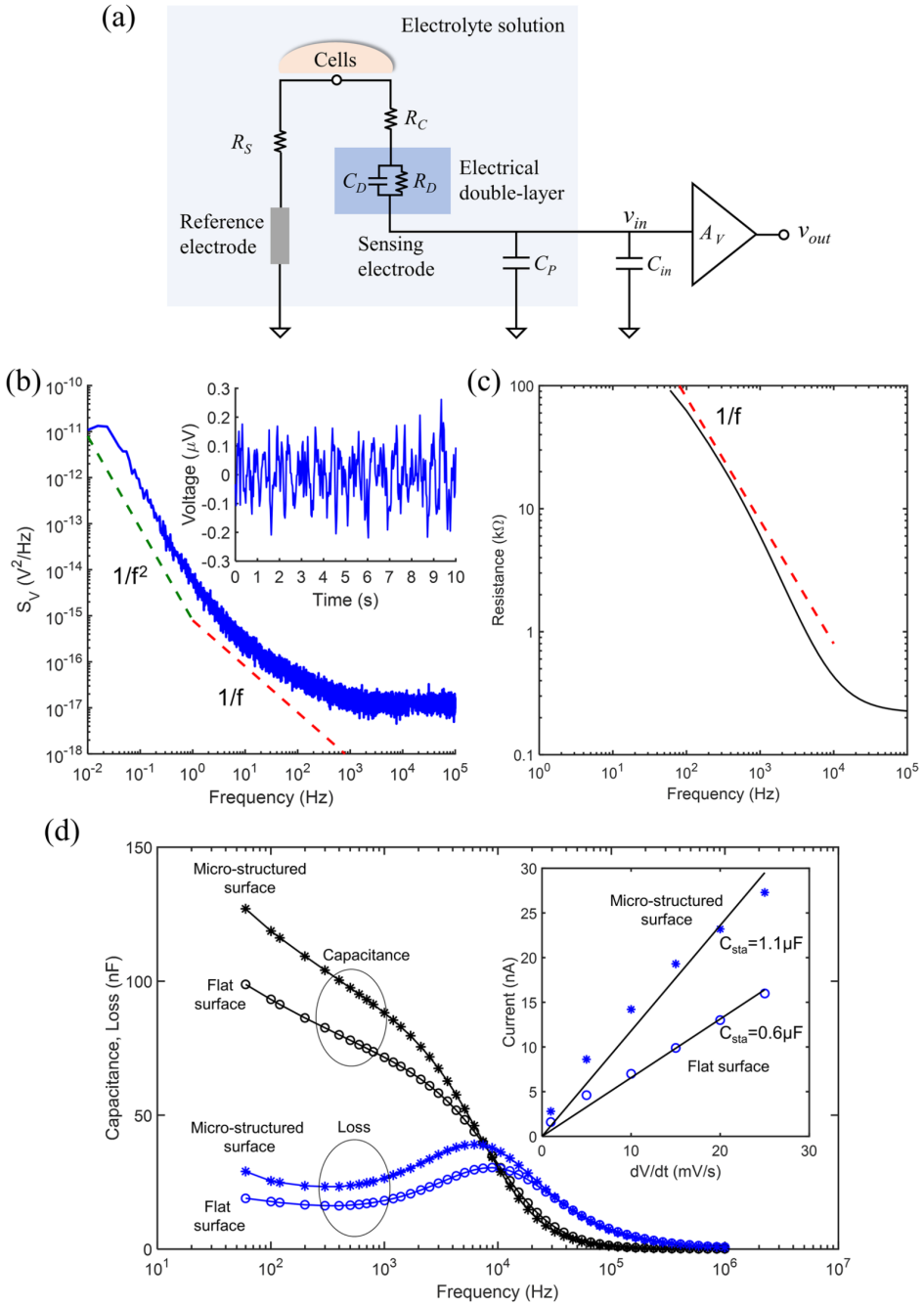

Figure 5.2 Electrical properties of the sensing electrodes. (**a**) Schematic diagram representing the electrical coupling between the cells and the measuring circuit. (**b**) Frequency dependence of the noise power density in voltage. (**c**) Frequency dependence of the total system resistance, *RP*. *SV* was measured by dividing the full frequency range (10^5 Hz) in several shorter ranges. The total smoothed power spectrum was obtained by joining the frequency segments. (**d**) Frequency dependence of the impedance components, Capacitance (C_P) and Loss ($L_P = 1/(\omega R_P)$). The inset compares the displacement current measured for a micro-structured and for a flat electrode[3].

5.3.2 Extracellular recording of Astrocytes signals using microstructured electrodes

The performance of the gold mushroom-like electrodes was assessed using populations of astrocyte cells *in vitro*. The astrocytes were isolated from mouse cerebral cortex, as described in the materials and methods section. Figure 5.3 (a) displays a typical time trace of the astrocyte electrical activity. Measurements were initiated after cell seeding. However, in the first hours only noisy fluctuations identical to bare electrodes (without cells) were measured. Cells only start to show a measurable activity approximately 3 hours after cell seeding. For simplicity, only a fraction of 20 minutes before the onset of activity is shown in Fig. 5.3 (a). Cell covered electrodes show a 3–4 μV (peak-to-peak) noise fluctuation, as shown on region labelled (A). The onset of electrical activity is preceded by an increase on the average noise fluctuations (see the region labelled (B) on Fig. 5.3(a)). The electrical activity starts suddenly as a burst of discrete signals. The burst is comprised of quasi-periodic signals with a broad distribution in amplitudes that vary from 10 to 60 μV. However, for some relatively short periods, the signals can show a quasi-periodic behaviour with a frequency of approximately 0.1 Hz and average amplitude of 50 μV. Figure 5.3(b) shows an example of this quasi-periodic behaviour recorded inside the burst of activity labelled (C**)**. The burst of electrical activity was recorded for 30 minutes, after which the cell culture medium was replaced with an extracellular calcium-chelating agent (ethylene glycol-bis(β-aminoethyl ether)-N,N,N',N'-tetraacetic acid; EGTA). The experiments were conducted using a concentration of EGTA of 10 mM. The histogram in the inset of Fig. 5.3(a) shows that in the presence of the calcium-chelating agent the frequency of signals lowers from an average value of 4 signals per minute (region (C)) to only 1 signal per minute (region (D)). Cells were kept in a medium with EGTA for 15 minutes, and then the electrolyte medium was replaced with fresh and normal cell culture medium.

After the EGTA removal the astrocyte population remained silent, with occasional spikes. One hour after the EGTA removal, the astrocyte population re-started activity. This activity, labelled as region (F), is characterized by signals also spaced by an average time of 10 seconds, as observed on the initial burst of activity (region (C)).

Although in region F, the signal amplitude is lower than in region A, the reduction in amplitude may be due to residual EGTA on the cell culture surface. The experiment was repeated three times and in all cases the activity was substantially reduced upon the addition of EGTA.

The addition of EGTA was conducted to inspect a possible relation between the observed signals and extracellular calcium waves commonly reported for astrocytes[124]. However, it has also been reported that the removal of calcium from the cell culture medium causes a disruption of the connections between cells (tight junctions) and also disturbs the cell attachment to the electrode surface[125–127]. In electrical terms, these perturbations on the tight junctions and cell adhesion properties will be reflected in a decrease in the seal resistance and imped the observation of signals. The tight junctions are re-established when the EGTA is washed and normal cell culture medium is used[125,127,128]. In order to inspect for changes in the cell adhesion and inter-connecting properties, small-signal impedance measurements were carried out. The impedance of the cell/substrate interface is sensitive to changes in morphology, adhesion and inter-cell connecting properties. This approach is referred to as electric cell-substrate impedance sensing (ECIS)[129]. According to the ECIS model, the high-frequency resistance should decrease when the tight junction is disrupted or when the cells are detached from the sensing electrodes[125]. The inset in Fig. 5.3 (a) shows that the resistance measured at 30 kHz decreases from 1.296 kΩ to 1.221 kΩ, a decrease of 75Ω, which corresponds to a 5.7% decrease in resistance. Although this change in resistance is relatively small, it may be enough to impede the propagation of cooperative signals across the cells. Alternatively, if the disruption is affecting the cells attachment to the electrode, it may decrease the seal resistance and compromise the ability of our electrodes to record the signals.

Figure 5.3 (b) shows a time trace of quasi-periodic signals inside the activity burst labelled (A) in Fig. 5.3(a). The signals are quasi-periodic, spaced by an average period of 10 sec. A detailed view of an individual signal is shown in Fig. 5.3(c). The signal shape is asymmetric and is characterized by a very fast time to peak (tr < 94 ms) and a slower decay to base line (td = 0.54 s). The average width of the signal is t_w = 2 s. During the signal decaying to baseline, the current often overshoots to a lower value than the steady state background noise.

We also recorded ultra-slow astrocyte activity. Slow signals do not appear in bursts, but sporadically, in clusters of 3 or 4 signals. A typical example of a cluster of signals is shown in Fig. 5.3 (d). Comparatively to the more rapidly varying signals, slow or long-lasting signals are weaker, sparser in time (several minutes), and last longer (10 to 20 s). Long lasting signals only reach amplitudes with a peak value of 5 µV, 4 times smaller than a typical fast signal with average amplitudes reaching 20 µV.

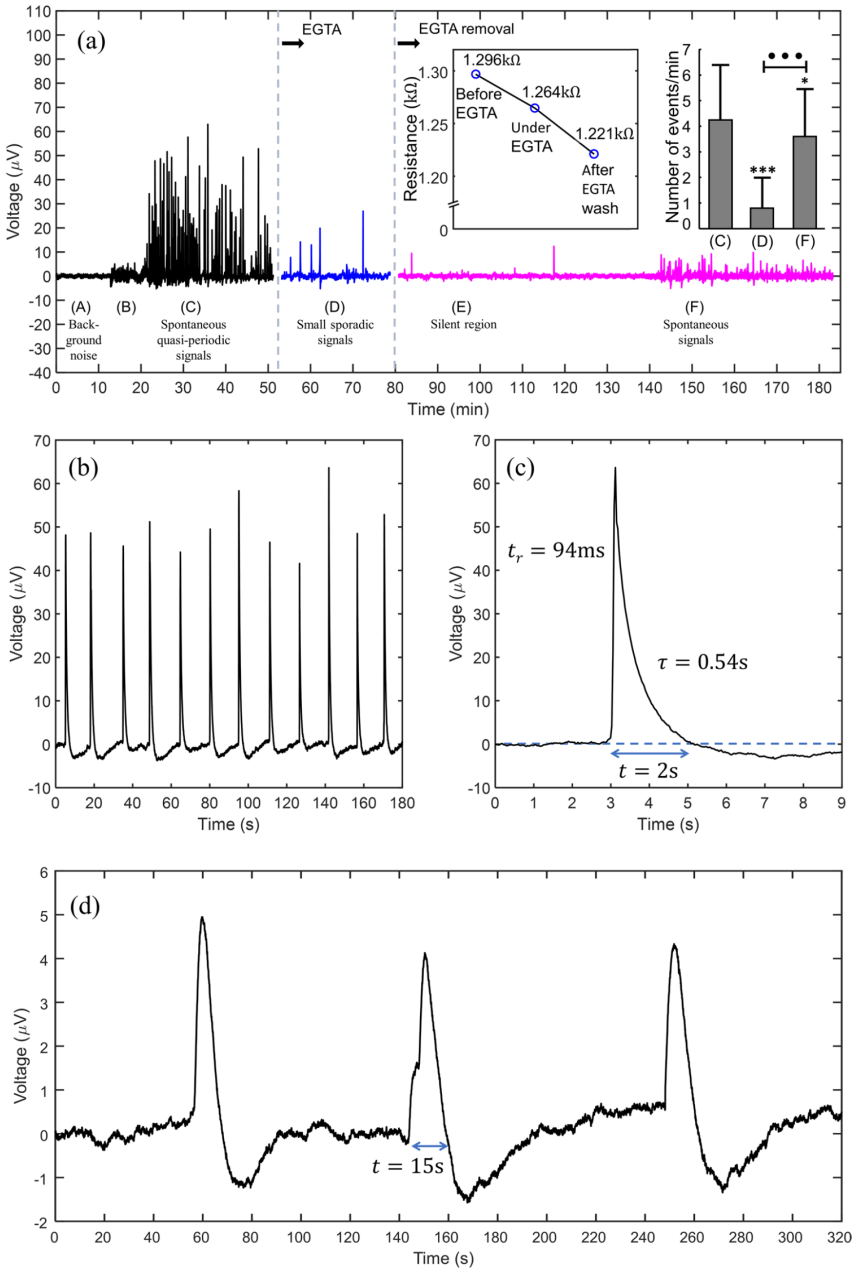

Figure 5.3 Electrical signals recorded in astrocytes populations. (a) An overview of a long-term recording of astrocyte population activity, with different experimental stages identified A-F. The inset shows how the high frequency (30 kHz) parallel resistance (*RP*) decreases upon the addition

of EGTA. The histogram in the inset shows the number of signals per minute, before and after the addition of EGTA. (b) Time trace of a quasi-periodic activity recorded in the burst of activity labelled (A). (c) Detailed view of an individual signal in Fig. 5.3(b). (d) Long-lasting, low amplitude and sporadic signals. The experiments were conducted using a concentration of EGTA of 10 mM^3.

5.3.3 Summary of the main results obtained using microstructured electrodes

In summary, astrocyte activity is characterized by discrete signals, with stereotyped shapes but different width, amplitude, and frequency. High amplitude signals are narrow, appear in bursts and are quasi-periodic ($f \approx 0.1$ Hz).

Low amplitude signals are long lasting and appear sporadically. Digital video image of fluorescence from intracellular Ca^{2+} signals reported by other authors[124,130,131] , show signals that are alike, in shape, length and frequency, to the signals presented in Fig. 5.3. For example, a study by Kuga *et al.*[132] report the observation of repetitive spikes with the periodicity of 1 minute and lasting for approximately 10–20 seconds (similar to the ones in Fig. 5.3 (d)). Other experiments[133] using rat hippocampal astrocytes show spontaneous calcium transients with a frequency of approximately 1.3 Hz. Each individual Ca^{2+} signal lasts for approximately 10–20 s. A recent study[134] using state-of-art image techniques in brain slices and *in vivo* showed astrocytes Ca^{2+} fluctuations lasting for approximately 14 s. The reported signals are also characterized by a fast rise time followed by a slower decay to the base line and a signal shape identical to the signals presented here.

The high-sensitivity of our measuring system is achieved by using large physical areas (4 mm^2) further enhanced by an array of mushroom-like structures. In comparison with a flat surface, the micro-structured surface significantly lowers the interfacial impedance between the cell and the electrodes. The interfacial quasi-static capacitance is increased by approximately 54%. There is also a corresponding decrease in the interfacial resistance that brings the thermal noise to approximately 0.3 μV (peak-to-peak).

The effective area of a micro-structured surface is much higher than its total base level area, therefore, micro-structured surfaces require less physical occupation area when compared with flat surfaces that provide identical impedances. Larger area flat electrodes probe larger ensembles of cells, and this may not be desirable if only a fraction of the cells synchronize to generate signals, while the remaining cells contribute to noise and

degrade the SNR. Therefore, the benefit of using micro-structured electrodes is the increase of the sensing electrode capacitance without the need to make very large base level area electrodes, hence, allowing a smaller population of cells to be probed. In addition to the obvious increase in capacitance, the group of M. Spira *et al.*[135] had also shown that the cells engulf the mushroom shapes. This engulfment leads to an improvement of the electrical coupling between cells and the sensing substrate, modelled through an increase in the seal resistance.

5.3.4 Bioelectrical signal modulation in amplitude and in frequency

This section presents the bioelectrical activity recorded using an interdigitated planar gold electrode. The device structure is depicted in Fig. 5.4. Further details about the device can be found in Chapter 4.

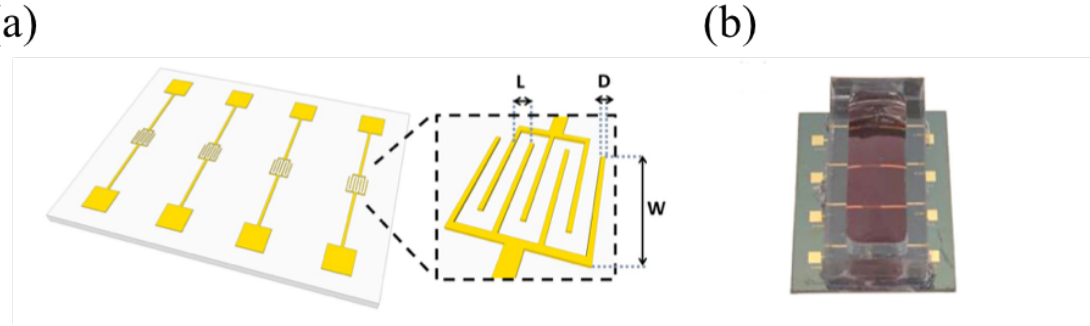

Figure 5.4 Planar sensing devices used in this study. (a) Schematic diagram of an interdigitated electrode fabricated on a silicon wafer. Device dimensions are W = 1000 mm, L = 10 mm, and D = 5 mm. The total number of fingers is 10. (b) Photo of the device mounted in a vessel with electrical connections[4].

The signal patterns recorded with the interdigitated electrodes shown similar behaviour to the ones observed on the microstructured surface. However, we conducted a more extensive number of experiments on the interdigitated type of device. Consequently, we were able to extensively characterize the bioelectrical signal patterns. These signal patterns reveal two types of signal modulation: modulation in amplitude (AM-amplitude modulation) and modulation in frequency (FM-frequency modulation). In this section, we provide a detailed discussion of the AM and FM bioelectrical signal patterns.

Figure 5.5 shows a typical time trace of astrocytes spontaneous activity. After 1–2 h of cell seeding on the device, astrocytes exhibit spontaneous weak signals. These early-stage signals are approximately 1.5 μV in amplitude, and they appear in cluster of a few (<10) discrete signals. With time, the astrocyte overall activity evolves to a new type of spontaneous activity, which is characterized by bursts of quasi-periodic signals and an increase of the signal magnitude. These bursts are briefly interrupted by shorter periods where both the signal rate and magnitude are lower. Bursts are characterized by a slow rise in signal amplitude until a maximum is reached. After attaining the maximum, the pattern decays following time dependence similar to the one followed during the rise in amplitude. This behaviour originates symmetric signal patterns modulated in amplitude. We refer to these patterns as amplitude modulated (AM) bursts.

Several AM bursts are visible on Fig. 5.5 (a). The temporal duration of an AM burst may vary from several minutes to hours.

Signals are approximately equidistant, with an inter-peak interval between 3 and 95 s. In order to identify firing patterns, we analysed the entire time bursting region of Fig. 5.5 (a) and constructed the statistics of the time between two consecutive spikes. These inter-peak intervals were estimated. The mean interpeak interval (± standard error of the mean) is 16.9 ±10.4 s. The skewness and kurtosis of the distribution appear significantly larger than their normal distribution thresholds. To evidence this, in the inset of Fig. 5.5 (a) we show the histogram obtained by distributing the time intervals into 10 s wide bins. Time intervals shorter than 3 s and longer than 95 s were not considered. The dominating frequency (*f*) is approximately 0.07 Hz (f =1/14 s).

Fig. 5.5 (b) shows a typical AM modulated burst. A burst can be characterized by its duration and by its peak in amplitude. The burst is fitted with a smooth curve that outlines the extremes. This is called the AM envelope. From this envelope we estimate the AM envelope peak. Fig. 5.5 (b) shows an AM burst of spontaneous activity with duration of 100 min. The estimated AM envelope peak is 74.5 μV. Fig. 5.5 (b) shows the relation between the burst duration and the burst amplitude. Long bursts have higher signal amplitudes. For short times the relation is approximately linear.

However, for very long times (t > 2 h) the fitting curve gently bends, suggesting that this signal amplitude will saturate.

An AM burst is comprised of discrete signals, as the ones shown in Fig. 5.5 (d). With time, the signals increase in amplitude without significant changes in the signal duration (1–2 s). An AM burst may also be comprised of biphasic signals, as the ones represented in Fig. 5.5 (e). The signal shape is asymmetric and characterized by a fast rise time to a peak value. Once the peak is reached the voltage decays, first slowly and then rapidly, to a minimum value lower than the baseline potential. This negative part of the signal relaxes slowly to the baseline.

The signals must be related to the inward and outward flow of ions across the membrane. The positive variation ($+\Delta V$) in respect to the baseline must correspond to an outward flow of positive ions and the negative variation ($-\Delta V$) to a net inward flow of positive ions.

The biphasic signal is clearly asymmetric because the upper and lower voltage peaks are different. However, if the areas under the voltage fluctuations are compared, this asymmetry in relation to the baseline is not so pronounced. For weak signals, the ratio between areas is approximately 0.7. For strong signals, this ratio is 0.9. Furthermore, there is evidence that this ratio is still underestimated because the positive variation does not have time to relax to the baseline, becoming slightly super-imposed in the negative variation. To some extent, both voltage fluctuations are mixed, and thus the area under the positive fluctuation is somewhat underestimated. It is reasonable to assume that the amount of charge involved in the positive voltage variation is equal to the amount of charge involved in the negative voltage fluctuation. Because the positive voltage variation occurs in a shorter time than the negative fluctuation, we propose that the apparent asymmetry is a consequence of a different ion flow rate.

The NCX channel operating in reverse mode is an obvious candidate to explain the positive voltage fluctuation (net positive outward current). However, further studies are required to elucidate the full signal shape.

A large area electrode cannot resolve single cell signals; the recorded trace reflects the combined activity of an astrocytic ensemble. If a large number of individual cells generate independent signals obeying to the same statistics, then, according to the central limit theorem, the resulting activity resembles noise since the distribution of the average of a large number of independent, identically distributed variables will be approximately

normal. To explain the observation of discrete, temporally structured signals, several hypotheses may be considered. An obvious one is that the population of cells is synchronized by a biological signaling process (pacemaker mechanism, just as in a cardiac beating signal, where individual signals sum up into an averaged discrete signal). However, a synchronized population of cells is not expected to generate modulating patterns. To explain the existence of AM- or FM-like modulated patterns we need to consider the existence of sub-populations of cells. A sub-population of cells is seen here as a relatively small number of cells that are synchronized. For the following reasoning a sub-population, in the limit, can be a single cell. These sub-populations may be sparse and distributed over the entire electrode area and generate signals with slightly different frequencies and phases, giving rise to patterns with an AM- and FM-like modulation.

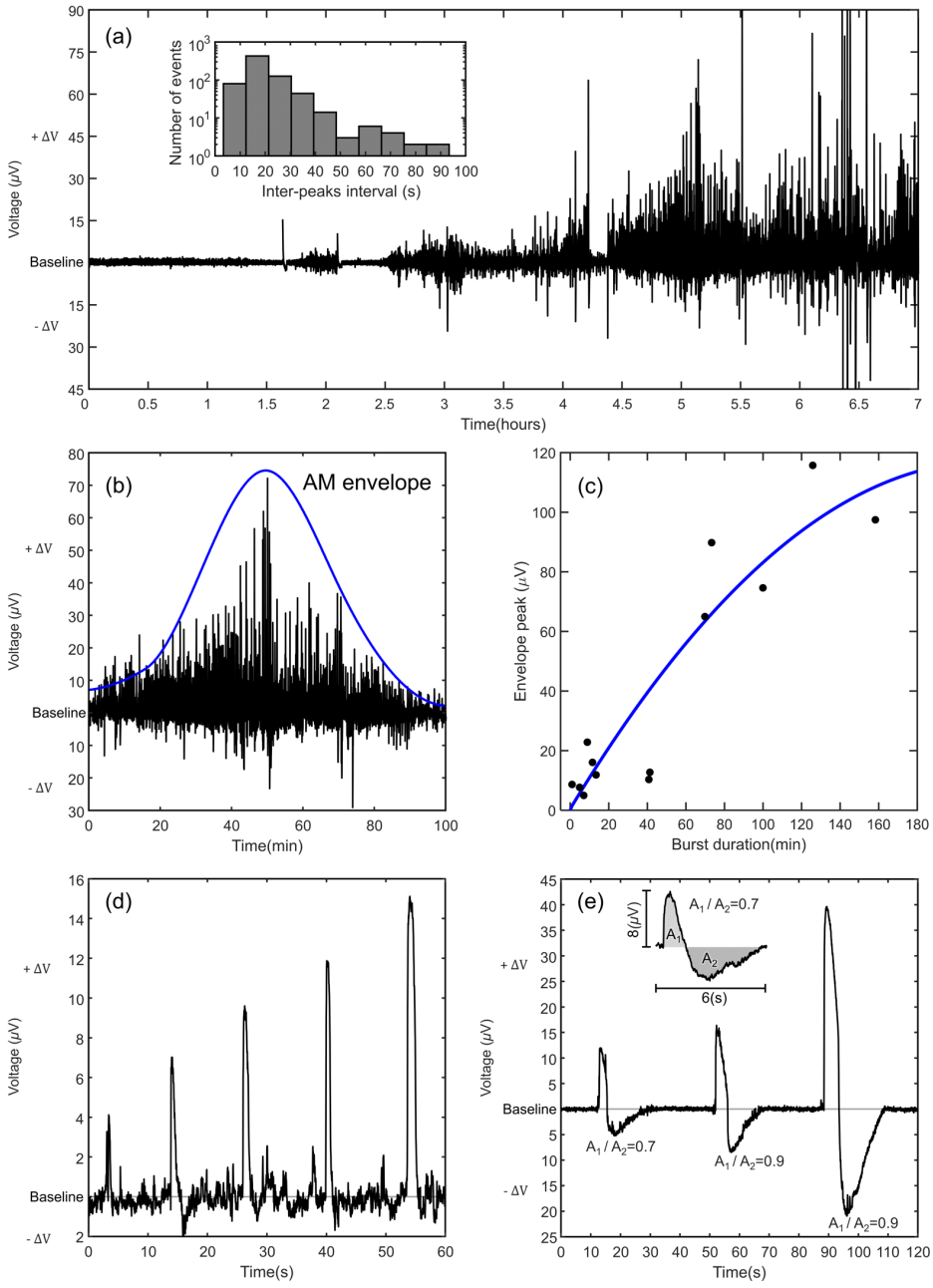

Figure 5.5 Electrical signals recorded in astrocytes populations. (a) An overview of a long-term recording of astrocyte population activity with different amplitude modulated (AM) bursts of activity. The inset shows a histogram of the inter-spike intervals recorded for the whole burst activity shown in (a). (b) Typical AM modulated burst. (c) Relation between the burst duration and the envelope amplitude. (d) Detailed view of several individual signals. (e) Asymmetric signals with increasing magnitude. As the signal amplitude increases, the ratio between the areas under positive and negative voltage fluctuations becomes 0.9[4].

Figure 5.6 (a) shows an example of a second type of burst also often recorded during our experiments. These bursts are characterized by a frequency modulation (FM). At the

onset of the burst, the frequency rises fast up to 15 spikes/min and then begins to decrease slowly until the signals disappear. The decrease in frequency can vary from a few minutes up to a half-hour. The progressively frequency shift to lower frequencies (red shift) is not necessary accompanied by a decrease in signal amplitude, as observed in the AM modulation discussed above. The FM modulation is clearly observed in Figure 5.6 (a) for $t > 50$ min. Interestingly, when all the clusters in Figure 5.6 (a) are analysed and the number of spikes per minute is represented in the form of a bar plot, all signal clusters in this time trace exhibit a similar red shift in frequency. Figure 5.6 (b) shows an example of a FM modulation recorded in a cluster of signals.

Calcium oscillations with AM and FM type of modulation have been reported by others[136,137]. However, in their studies signal modulation appears as a response to a chemical stimulus and it is usually reported in independent time traces[138,139]. To the best of our knowledge, we show for the first time non-interrupted experimental time traces with a clear FM modulation. Furthermore, this frequency shift repeats itself in few consecutive bursts, is spontaneous and is recorded using extracellular electrodes.

In order to highlight the electrical sensitivity of our sensing electrodes and method, we showed in Figure 5.6 (c) a detailed view of the weakest signals measured on the time trace of Figure 5.6 (a). One cluster is also shown in detail after the noise was removed for clarity (Figure 5.6 (d)). The signals are monophasic and approximately 1.5 μV in amplitude. In the beginning of the cluster the signals are about 1 s long but get shorter and weaker until the cluster fades away.

In order to gain insight into the possible biological process connected to the signals, the astrocyte population was exposed to glutamate (0.1 mM) for 10 min and then removed. In a time span of 20 min after glutamate removal, discrete signals were induced.

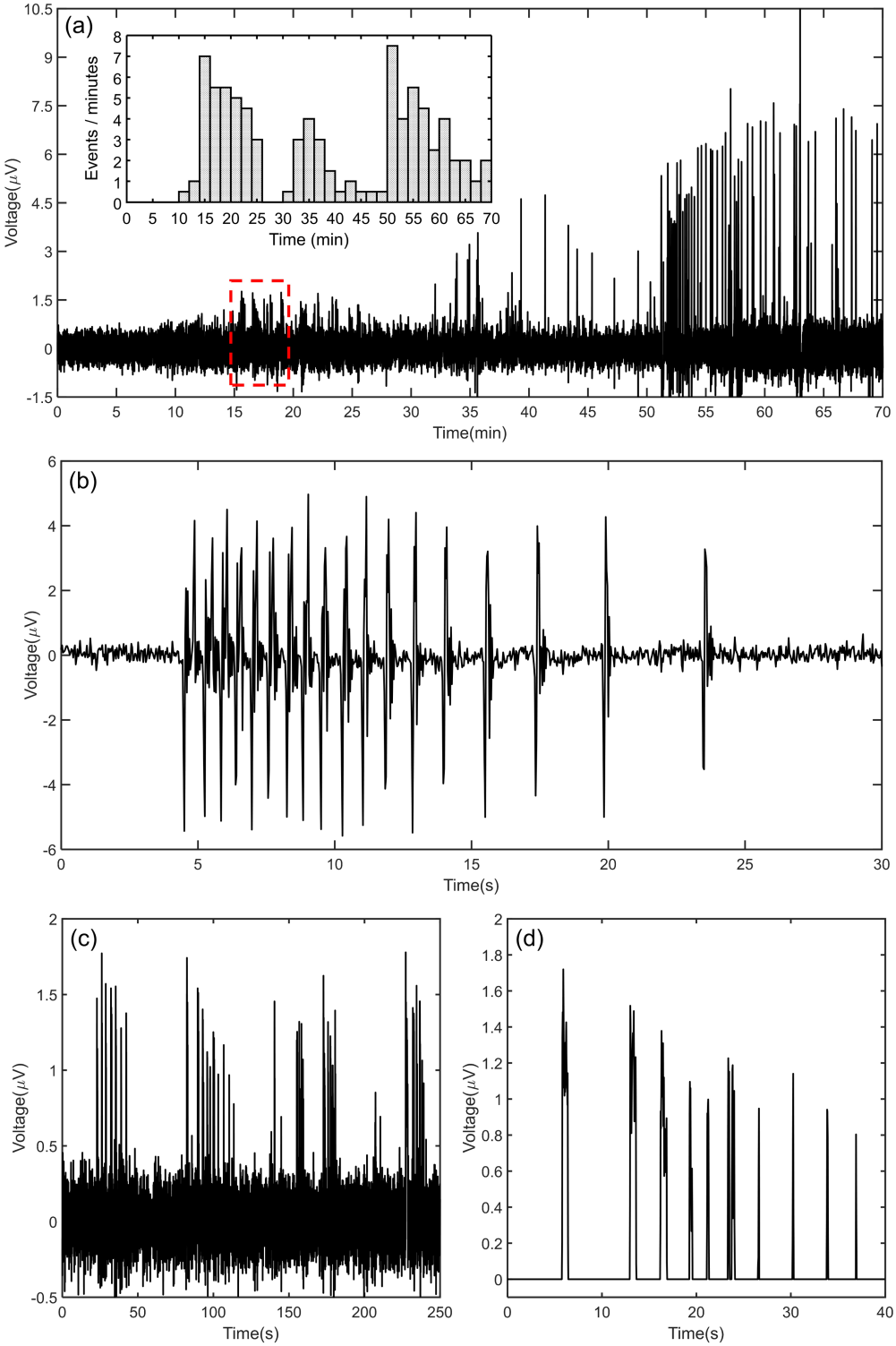

Figure 5.6 Signal patterns with frequency modulation (FM). (a) Time trace showing several distinct bursts. The bar plot in the inset shows that the signal rate decreases with time (FM). (b) Typical FM modulation recorded in a cluster of relatively fast signals. (c) Detailed view of the clusters of signals inside the dashed square of (a). (d) Detailed view of an individual cluster with the noise removed to highlight the changes with time in signal width[4].

The effect of glutamate exposure on the astrocyte activity is shown in Figure 5.7 (a). The inset shows a detailed view of two discrete signals inside the burst of activity. The signals triggered upon glutamate exposure are monophasic, with a negative voltage fluctuation in relation to the baseline. A detailed view of two signals is shown in the inset of Figure 5.7 (a). In this respect they are slightly different from the spontaneous signals, which can be monophasic or biphasic.

As explained in the Introduction section, most of the electrical fluctuations reported for astrocytes populations have been directly related with Ca^{2+} signaling. To assess the possible involvement of calcium on our signals we deliberately deprived the cell culture medium of calcium cations and looked at the possible effects on the signals. Figure 5.7 (a) shows that the signals can be substantially inhibited when the cell-surrounding medium is replaced by calcium deprived medium, through the addition of a 10 mM solution of ethylene glycol-bis (b-aminoethyl ether)- N,N,N0,N0-tetraacetic acid (EGTA), a calcium-chelating agent.

Figure 5.7 (b) shows the effect of EGTA exposure in a burst of spontaneous signals. The addition of EGTA also successfully stops astrocyte spontaneous activity. The bar plot in the inset of Figure 5.7 (b) shows that in the presence of the calcium-chelating agent, both the average spike rate and the signal amplitude are lowered. The frequency of signals decreases from an average value of 3 signals per minute to only 1 signal per minute. The average amplitude of the signals lowers from approximately 6 μV to 1 μV.

Cells were kept in a medium with EGTA for 15 min, and then the electrolyte medium was replaced with fresh and normal cell culture medium. After removal of the EGTA the astrocyte population remained silent, with occasional signals. One hour after the EGTA removal the astrocyte population re-started activity. This pattern of behaviour was observed in all experiments ($n = 3$), with EGTA addition substantially reducing the activity ($p < 0.001$).

The addition of 10 mM of EGTA was conducted to inspect a possible relation between the observed signals and extracellular calcium waves commonly reported for astrocytes. However, it has also been reported that the removal of calcium from the cell culture medium causes a disruption of the connections between cells (tight junctions)[127]. These perturbations may also affect the signaling process.

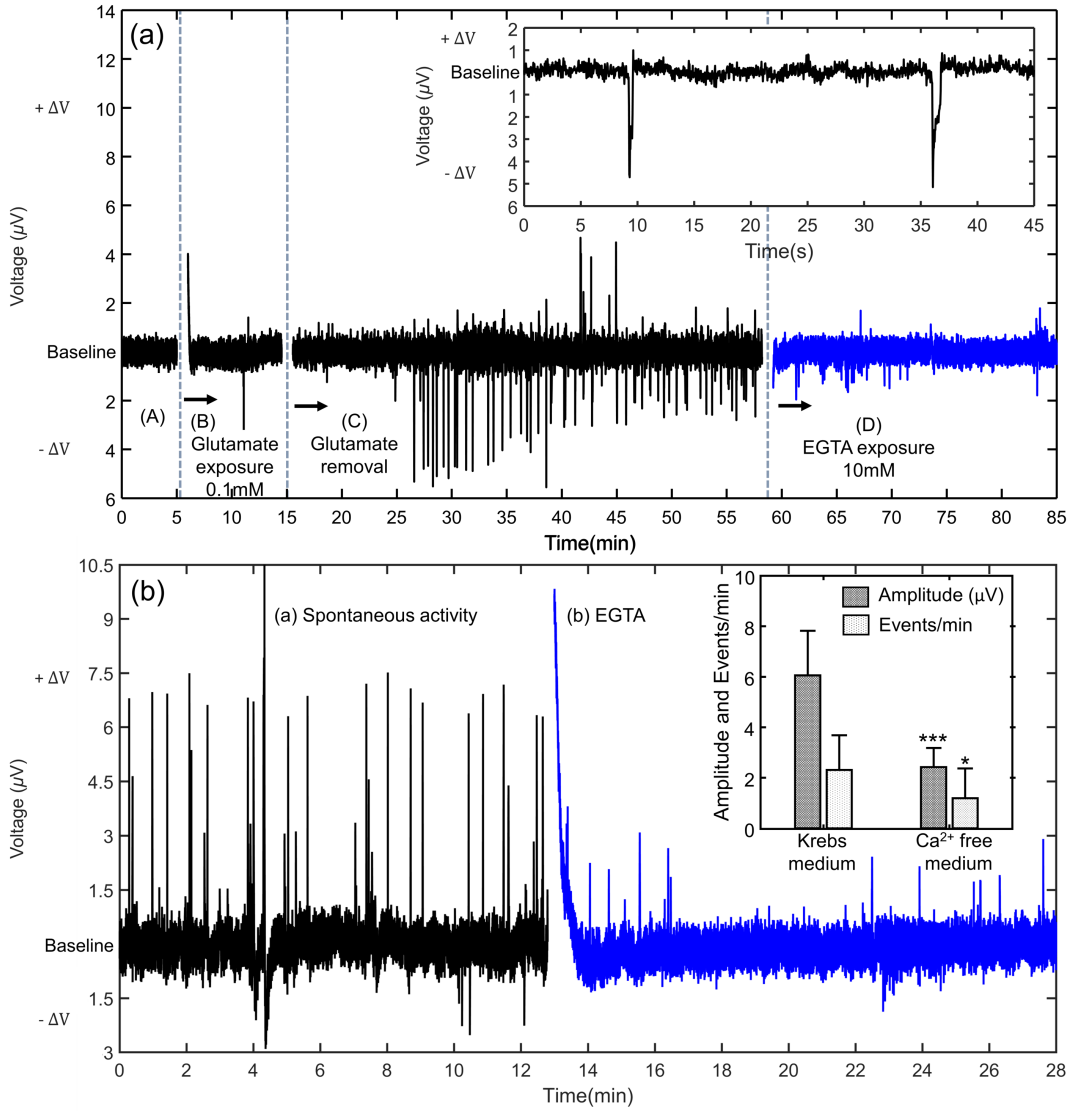

Figure 5.7 Signal-enhancing and signal-inhibiting agents. (a) Typical example of the effect of glutamate exposure. Signals appear with a delay of approximately 20 min. The induced signals are inhibited by an extracellular selective calcium chelator (EGTA). The inset shows a detailed view of two signals. (b) The effect of calcium deprivation in a burst of spontaneous signals. The inset shows the average changes, plotted as mean ±SD, caused in the signal rate and signal amplitude, compared to the baseline activity. *$p < 0.05$; ***$p < 0.001$[4].

5.4 Discussion

The electrode and the measuring methodology were evaluated by recording signals from astrocytes isolate from mouse cerebral cortex in primary culture. The measured signal is a superposition of the individual responses of an ensemble of cells adherent on the electrode. We ascribe these quasi-periodic signals to the collective electrophysiological behaviour and synchronization of the activity across a population of cells on the electrode; thus, they arise from a cooperative phenomenon.

Although astrocytes do not fire action potentials, they are not electrically silent cells. Electrophysiological recordings using patch clamp methods revealed that astrocytic membranes are animated by very slow fluctuations that are intimately related to changes in neuronal activities[110,140–143]. Astrocytes do indeed exhibit a form of excitability, albeit one quite different from the known membrane electrical excitability of neurons. Astrocyte excitation is expressed as oscillations in cytosolic Ca^{2+} concentration and an increase in propagating waves of free Ca^{2+} increase[124,140,142,144]. This form of excitation is in line with the results reported herein, where the astrocyte activity is partially inhibited by chelation of the extracellular Ca^{2+}. Furthermore, the frequency and shape of the electrical extracellular signals match the ones using optical fluorescence probes reported in literature[143]. The oscillations occur at frequencies in the order of 0.1 Hz. Astrocytes excitability progress thousands of times more slowly than do their neuronal electrical counterparts. Activity waves spread from astrocyte to neighbouring astrocyte by means of gap junctions, which interconnect adjacent astrocytes into functional networks, both in brain tissues and under cell culture conditions[142,145,146].

Although, the signals reported here have electrical characteristics in line with those reported as calcium waves, further experiments are required to establish an unambiguously link to calcium waves. The elimination of signals in the presence of calcium chelating agent EGTA is by itself not conclusive because calcium deprivation causes a disruption of the electrical coupling between cells and the sensing electrode as described in the Results section.

A search in the literature revealed that weak and slow signals, such as intercellular calcium waves, have been addressed using extracellular ion-selective probes. However, probes and optical methods have a low signal-to-noise ratio and may impact in the

physiological functions of the cell membrane. Moreover, the lifetime of fluorescence dyes limits the observation to a few hours. Extracellular electrodes offer the advantage of being totally non-invasive and enable monitoring cells and tissues for periods of time as long as weeks.

This study has demonstrated that extracellular electrophysiological measurements show a richness of detail never reported before using imaging methods. For example, electrical signals rarely start abruptly. Often, a signal pattern is preceded by a sudden increase in noise. Once the signals start, they gently increase in amplitude and rate, showing that an increasing number of cells get synchronized or are somehow correlated. The temporal dependence of the cell synchronization process can be followed in real time. This is a feature not entirely perceived using fluorescence techniques. In imaging techniques, the signal-to-noise ratio (SNR) is relatively low. For example, with voltage sensitive dyes, an alternative to calcium imaging which potentially interferes less with the cellular intrinsic dynamics, the fractional change in fluorescence is in the order of 0.1% to 0.5%. The SNR associated to the signals presented here depends on the signal amplitude. However, SNR higher than 3 can be obtained if strong signals as the ones shown in Fig. 5.5 (e) are generated.

The electrodes and the measuring methodology issued from our investigations and described herein are thus highly relevant for a community of neuroscientists and biologists interested in the study on how electrical signals are used by cells to communicate and coordinate their activities. There is a large body of evidence supporting the view that these slow signals are important regulators of cell behaviour, controlling cell proliferation, migration, and differentiation[147,148]. Thus, while providing new tools, this study opens new directions for assessing biological events based on cooperative communication.

It is shown signal patterns with FM and AM modulation that repeat in a quasi-periodic trend. These modulations are known and have been proposed as a way to encode biological information[149]. Previous studies have shown that the modulations occur in response to chemical stimuli[138] and have been recorded in distinct time traces. To the best of our knowledge, this work provides the first report on FM and AM signal modulations occurring spontaneously, monitored in real time in a single time trace.

5.5 Conclusions

In summary, our work yielded a new methodology to measure extracellular signals in astrocytes populations. This experimental approach enables the study of astrocyte physiology in a totally non-invasive manner, with a high temporal resolution, and over extended periods of time. The advantages of the method were demonstrated by showing a variety of spontaneous signals, in close agreement with previous reports using optical fluorescence methods. Furthermore, newly revealed signals and signal patterns, which had remained inaccessible using conventional imaging and patch-clamp methods, have also emerged.

We believe the methodology used here can be applied to brain slices and to mixed cell populations to study neuron-glia interactions. This is because, while action potentials are relatively fast signals (milliseconds) detected in a frequency range of kHz, signals from astrocytes populations are observed in a spectral region below 10 Hz. Therefore, both types of signals should not interfere with each other.

It is proposed that extracellular measurements in astrocytes, complemented with other methods, will hopefully produce a more detailed knowledge of astrocytes signaling, paving the way towards a better understanding of the brain information processing.

CHAPTER 6

Extracellular electrophysiological based sensor to monitor cell migration

"Life is like riding a bicycle. To keep your balance, you must keep moving."
Albert Einstein

This chapter explores the use of bioelectrical activity generated by migrating cells as a tool for extracting quantitative information on cell motility, spatial organization, and cell-cell communication. The chapter presents results for various cell types (dermal fibroblast and C6 cells) and discusses migration patterns exhibited by each type of cell. Additionally, it discusses the effect of sex hormones during the wound-healing process of dermal cells.

6.1 Introduction

Our research group has developed a sensor based on electrophysiology that enables real-time monitoring of cancer cell migration[150]. The method involves measuring the bioelectrical activity of cells as they move from a densely populated area to a region without cells. In this chapter, we aim to extend our research and evaluate the usefulness of our method and electrodes in monitoring the migration of other cell types.

Our goal is to validate the technology and develop a new instrument or biological assay for monitoring cell migration.

To validate our technology, we decided to use dermal or skin cells. We justify our selection because skin cells play a crucial role in wound healing, which involves complex cellular activities that must be synchronized and coordinated[151]. During wound repair, cells must perform a complex number of tasks in a coordinated manner[152]. Cells must detach from their neighboring cells, release from the substrate, and initiate migration in a well-defined direction. To illustrate the complexity of damage repair, Fig. 6.1 shows fluoresce microscopy photographs of an *in vitro* culture of BJ-5ta cells near a damaged site. The tightly packed cell structure is still evident six hours after the damage, but after twelve hours, the closely packed cell population is already disconnected, and the isolated cells begin their migration towards the empty region, as seen in the image taken 12 hours after the damage (see Fig. 6.1 (b)).

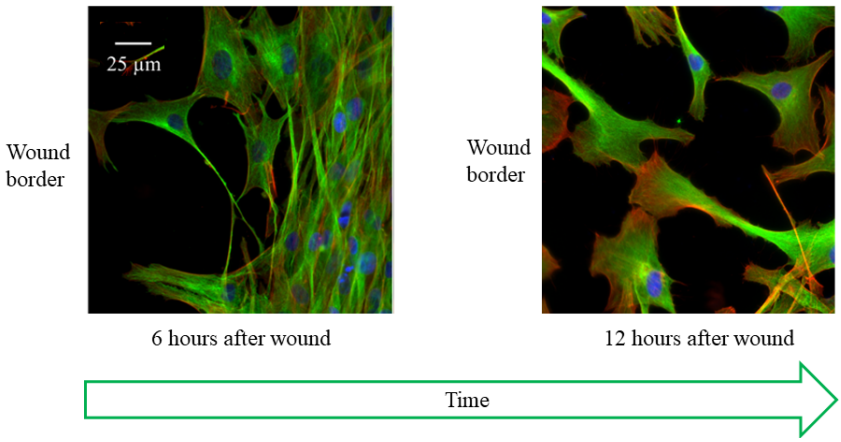

Figure 6.1 Immunocytochemistry of BJ-5ta cells in a cell monolayer *in vitro*. BJ-5ta cells were labelled with a monoclonal anti-α-tubulin antibody produced in mouse and detected with a goat anti-mouse IgG (H+L). Antibody conjugated to Alexa Fluor 488 (alpha tubulin in green) and stained with Texas Red®-X Phalloidin (actin filaments in red) and DAPI (nuclei in blue). The images are representative of cells 6h after scratching (in the left image) and 12h after scratching (in right image).

Additionally, cells must generate instructions (chemical or electrical signals) to manage all the organized cell activity during the damage repair and this also requires some sense of time. It is reasonable to assume that cells during damage repair activate biological clocks or rhythms, making it a complex process that requires a sophisticated cell-cell communication mechanism[153]. Cells communicate using ion channels; Therefore, monitoring extracellular ionic fluctuations would be an ideal method to gain insight into the mechanisms involved in cell migration during damage repair[154].

There is some evidence that women can repair wounds faster than men. It has been proposed that this difference is due to the direct impact of sex hormones on wound healing speed, possibly through their modulating effects on inflammation[155]. This hypothesis provides an interesting playground for designing experiments where cell migration speed and damage repair of cells in culture is studied when cells are exposed to different sex hormones[156], such as estrogen[157] or testosterone[158].

The hypothesis of whether different sex hormones (such as estrogen or testosterone) affect the speed of wound healing is a very interesting topic for the design of experiments.

With the intention of exploring the role of sex hormones in repairing wounds, we planned a set of *in vitro* experiments. We used two different types of skin fibroblasts. HDF cells and BJ-5ta cells. HDF cells are originally from a human adult female, and BJ-5ta cells are originally from a human neonate male. The detail of whether the cells are from an adult, or a new-born is relevant because neonatal cells have a lower immune response than adult cells. The immune response is certainly a parameter important to consider in a wound (or damage) repair.

The first part of this chapter is focused on the sedimentation and migration of the fibroblast under study. The migration process is studied using electrical based methods and conventional methods based on optical inspection of the damage (scratch) closure. The second part on this chapter provides a comparison between the electrophysiological pattern generated by different types of cells as they migrate to repair a damaged area. This comparison was carried out using brain cancer cells (glia cells) and 3 types of dermal fibroblasts.

It is worth noting that dermal fibroblasts differ greatly from glia-derived cancer cells. Skin cells coordinate their activity to repair a damaged tissue, while cancer cells migrate

to invade surrounding tissues. As a result, we expected to see differences in the migration behaviour of these two cell types. This chapter presents experimental work aimed at addressing several key questions related to electrophysiological measurements and their application in the study of damage repair. Specifically, the research investigates the potential of electrophysiological based methods to detect differences in migration behaviour among various cell types. Additionally, it examines the kind of information that can be obtained through electrophysiological measurements, and how this technology can be used as an assay tool for biologists seeking to study damage repair.

Our technology to monitor cell activity during migration are of interest to various scientific communities. Researchers interested in developing methods and devices to promote wound healing *in vivo*, researchers studying tissue regeneration and organ formation, researchers studying cancer cell invasion, and those exploring the role of internal "clocks" in coordinating cellular and physiological processes, will all find this work particularly attractive.

6.2 Materials and Methods

6.2.1 Cell cultures

(a) C6 glioma cells

C6 glioma cells (American Type Culture Collection, USA) were cultured in F-12K nutrient medium supplemented with 15% fetal horse serum, 2.5% fetal bovine serum, and 1% penicillin and streptomycin. The cells were maintained under aseptic conditions at 37ºC in a CO_2 incubator (Thermo Scientific Midi 40) containing a 5% CO_2/air gas mixture that was automatically controlled. UV sterilization was accomplished using an Olympus TH4-200 and the exposure time was 5 minutes, to prevent damage to the vessel sealant. The C6 glioma cells were harvested from the culture plates using a cell scraper and diluted in culture medium to yield a cell suspension (in F-12K nutrient mixture) containing from 50,000 up to 300,000 cells. The cell suspension was used to seed the device, which was maintained in an incubator for 24h until a confluent monolayer had covered the entire surface of the device including the sensing electrode. The cells were mechanically removed from the sensing electrode using a pipette tip hand-held scraper. The detached cells were then washed using several changes

of cell culture medium. Digital images of the migrating cell were captured using an Olympus BX41 and a camera coupled to a computer. C6 glioma cell number and viability were assessed using a Neubauer chamber and a trypan blue live/dead exclusion assay. The average viability of cultures remained at all points ≈80% (±12%). The cells were highly viable during the migration experiments.

(b) Human skin cell culture

A commercially available BJ-5ta immortalized neonatal fibroblast cell line from human male foreskin (ATCC® CRL-4001™, USA) and HDF immortalized fibroblast cell line from an adult human female (HDF/TERT164, Everycyte GmbH, Viena, Austria) were used in the study. Dulbecco's modified Eagle's medium (DMEM) (Sigma-Aldrich, Germany) and Medium 199 were mixed (4:1 v/v) and supplemented with 0.01 mg/mL hygromycin B (Sigma-Aldrich, Germany) 1 % penicillin and streptomycin (Sigma-Aldrich, Germany), and 10 % fetal bovine serum (Sigma-Aldrich, Germany) was used for the BJ-5ta fibroblast cell maintenance. A mixture (1:1) of DMEM (Sigma-Aldrich, Germany) and Hams F12 medium (HyClone-Cytiva, Belgium), 1% Glutamate (Sigma-Aldrich, Germany), 10% fetal bovine serum (Sigma-Aldrich, Germany) and antibiotic G418 100 μg/mL (InvivoGen, Toulouse, France) was used for HDF cell maintenance. The cells were maintained at 37 ºC and 5% CO_2 in an incubator as recommended by the supplier. Evaluation of the general cell characteristics revealed that HDF cells are slight larger in size than BJ-5ta cells. Another differentiating feature is the duration of the cell cycle and BJ-5ta cells duplicate in a cycle of 24h, while HDF cells duplicate in approximately 48 hours.

Fig. 6.2 shows optical photographs of confluent cell populations of BJ-5ta and HDF cells. When adherent to the sensing electrode both type of cells has a fusiform shape.

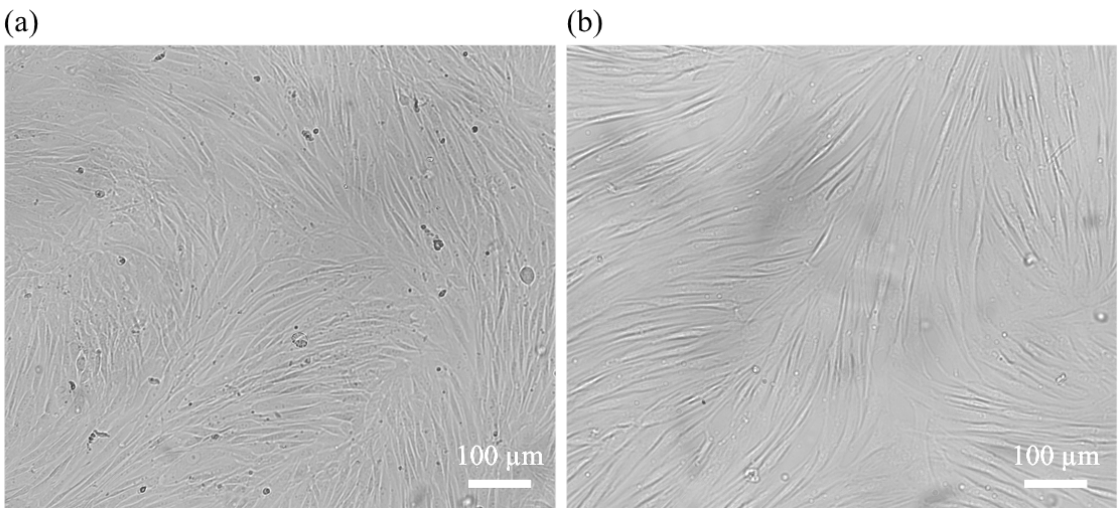

Figure 6.2 Photograph of populations of confluent cells population adherent to the sensing electrodes. (a) BJ-5ta cells and (b) HDF cells.

6.2.2 Electrical measurements

Extracellular voltage measurements were carried out using the experimental set-up described in Chapter 4. Damage was caused using an electrical discharge and a protocol defined by the company Applied Biophysics for an electrode with an area of 250 µm of diameter. This protocol consists of administering a series of short electrical pulses, which were optimized for each confluence monolayer of cells. For the BJ-5ta cells, a train of current pulses reaching 1.2 mA with a frequency of 4 kHz was applied across 10 seconds. HDF cells were dissociated from the electrode using a train of electrical pulses with a current of 800 µA at a frequency of 40 kHz across 20 seconds. The cell membranes were disrupted by the high current pulses and the cells sitting on top of the electrode were lysed and dissociated. To obtain a cell free electrode, the dead cells were then washed with fresh medium.

6.2.2.1 Electrodes

Commercially available electrodes with built-in vessels to hold the cell cultures were used. These devices were supplied by the company Applied Biophysics. These electrodes were made of semi-transparent gold on a plastic substrate (PET). The electrodes used were 8W1E. A single circular gold electrode with a diameter of 250 µm was used. For further details see Chapter 4.

6.2.3 Steroid hormones preparation and toxicity evaluation

Steroid hormones used in the study were 17β-Estradiol (≥ 98% purity, 1,3,5-Estratriene-3.17β-diol, Sigma-Aldrich, Germany) and testosterone (> 98% purity, 4-Androsten-17β-ol-3-one, Sigma-Aldrich, Germany). Solutions of the steroid were prepared by diluting them in alcohol (70%) and then for use in assays, the stock was diluted to an appropriate concentration in the cell-appropriate culture medium.

In the experimental work, several biological assays were used, namely, MTT, cell proliferation, scratch assays and immunocytochemistry as described in Chapter 4. To assess the cytotoxicity of steroid hormones, (17β-Estradiol and testosterone), the BJ-5ta and HDF cells were exposed to serial dilutions (0.001 μM and 0.01 μM) of hormone and an MTT assay was performed. Upon exposure of BJ-5ta and HDF cells no cytotoxic effects were noticed at most of the hormone concentrations tested (Figure 6.3). Based on cell cytotoxic effects we selected to expose the cells to a physiological concentration of hormone (0.1 μM) in all the experiments.

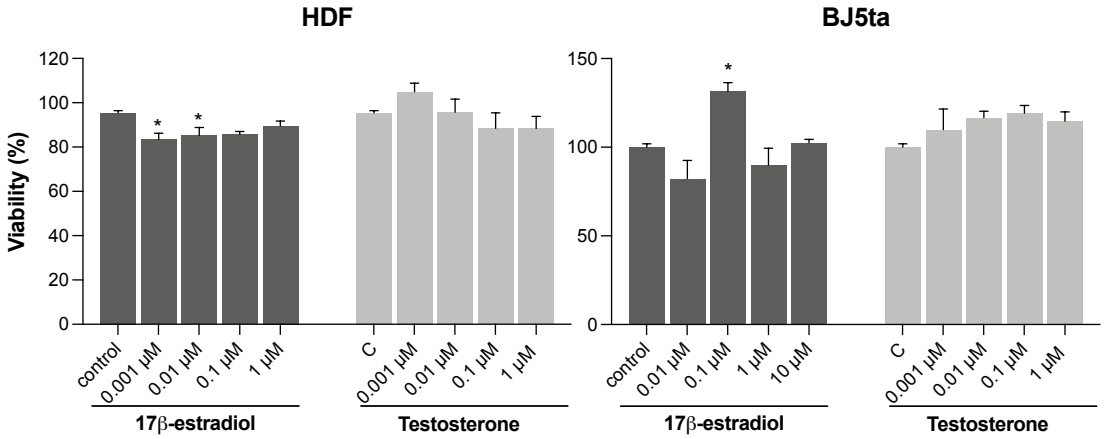

Figure 6.3 MTT assay for HDF and BJ-5ta cells exposed to different concentrations of 17β-Estradiol and testosterone. Results are showed as the average ± SEM of 4 technical replicates. Data was analysed using a One-way Anova and the statistical analysis was performed using GraphPad Prism version 7.0a. $p < 0.05$(*) was considered significant.

6.2.4 Electric cell-substrate Impedance Sensing (ECIS)

Electric cell-substrate Impedance Sensing (ECIS) assays were performed with an ECIS Model Z Theta® (Applied Biophysics, USA) instrument. The ECIS assays were used in the multiple frequency scanning mode from 62.5 Hz to 64 kHz. The coating of

the electrodes by the cells was monitored by measuring the electrode/electrolyte resistance at a constant frequency of 4 kHz.

The electrodes were firstly stabilized following the manufacturers recommendation and one hour of measurements were performed before the addition of 50,000 cells to each well of the biosensor device. All devices used in the experiments were pre-treated with cysteine (10 mM), following the manufacturers recommendation. For migration assays, control (cells without treatment), 17β-Estradiol treatment (0.1μM in cell culture medium) and testosterone treatment (0.1μM in cell culture medium) were assayed simultaneously with two replicates/ treatment. For cell migration, a single electrode of 250 μm diameter (8WE1, IBIDI®) was used.

6.2.5 Statistics

To assess the effect of different concentrations of steroid hormones on cell viability and cell proliferation a One-way Anova test was performed for each compound and cell line. Statistical analysis of the results of the scratch recovery data was performed using a two-way ANOVA test followed by a Tukey's Multiple Comparison test. All statistical analysis was performed using GraphPad Prism version 8.4 for MacOSX, GraphPad Software, La Jolla California USA). For ECIS experiments, the data were analysed using a one-way ANOVA followed by a Tukey's Multiple Comparison test. The statistical analysis was performed using SPSS and $p < 0.05$ (*) was considered significant.

6.3 Results and discussion

This section begins by presenting the study of the sedimentation and adhesion of the cells to the sensing electrodes. The behaviour of the BJ-5ta cells is presented first and then it is compared with the behaviour of the HDF cells.

6.3.1 Sedimentation, adhesion, and migration of BJ-5ta and HDF cells

Figure 6.4 plate **A** shows a photograph of the sensing electrode used to measure the migration. Cells (50,000) were seeded and left to sediment and coat the entire electrode and the surrounding region (photograph (a)). Once cell confluence was reached, a train

of electrical pulses was applied to the sensing electrode to kill the cells on top of the sensing electrode. Details of the electrical pulse used are explained in the Materials and Methods. Once dead cells were removed by washing the chambers of the device several times with fresh medium, a perfect and cell free round area was evident. The cell free area on the electrode was surrounded by healthy attached cells (see photograph (b) in Fig. 6.4.). The cells at the electrode border started to migrate onto the empty electrode until it was totally covered by a confluent monolayer (see photograph (c) in Fig. 6.4).

The cell sedimentation and attachment on the electrode surface was monitored by measuring the bioelectrical activity generated on top of the sensing electrode and also by the corresponding changes in the electrode/cell impedance. A consideration is first provided about the changes in impedance and subsequently changes in electrophysiology. During settlement and adhesion, the resistance increases from less than 2 kΩ up to 12 kΩ showing that the electrode is full coated with a cell population (Plate **B** on Fig. 6.4). Once the cells are killed (by a train of electrical pulses) the electrode resistance drops to the original values (cell free electrode). As the cells move into the electrode the resistance begins to rise, first slowly and then with an increasing rate as the electrode coverage by the cells increases. The corresponding time trace of cell impedance is show in Fig. 6.4 Plate **B**. As expected, the resistance increases with time until it reaches a noisy plateau at approximately of 15 kΩ. The time that it takes to reach the plateau is approximately 30 hours. The slope of the impedance curve is proportional to the rate of the electrode coverage by the cells. Initially, the slope of the resistance curve is very small, showing that there is a delay before the onset ofcell migration. To estimate the migration speed only the steepest slope of the resistance curve was considered. Assuming that the cells only have to travel half of the electrode diameter (125 μm), the average cell migrating speed was estimated to be approximately 14 μm/h. This speed is significant lower that the values of 30 μm/h reported by others[159].

Interesting, the plateau induced by the cell migration process occurs at higher resistance than the first plateau caused by the cell settlement and attachment. Cells establish a more compact cell population when they move by migration than when they move by a sedimentation process. When analysing the resistance plots two important aspects should be considered; (i) the slope of the curve monitors the rate of electrode coverage, therefore it can be assumed to be a direct indication of the cell migration speed; (ii) the magnitude

of the resistance plateau is proportional to the tissue compactness. The higher the electrode/cell resistance the more compact is the cell population.

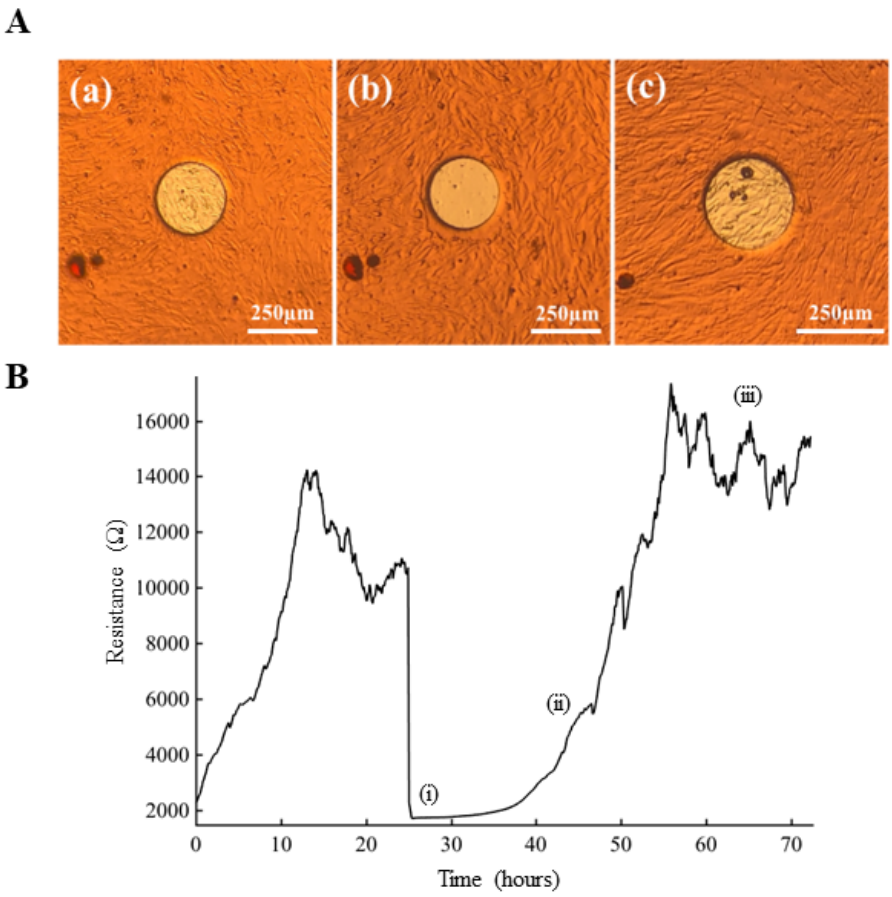

Figure 6.4 Cell settlement (sedimentation) and damage repair recorded for BJ-5ta cells. (A) microphotographs of BJ-5ta cells cultured on a gold electrode, (a) a confluent monolayer of cells, covering the electrode, (b) photograph of an empty electrode surrounded by cells; and (c) an electrode with a confluent monolayer of cells after damage repair. (B) Time dependence of electrical resistance measured at 4 kHz with the ECIS method. Region (i) correspond to the moment after damage; Region (ii) is the moment while cells are migrating and region (iii) when a monolayer is reestablished.

Wound healing experiments were also carried out using HDF cells following the same procedure as described for the BJ-5ta cells. Figure 6.5 represents the electrodes and the evolution of the electrode/cell resistance with time after cell settlement (sedimentation) on top of the electrode and during the damage repair.

Figure 6.5 plate **A** (a) is a photograph of the sensing electrode used to record the migration. Figure 6.5 plate **A** (b) represent the empty electrode and finally Figure 6.5

plate **A** (c) represent the wound repaired. Figure 6.5 plate B shows a time-trace of electrode resistance. Plateau reached a maximum value of 10.5 kΩ in the first 5 hours, and then, decreased to 8 kΩ. The maximum value was achieved much faster than BJ-5ta cells, however the plateau stabilised at lower values.

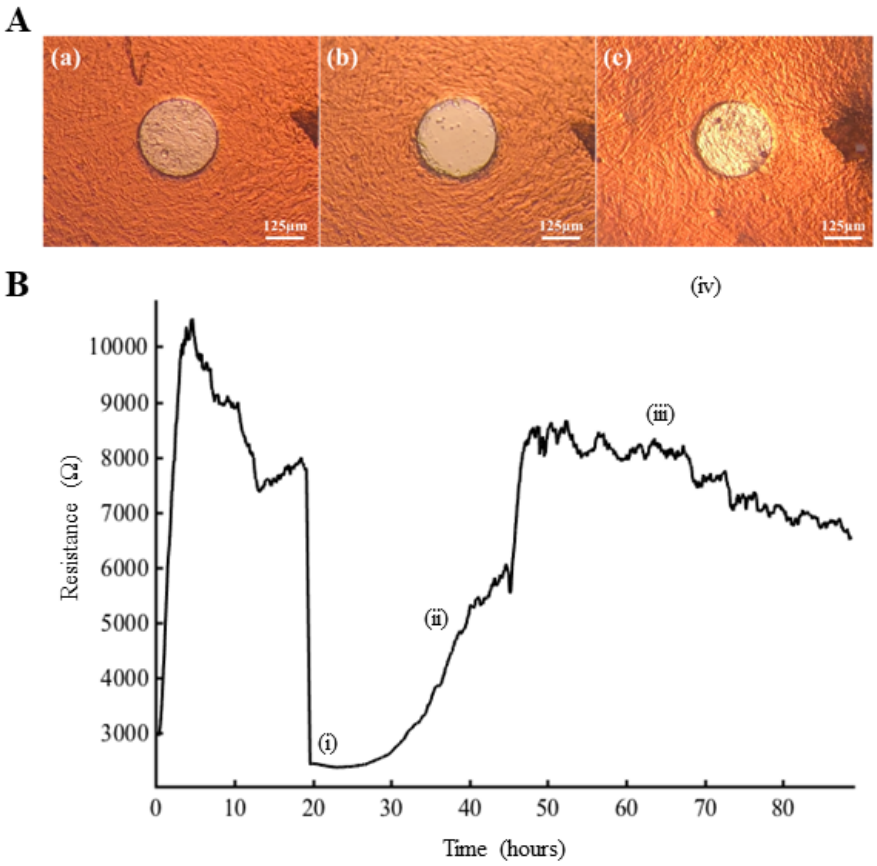

Figure 6.5 Cell sedimentation and wound healing record for HDF cells. (A) microphotographs of BJ-5ta cells cultured on a gold electrode, (a) a confluent monolayer of cells, covering all electrode, (b) photograph of empty electrode surrounded by cells; and (c) electrode after wound healing with a monolayer of cells on top of the electrode. (B) Time dependence of electrical resistance measured at 4 kHz with ECIS method. Region (i) correspond to the moment after damage; Region (ii) is the moment while cells are migrating and region (iii) when a monolayer is reestablished.

6.3.2 The effect of sex hormones on cell adhesion

Upon seeding (50,000) cells onto the electrode, noticeable differences were observed in the way different cells organize on top of the sensing electrode. Specifically, the BJ5-5ta cells gradually coated the sensing electrode, while the HDF cells underwent a distinctive re-organization within the cell population. The changes in electrode/cell resistance upon cell settlement (sedimentation) is presented in Fig. 6.6 for the two types

of cells and under exposure to different sex hormones. Initially, the HDF cells take approximately 5 hours to settle and the resistance rises to a maximum at this time and then drops until it reaches a plateau at a significantly lower resistance value. The attainment of a plateau strongly suggest that the cells undergo a re-arrangement process that results in a population of cells that are less compact and more permeable to the electric field than the population at time t=5 hours.

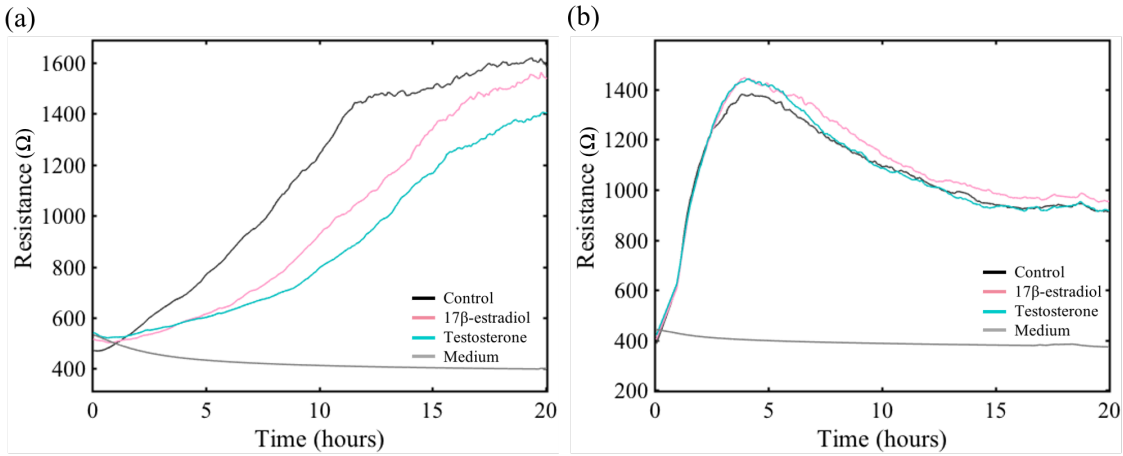

Figure 6.6 Electrode/cell resistance changes during cell seeding and attachment to the sensing electrode under exposure to different sex hormones. Assays were performed using ECIS and an 8WE10 device. (a) Change in resistance associated with BJ-5ta cell (b) Change in resistance associated with HDF cell attachment. The results represent the average of two experiments. Control: black line; 17β-Estradiol: red line; testosterone: blue line; cell culture medium alone: grey line.

This change in behaviour is not observed in the BJ-5ta. Furthermore, BJ-5ta cells coat the electrode at a slower rate.

6.3.3 Damage repair under exposure to different sex hormones

The damage repair process was monitored by the electrical resistance method when the cells were exposed to different sex hormones, testosterone, and estradiol. The results obtained are shown in Fig. 6.7 for the two cell types.

In the damage repair assays, the BJ-5ta migrated onto and recovered the electrode faster than HDF cells. This can be explained by the much longer delay before HDF cells start to migrate coupled to their slower rate of migration. Furthermore, the analysis of all the

experiments showed that there was large variability in the delay time for HDF cell migration. The reasons for this delay time are not know.

During damage repair, the striking difference between the two types of cells was the compactness of the cell monolayer covering the electrode in the BJ-5ta cells compared to the HDF cells. The resistance of the BJ-5ta cells on the electrode was twice the resistance of the electrode covered with HDF cells. This means that HDF monolayer on the electrode was much more permeable to the electric field. These results highlight the significant impact that variations in cell morphology and tissue structure can have on electrical resistance measurements during damage repair.

The difference in electric field permeability between the two types of cell populations was already discussed above in relation to settlement (sedimentation) and adhesion of the cells to the electrode. It is important to note there are some differences between the settlement and damage repair experiments. During settlement/sedimentation, cells fall from a suspension onto the electrode and later re-organize to make a monolayer. In the damage repair process, cells move from the electrode border over the empty electrode. Although the resistance plateau is noisy, a pronounced and systematic decrease in the resistance is not observed in damage repair, which means that the cells do not reorganize into a new morphological or structural arrangement. We propose that this organizational state was naturally reached during the cell migration process.

One notable and significant finding is that the electrical resistance technique can effectively distinguish between the formation of an adherent monolayer from a cell suspension and a monolayer that has migrated to the electrode.

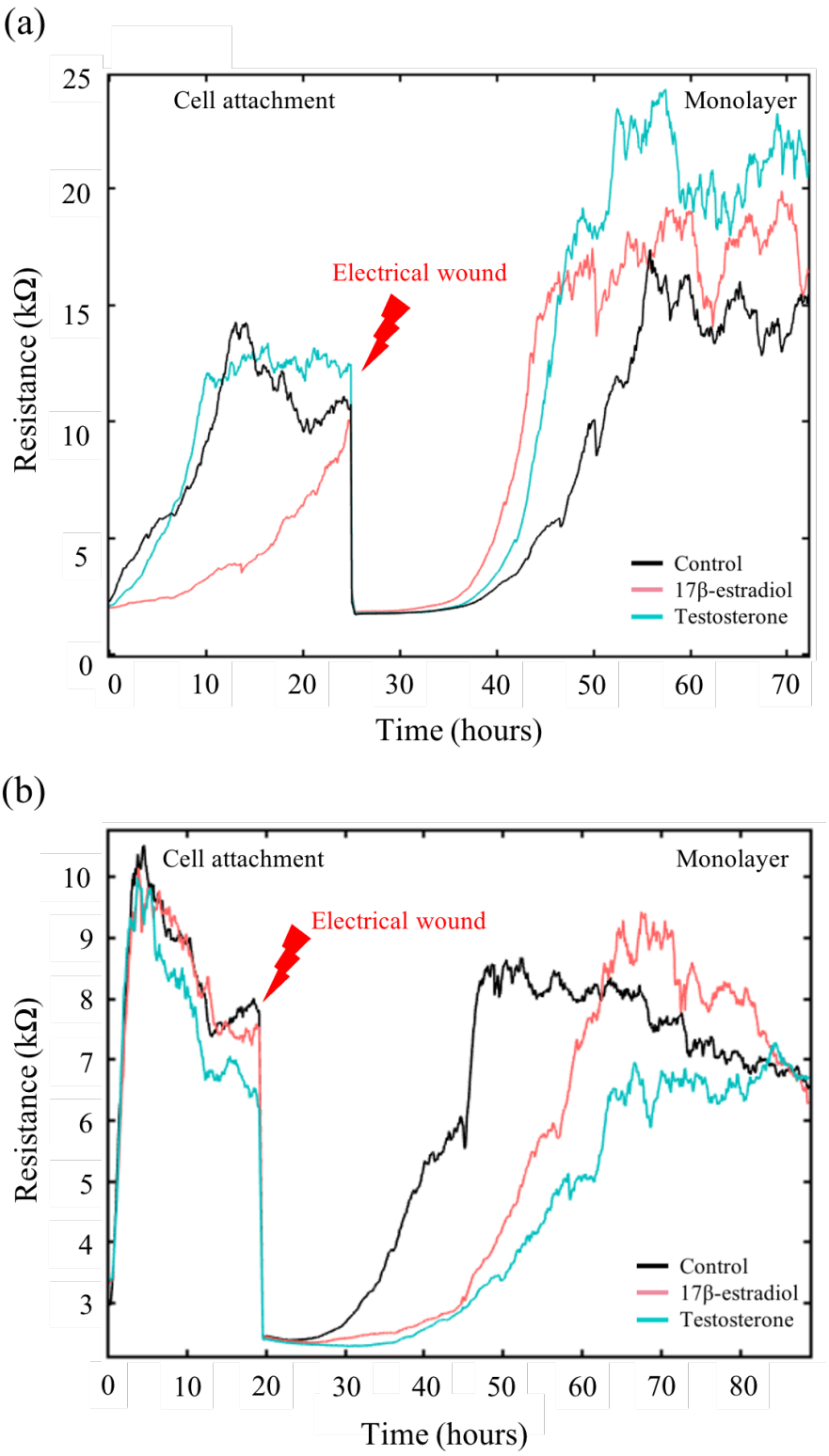

Figure 6.7. Cell seeding and damage repair experiments recorded using the time dependence of the electrical resistance of the cell/electrode interface. Changes in resistance are present in different colours for each group of treated cells in both figures (a) and (b): control cells (black), 17β-estradiol (pink) and testosterone (blue). Data are presented as the average resistance of at

least three independent experiments performed with two/three replicates for each experimental group. (a) Migration BJ-5ta cells in 8WE1. (b) Migration HDF cells in 8WE1 type of electrodes.

In damage repair experiments there are always two processes occurring, migration and proliferation and these parameters were compared in BJ-5ta and HDF cells. In addition, the effect of steroid hormones in cell proliferation was assessed. BJ-5ta and HDF cells were counted over 8 days. Cells were counted every 24 hours for the BJ-5ta cells and every 48 hours for HDF cells. The results are shown in Figure 6.8. Although in the first days after damage the HDF cells proliferated more than BJ5tA, in the long term (8 days) the number of cells was approximately equal for both types of cells. Furthermore, exposure of the cells to sex steroids did not cause any detectable difference in the proliferation rate for both types of cells.

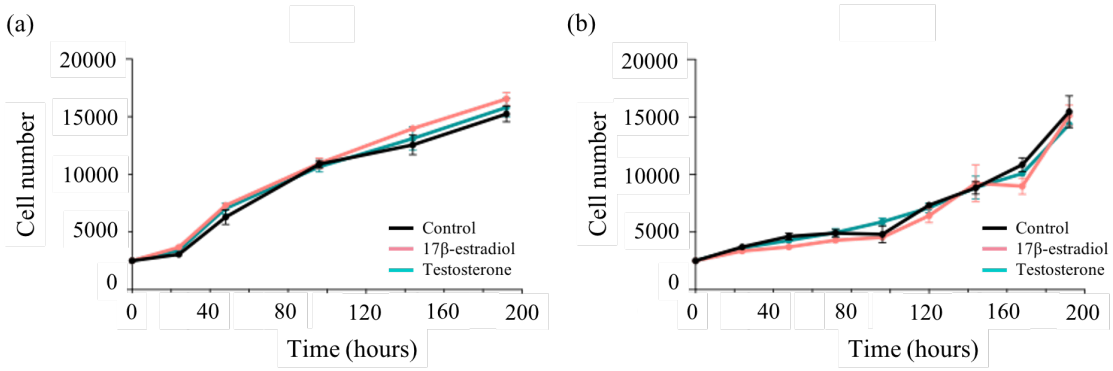

Figure 6.8 Proliferation curves of HDF (female origin) and BJ-5ta (male origin) skin fibroblasts in control conditions (normal medium), cells treated with 0.1 μM 17β-Estradiol and cells treated with 0.1 μM testosterone. The black line corresponds to the control, the pink line represents 17β-Estradiol treatment, and the blue line represents testosterone treatment for both cell lines. The results are shown as the average ± SEM of 3 technical replicates Data was analysed using a Two-way Anova followed by a Tukey's multiple comparison test and the statistical analysis was performed using GraphPad Prism version 7.0a.

6.3.4 Conventional scratch assay

To validate our electrical based measurements, we also conducted a conventional scratch assay. In this method the damage was caused by a mechanical scratch with a sharp 200 μL tip in a confluent cell layer and then the repair was monitored by visual inspection. The damage repair rate was quantified by measuring the damaged area at different time points after scratching with a microscope and the area of the gap between the cells on either side of the scratch was estimated. The results of the scratch assays performed with

both BJ-5ta cells and HDF cells are shown in Figure 6.9 and 6.10, respectively. Both HDF cells and BJ-5ta cells take a similar time to repair the damage and full repair occurred after 24 hours.

6.3.4.1 Immunocytochemistry of cytoskeleton

To further investigate the cellular effect of sex steroid on skin fibroblasts immunocytochemistry of the cytoskeleton was studied. If the steroids modified the cytoskeleton, this might explain their different migratory capacity.

Immunocytochemistry analysis showed when cells were exposed to steroids the cell cytoskeleton was changed. Figure 6.9 (c) shows in green, the tubulin filaments throughout the cell cytoplasm of BJ-5ta cells, while actin filaments (red) were concentrated in cells at the migration front. In HDF cells, Figure 6.10 (c), tubulin filaments (green) were concentrated near to the nucleus, while actin filaments (red) were intense throughout the cell cytoskeleton. The actin and tubulin filaments were modified in appearance when steroids were present. I particular actin filaments tended to be condensed in cells at the damage repair front and similar observations have previously been reported[160], and actin is suggested to drive cell migration during damage repair[161].

Although the cell cytoskeleton changed in the presence of steroids, both the scratch assay and the electrical impedance measurements did not reveal a significant change in the rate of damage repair.

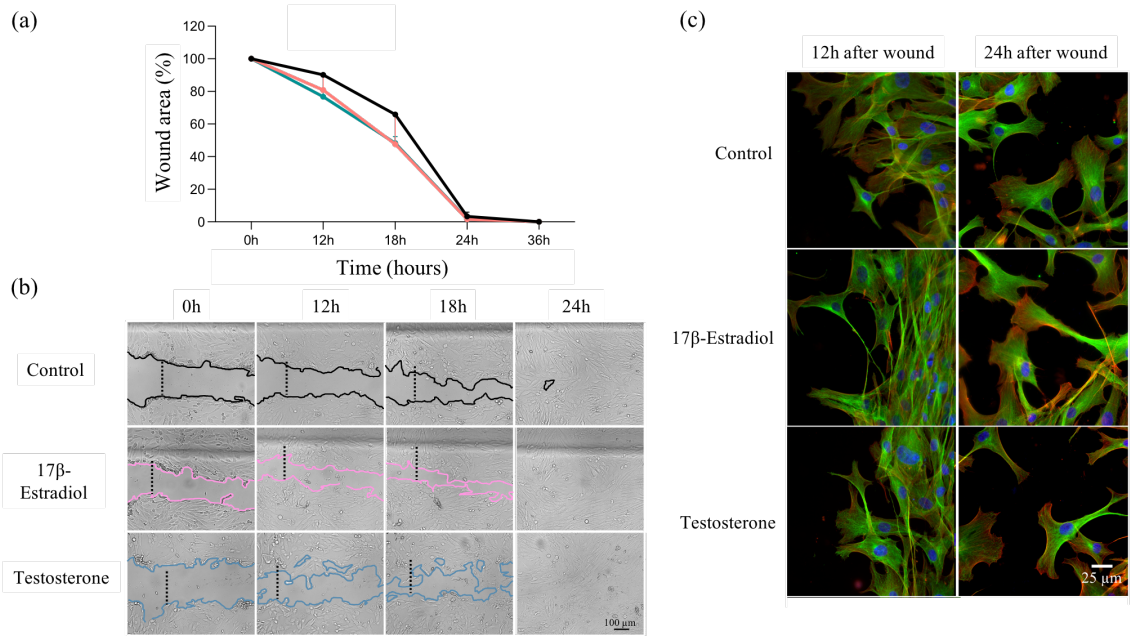

Figure 6.9 BJ-5ta cells during scratch assays. (a) Scratch area (percentage) was measured at 0 h, 6 h, 12h and 24 h in relation to the area immediately after the scratch was made (100%). The results are shown as the average ± SEM of one experiment with 3 technical replicates. The data were analysed using a two-way ANOVA followed by Tukey's Multiple Comparison test. (b) Scratch assay (10x) of BJ-5ta cells showing the progression of the scratch recover across time on Control with no treatment is in black, 17β-Estradiol in pink and testosterone in blue. The scale bars indicate 100 µm. (c) Immunocytochemistry of BJ-5ta cells with 0.1 µM 17β-Estradiol and 0.1 µM testosterone at 6h and 12h after wound. BJ-5ta cells were labelled with a monoclonal anti-α-tubulin antibody produced in mouse and detected with a goat anti-mouse IgG (H+L) Secondary antibody, Alexa Fluor 488 conjugate (alpha tubulin in green) and stained with Texas Red®-X Phalloidin (actin filaments in red) and DAPI (nuclei in blue). The images are representative of cells after 6h after scratching (on the left) and 12h after scratching (on the right), for control, 17β-estradiol and testosterone (first, second and third line, respectively). The scale bars indicate 25 µm. All images were obtained with a Leica DM IL microscope coupled to a Visicam HDMI 6 digital camera and analysed using image J.

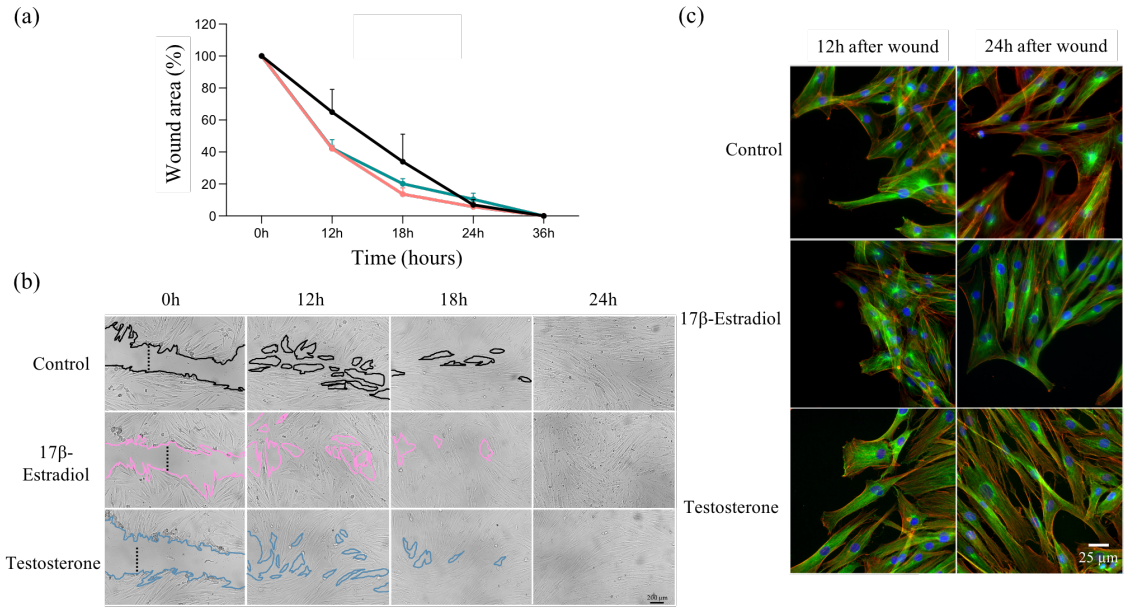

Figure 6.10 HDF cells during scratch assay. (a) Scratch area (percentage) was measured at 0 h, 12 h, 18h and 24 h in relation to the area immediately after the scratch (100%). The results are shown as the average ± SEM of one experiment with 3 technical replicates. The data were analysed using a two-way ANOVA followed by Tukey's Multiple Comparison test. (b) Scratch assay (10x) of HDF cells showing the progression of the scratch recover across time on Control with no treatment is in black, 17β-Estradiol in pink and testosterone in blue (c) Immunocytochemistry of HDF cells with 0.1 µM 17β-Estradiol and 0.1 µM testosterone at 12h and 24h after wound. HDF cells were labelled with a monoclonal anti-α-tubulin antibody produced in mouse and detected with a goat anti-mouse IgG (H+L) Secondary antibody, Alexa Fluor 488 conjugate (alpha tubulin in green) and stained with Texas Red®-X Phalloidin (actin filaments in red) and DAPI (nuclei in blue). The images are representative of cells after 12h after scratching (on the left) and 24h after scratching (on the right), for control, 17β-estradiol and testosterone (first, second and third line, respectively). The scale bars indicate 25 µm. All images were obtained with a Leica DM IL microscope coupled to a Visicam HDMI 6 digital camera and analysed using image J.

6.3.5 Electrophysiological activity of dermal fibroblast cells

In this section we discuss the electrophysiological activity of a cell population under two distinct situations: (i) activity upon cell seeding and attachment to the electrodes and (ii) activity during damage repair. The differences and similarities are discussed for both types of dermal fibroblast cells (HDF and BJ-5ta) and compared with the migration of C6 (glial) cells.

6.3.5.1 Electrophysiology of dermal fibroblast during cell attachment

Above, when discussing cell attachment to the electrodes, we reported a peculiar behaviour only observed in the HDF cells (cells with a female origin). After 5 hours elapsed from cell seeding, HDF cells underwent a reorganization on the electrode surface that led to a less compact population, or to a population that was more permeable to the electric field. This reorganization should in principle also be detected in the electrophysiological data.

To confirm the above hypothesis, several electrophysiological time traces recorded on HDF cells, indeed showed a silent region of 5-6 hours followed by a strong activity burst. Fig. 6.11 shows an example recorded for HDF during cell seeding. This behaviour was not observed in the BJ-5ta cells.

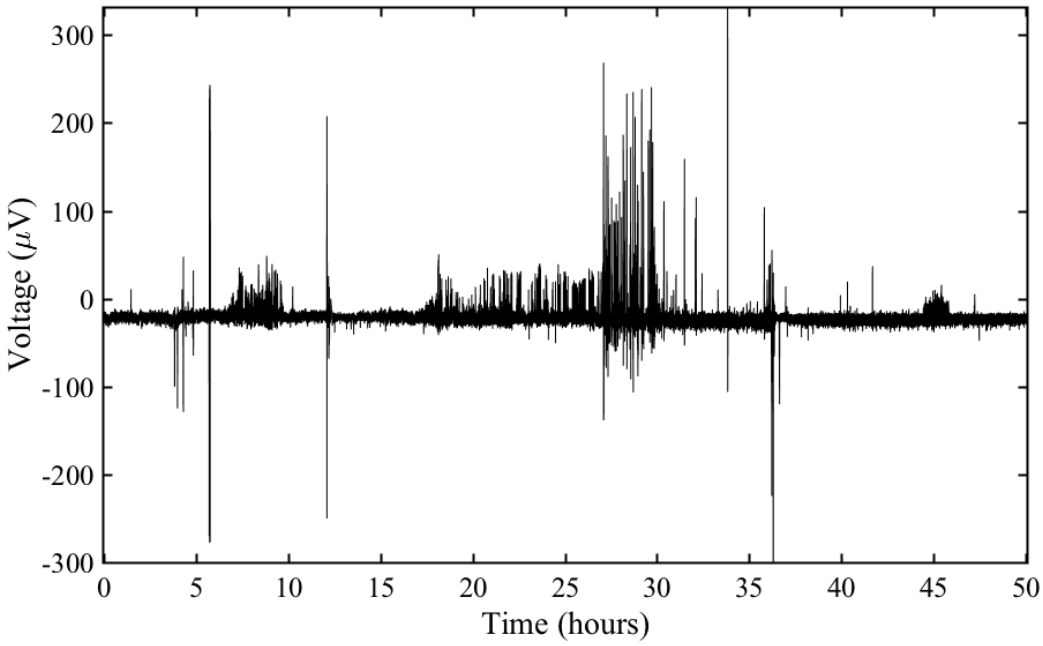

Figure 6.11 Electrophysiological time trace recorded on a population of HDF cells upon cell seeding on top of gold electrode.

According to the impedance data, the change in behaviour after a 5-hour period, was exclusively observed during cell settlement (from a suspension) on the electrode surface. However, we found a remarkable example with the NHDF cells in which the

electrophysiological behaviour also changes 5 hours after damage was inflicted on the cell population. This striking example is shown in Fig. 6.12. After damage caused by an electrical discharge the cells remained silent for 5 hours after which a strong burst of activity was observed.

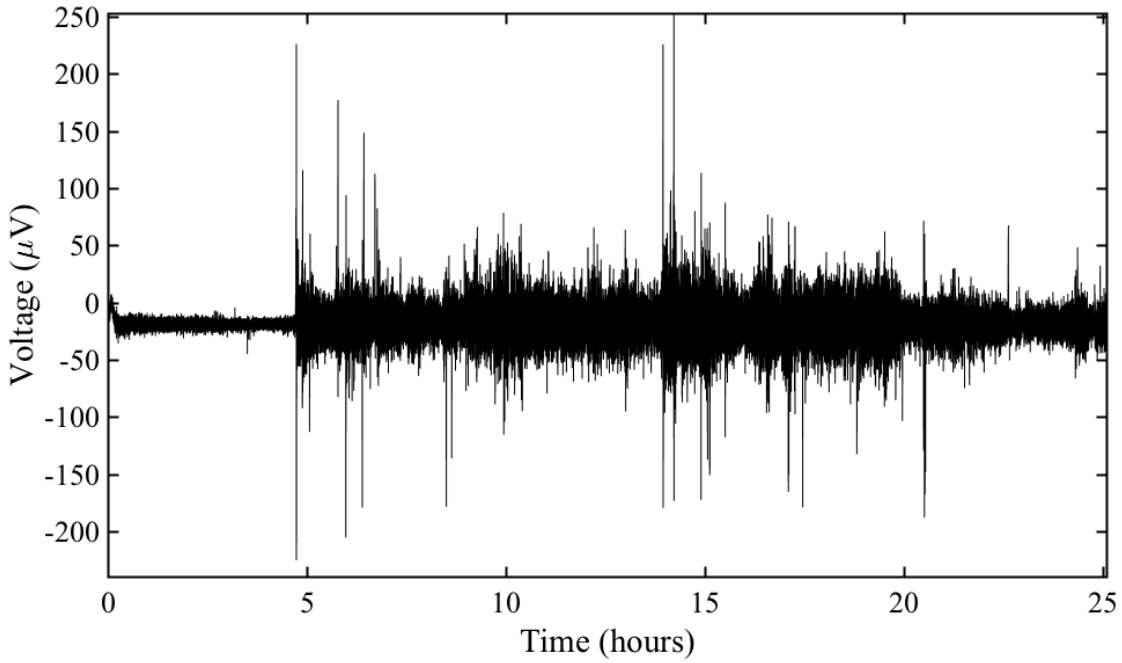

Figure 6.12 Electrophysiological time trace recorded on a population of NHDF cells upon a wound was created by a train of electrical pulses.

6.3.5.2 Electrophysiology activity during wound healing

In a previous study[150] our research group reported the electrophysiological behaviour of a migrating cancer cell population. We reported that as the cells migrate onto the sensing electrode discrete signals were recorded. The frequency and the amplitude of the signals increased with the number of cells covering the sensing electrode. The overall electrophysiological time trace recorded from the onset of the migration until the full electrode coverage was reached led to an electrophysiological time trace that was comprised of signals with an increased signal amplitude until saturation was reached. This behaviour leads to a signal time trace with a V-shape as shown in Fig. 6.13. The cell migration was also monitored using impedance-based methods, and as expected the resistance as a function of the time also saturates into a resistance plateau which coincides in time with the appearance of the plateau in the electrophysiological signal time trace. The strong correlation between the two, the electrophysiological time trace and the impedance time trace led us to propose that electrophysiological devices can be used to

monitor in real time the migration of cancer cells. A typical migration experiment of C6 cells is illustrated in Fig. 6.13.

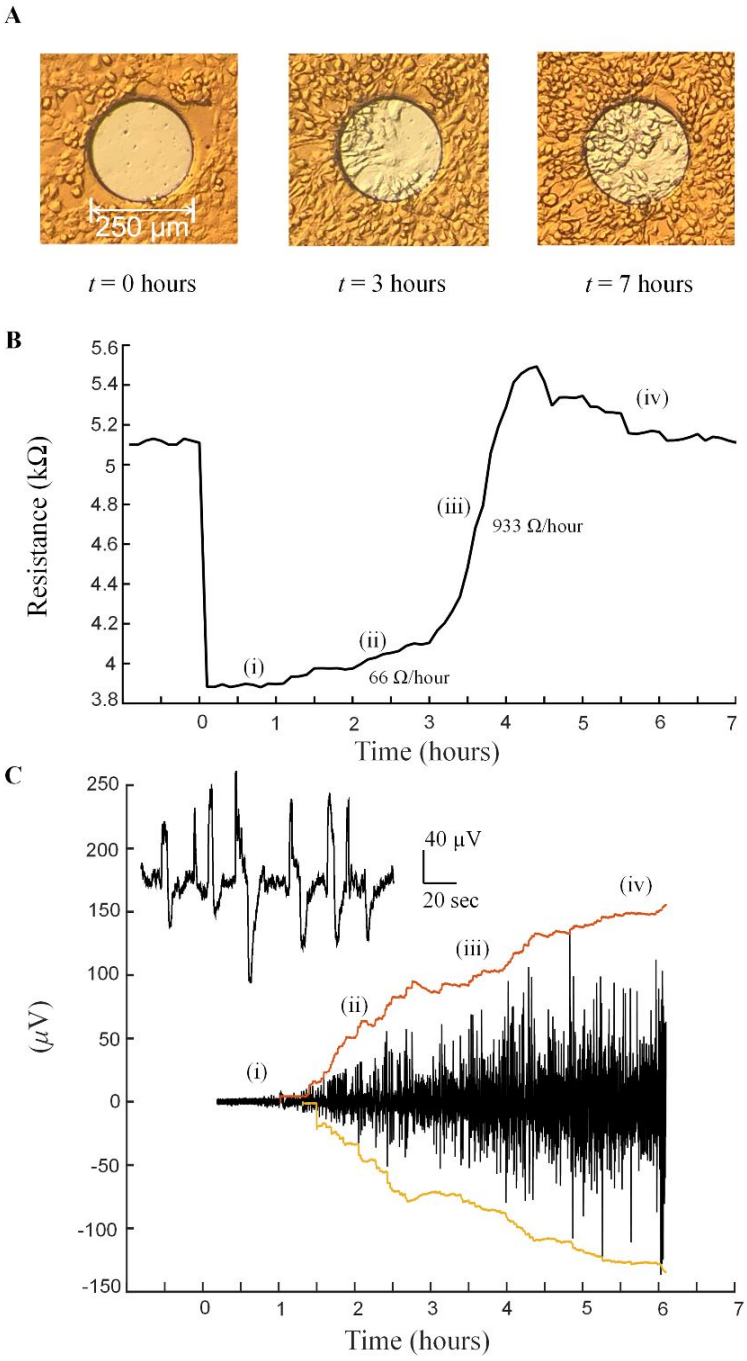

Figure 6.13 Migration of C6 glioma cells monitored by microscopy, electrophysiological measurements and small signal impedance measurements. (A) A sequence of photographs showing the migration of the C6 glioma cells onto the central sensing electrode. (B) The time dependence of the electrical resistance measured at a frequency of 10 kHz (ECIS method). (C) The time dependence of the electrophysiological signals generated by the C6 glioma cells as they migrate onto and cover the sensing electrode surface. The inset in (C) gives a detailed view of the

signal recorded 3 hours after the start of the experiment. The red line represents the cumulative sum of the signals over intervals of 5 minutes.

Figure 6.14 shows two typical electrophysiological time traces recorded for the BJ-5ta cells and for the HDF cell.

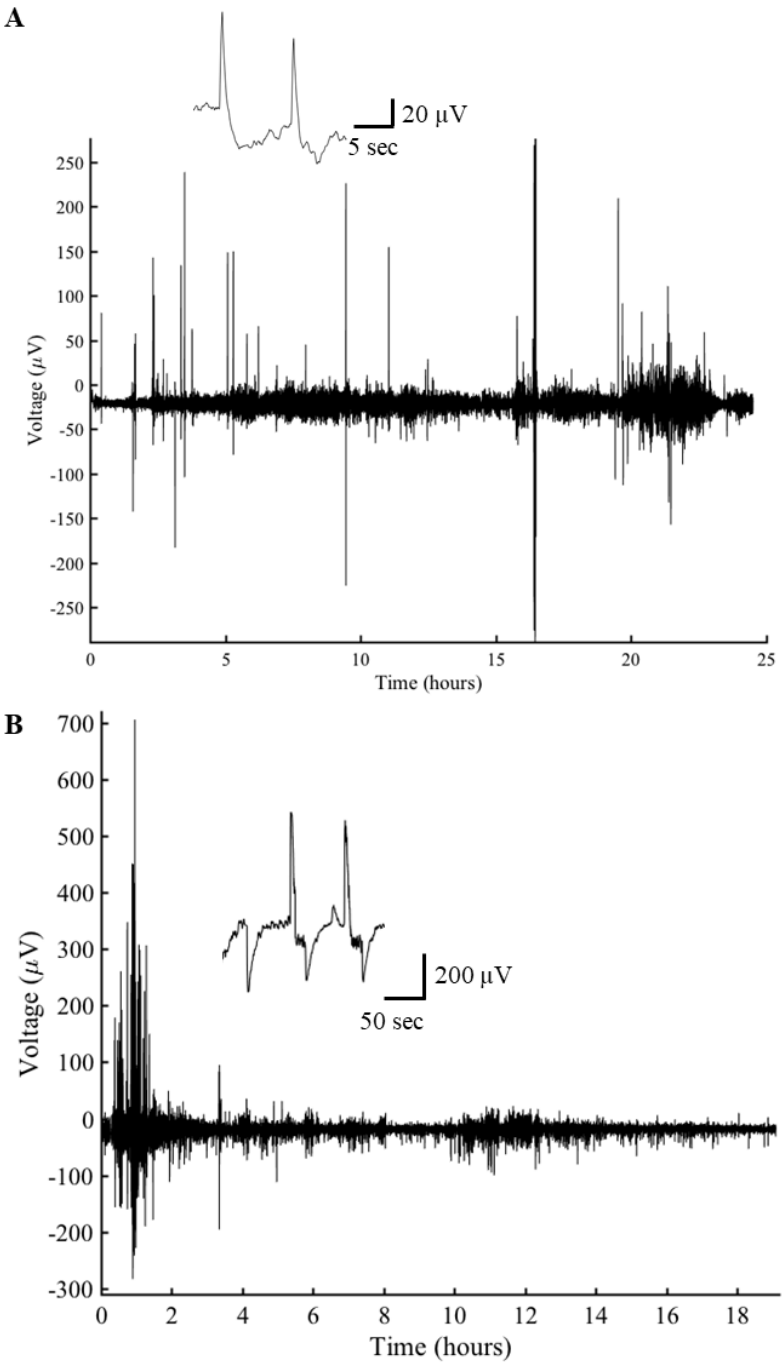

Figure 6.14 Electrophysiological time traces of migrating fibroblast cells after an electrical wound were inflicted in the cell population. (A) the BJ-5ta cell population and (B) for a HDF cell population. Both signal traces were measured in a in 8WE1 device.

The electrophysiological time trace of dermal fibroblast does not show the typical V-shape recorded for the C6 cells. Instead, the amplitude of the signals fluctuates randomly.

A few interesting differences between the HDF cells and the BJ-5ta cells are worth mentioning. The electrophysiological time trace recorded in the BJ-5ta cells is not characterized by any particular periodic behaviour. Bioelectrical signals appear very early, just a few hours after the wound. The overall signal pattern is comprised of burst of activity often modulated in amplitude. A specific long-term burst pattern was not identified. A typical example of an electrophysiological time trace recorded on BJ-5ta cells is show in Fig. 6.14 **A**.

HDF cell population also showed bursts of activity within a few hours after the wound. The activity remained intense for a couple of hours. After this early strong activity, the remaining bioelectrical recording remains relatively quiet for relatively long periods. Fig. 6.14 B shows a typical time trace recorded on HDF cells after a wound.

6.4. Conclusions

The mains conclusion of this study can be summarized as follows:

(a) Establishment of a cell population in a sensing electrode. Differences between the two types of dermal fibroblast cells.

When seeded onto an electrode, BJ-5ta and HDF cells exhibited distinct behaviours. BJ-5ta cells formed a progressively denser population that completely covered the electrode surface. On the other hand, the HDF cell population initially showed a similar trend to the BJ-5ta, but after the first 5 hours, the resistance slowly decreased with time to a steady state plateau, indicating that the population began to re-organize in a way that was more permeable to the electric field. This suggests a morphological reorganization of the cell and a less compact cell population.

This cell seeding behaviour can be effectively observed through electrical methods, highlighting the power of these techniques for monitoring cell populations. Interestingly, such phenomenon is not easily detected through visual inspection using microscopy techniques.

(b) Effect of hormones on damage repair.

When exposed to estradiol, a female hormone, cells of female origin (HDF) exhibited a more compact cell population. Similarly, exposure to testosterone led to a more compact cell population in cells of male origin (Bj-5ta). However, the number of experiments was insufficient to obtain statistically significant results.

Interestingly, exposure to sex hormones does not seem to affect the speed of cell migration in both types of dermal fibroblast cells. Nevertheless, to fully repair damage, HDF cells were slower than BJ-5ta cells due to a longer delay time before the onset of migration, rather than differences in migration speed, which was approximately 14 μm/hour for both cell types.

(c) Electrophysiological behaviour during a wound repair.

This study revealed that different cell types exhibited different migration patterns. Specifically, C6 cells rapidly covered the electrode surface and organized themselves into clusters, generating electrophysiological signals with increasing power. The maximum amplitude of these signals was reached when the cells achieved confluence. The V-shape of the electrophysiological time trace indicated when the electrode was fully coated, allowing for easy extraction of the migration speed.

When compared to C6 cells and dermal fibroblasts different electrophysiological activity was exhibited. After damage to the monolayer occurred, dermal cells produced strong electrophysiological signals within a few hours, which might be the instruction for initiating wound repair. It is speculated that this burst of signals at the onset of migration could be due to a chemical cue released by the damaged cells into the medium.

The electrophysiological activity of dermal fibroblast cells is different from the C6 cells. Dermal cells generate strong electrophysiological signals within a few hours after damage. We speculate that the strong burst of signals at the onset of migration in the fibroblast type of cells, is an instruction to begin the wound repair. It is possible that the instruction may have its origin in a chemical cue released into the medium by the damaged cells.

During the course of cell migration, bursts of signals modulated in amplitude were typically observed. The highest power bursts were typically recorded when cells had reached confluence. However, cells also became silent when they were confluent, and

this seemingly random behaviour precludes obtaining information about migration speed as was possible in the case of C6 cells. Consequently, further research is necessary to extract relevant insights from the electrophysiological behaviour of dermal fibroblasts.

CHAPTER 7

Conclusions and further work

"It's always seems impossible until it's done" Nelson Mandela

This chapter is to provide an overview of the key achievements and conclusions from the work carried out in this thesis. It includes a discussion of the correlations between the major findings and how they contribute to our understanding of how cells organize and communicate. Additionally, this chapter highlights the ongoing challenges involved in interpreting electrophysiological data from cell populations, along with suggestions for further research in this field.

7.1 Summary of the major findings

This thesis aimed to investigate the measurement of cell bioelectrical activity using extracellular electrodes *in vitro*. One of the primary accomplishments was the successful development of electrodes with an intrinsic noise level below 1 microvolt *r.m.s*. These electrodes were then utilized to measure the bioelectrical activity of populations of immortal cells, primary cell cultures, and *ex-vivo* tissues. In the following topics, we outline the major contributions of this thesis.

1. Extracellular devices to measure the electrophysiological activity of astrocytes populations

We conducted a study in which a population of primary cultured astrocytes was grown on top of large-area microstructured electrodes. Compared to conventional microelectrode arrays (MEAs), the microstructured electrodes utilized in this study offered significantly lower impedance and very low intrinsic thermal noise. These features enabled us to measure low-frequency astrocyte signalling for the first time using extracellular electrodes.

2. Extracellular electrophysiological based sensor to monitor cell migration

An electrophysiological-based method was developed by our group to quantify cell migration speed and the establishment of cell-cell connections seeded on top of electrodes. The work carried out in this thesis aimed to validate the technology and develop a new instrument or biological assay for monitoring cell migration. We conducted evaluations of our method on two distinct cell types, dermal fibroblast cells, and C6 glia cells. It was observed that the electrophysiological time trace properties varied significantly based on the cell type under study. This variability is not surprising since each migrating cell type serves a different purpose. C6 cancer cells aim to infiltrate surrounding tissues, while dermal fibroblasts aim to repair a damaged tissue. As a result, we conclude that our electrophysiological method for monitoring cell migration must be tailored to the specific properties of the cell type being studied and, therefore, cannot be universally applied.

7.2 Suggestions for further work

Our primary objective is to optimize our sensing devices and validate them through measurements in cell cultures, in order to better understand the cellular behaviour of astrocytes and neurons in both healthy and cancerous states. Given the prevalence of astrogliosis in nearly all neurodegenerative disorders, we believe it should be a subject of more intense study. In addition, to its relevance to neurodegenerative diseases, bioelectronic communication also plays a crucial role in tissue regeneration. Therefore, we anticipate that our research will ultimately contribute to the development of technologies and tools in the areas of tissue engineering and regenerative medicine. Below, we outline specific research topics that are timely and relevant to this field.

A) Artificial intelligence tools for signal pattern recognition in cell populations

Measuring cell populations is a major challenge as the sensing electrode does not probe a single cell but rather an ensemble of cells. This often leads to measuring the collective electrophysiological activity, which can result in a noisy overall electrophysiological time trace. This is expected when the cells or a large number of cell clusters are not synchronized with each other. To address this challenge, we propose that artificial intelligence (AI) tools should be used to decipher the signal patterns generated by the superimposed signals in the electrophysiological time trace. AI algorithms can differentiate the underlying signals and separate out the noise caused by overlapping signals.

B) Optimization of the electrode geometrical parameters

It is important to have an idea of what is the typical size of a coordinated or synchronized cell cluster. In other words, what is the typical number of cells that can be synchronized? If we know the number of cells, that on average can be synchronized, we can design electrodes with the ideal area to pick these synchronized cell ensembles. The information gathered from the AI tools (described in the above point) may help us to get an idea of the number of cells that on average can synchronize and lay down some rules for the design of the electrodes.

Another important aspect to take into consideration in the design of the electrodes is the type of biological signal that is generated by the cells. If it is a static signal or a traveling wave. By static signal, we understand a signal generated by a cluster of cells that

synchronize to produce an oscillation. However, this oscillation remains within the boundaries of the cell population (cluster) generating it and does not travel to the nearby cells. If the oscillation travels, then it is defined as a traveling wave. Static signals and traveling waves require a different type of electrode geometries. If the signal is a traveling wave, finger-like electrodes with specific width and space between fingers should be used. A proper design will allow us to obtain the wave speed and the traveling distance along the population of the cell.

C) Implantable device

The findings reported in this thesis represent a significant step forward in the development of a device capable of recording and modulating the electrical activity of brain tumours. Our short-term goal is to develop electrodes based on polymers printed on soft, flexible, and biocompatible cellulose substrates to record the electrical activity of brain tumours, while also providing the ability to electrically stimulate or inhibit tumour growth. These devices should have the potential to serve as implantable electroceutical devices that can inhibit cell migration and proliferation.

D) Drug screening platform

This thesis demonstrates the spontaneous and evoked activity of a population of non-electrogenic cells using extracellular electrodes. Our novel electrode design has the potential to be used to evaluate new drugs developed to restore normal bioelectrical activity and stop the irregular activity of cells, potentially contributing to new drug discovery. Our electrophysiological method is non-invasive and allows for real-time measurements, making it a promising approach for the development of new diagnostic and therapeutic tools. A particular interesting area is the development of novel drugs to promote tissue regeneration.

References

1. Purves, D. *et al. Neuroscience, 5th Edition*. *Nature Reviews Neuroscience* (2012). doi:978-0878937257

2. Medeiros, M. C. R. *et al.* An electrical method to measure low-frequency collective and synchronized cell activity using extracellular electrodes. *Sens. Bio-Sensing Res.* **10**, 1–8 (2016).

3. Mestre, A. L. G. *et al.* Ultrasensitive gold micro-structured electrodes enabling the detection of extra-cellular long-lasting potentials in astrocytes populations. *Sci. Rep.* **7**, 14284 (2017).

4. Mestre, A. L. G. *et al.* Extracellular Electrophysiological Measurements of Cooperative Signals in Astrocytes Populations. *Front. Neural Circuits* **11**, 1–9 (2017).

5. Özsoylu, D., Wagner, T. & Schöning, M. J. Electrochemical Cell-based Biosensors for Biomedical Applications. *Curr. Top. Med. Chem.* **22**, 713–733 (2022).

6. Tanwar, A., Gandhi, H. A., Kushwaha, D. & Bhattacharya, J. A review on microelectrode array fabrication techniques and their applications. *Mater. Today Chem.* **26**, 101153 (2022).

7. Baer, M. L., Henderson, S. C. & Colello, R. J. Elucidating the role of injury-induced electric fields (EFs) in regulating the astrocytic response to injury in the mammalian central nervous system. *PLoS One* **10**, (2015).

8. McCaig, C. D., Rajnicek, A. M., Song, B. & Zhao, M. Controlling Cell Behavior Electrically: Current Views and Future Potential. *Physiol. Rev.* **85**, 943–978 (2005).

9. Hamill, O. P., Marty, A., Neher, E., Sakmann, B. & Sigworth, F. J. Improved patch-clamp techniques for high-resolution current recording from cells and cell-free membrane patches. *Pflügers Arch. - Eur. J. Physiol.* **391**, 85–100 (1981).

10. Stett, A. *et al.* Biological application of microelectrode arrays in drug discovery and basic research. *Anal. Bioanal. Chem.* **377**, 486–495 (2003).

11. Martinoia, S. *et al.* Development of ISFET array-based microsystems for bioelectrochemical measurements of cell populations. *Biosens. Bioelectron.* **16**,

1043–1050 (2001).

12. Thompson, E. G. & Sontheimer, H. A role for ion channels in perivascular glioma invasion. *European Biophysics Journal* (2016). doi:10.1007/s00249-016-1154-x

13. Haas, B. R. & Sontheimer, H. Inhibition of the sodium-potassium-chloride cotransporter isoform-1 reduces glioma invasion. *Cancer Res.* (2010). doi:10.1158/0008-5472.CAN-09-4666

14. Rooj, A. K. *et al.* Glioma-specific cation conductance regulates migration and cell cycle progression. *J. Biol. Chem.* **287**, 4053–4065 (2012).

15. Veiseh, O., Kievit, F. M., Ellenbogen, R. G. & Zhang, M. Cancer Cell Invasion: Treatment and Monitoring Opportunities in Nanomedicine. *Advanced Drug Delivery Reviews* (2011). doi:10.1016/j.addr.2011.01.010

16. Morrone, F. B., Gehring, M. P. & Nicoletti, N. F. Calcium Channels and Associated Receptors in Malignant Brain Tumor Therapy. *Mol Pharmacol* **90**, 403–409 (2016).

17. Munaron, L., Antoniotti, S., Fiorio Pla, A. & Lovisolo, D. Blocking Ca2+entry: a way to control cell proliferation. *Curr. Med. Chem.* (2004). doi:10.2174/0929867043365008

18. Olsen, M. L., Schade, S., Lyons, S. A., Amaral, M. D. & Sontheimer, H. Expression of voltage-gated chloride channels in human glioma cells. *J. Neurosci.* **23**, 5572–82 (2003).

19. Yang, M. & Brackenbury, W. J. Membrane potential and cancer progression. *Frontiers in Physiology* (2013). doi:10.3389/fphys.2013.00185

20. Soroceanu, L., Manning, T. J. & Sontheimer, H. Modulation of glioma cell migration and invasion using Cl(-) and K(+) ion channel blockers. *J. Neurosci.* (1999).

21. Weaver, A. K., Bomben, V. C. & Sontheimer, H. Expression and function of calcium-activated potassium channels in human glioma cells. *Glia* (2006). doi:10.1002/glia.20364

22. Giaume, C. & Naus, C. C. Connexins, gap junctions, and glia. *Wiley Interdiscip. Rev. Membr. Transp. Signal.* **2**, 133–142 (2013).

23. Dere, E. & Zlomuzica, A. The role of gap junctions in the brain in health and disease. *Neurosci. Biobehav. Rev.* **36**, 206–17 (2012).

24. Bruzzone, R. & Dermietzel, R. Structure and function of gap junctions in the developing brain. *Cell Tissue Res.* **326**, 239–248 (2006).

25. Nakase, T. & Naus, C. C. G. Gap junctions and neurological disorders of the central nervous system. *Biochim. Biophys. Acta* **1662**, 149–58 (2004).

26. Giaume, C. & McCarthy, K. D. Control of gap-junctional communication in astrocytic networks. *Trends Neurosci.* **19**, 319–25 (1996).

27. Zhang, W. *et al.* Direct gap junction communication between malignant glioma cells and astrocytes. *Cancer Res.* **59**, 1994–2003 (1999).

28. Oliveira, R. *et al.* Contribution of gap junctional communication between tumor cells and astroglia to the invasion of the brain parenchyma by human glioblastomas. *BMC Cell Biol.* **6**, (2005).

29. Lin, J. H. C. *et al.* Connexin 43 enhances the adhesivity and mediates the invasion of malignant glioma cells. *J. Neurosci.* **22**, 4302–4311 (2002).

30. Lee, S. H., Kim, W. T., Cornell-Bell, A. H. & Sontheimer, H. Astrocytes exhibit regional specificity in gap-junction coupling. *Glia* **11**, 315–25 (1994).

31. Cervera, J., Alcaraz, A. & Mafe, S. Membrane potential bistability in nonexcitable cells as described by inward and outward voltage-gated ion channels. *J. Phys. Chem. B* (2014). doi:10.1021/jp508304h

32. Chappell, M. & Payne, S. The Action Potential. in *Biosystems and Biorobotics* (2020). doi:10.1007/978-3-030-39705-0_3

33. Perea, G., Navarrete, M. & Araque, A. Tripartite synapses: astrocytes process and control synaptic information. *Trends in Neurosciences* **32**, 421–431 (2009).

34. Parpura, V., Grubišic, V. & Verkhratsky, A. Ca2+ sources for the exocytotic release of glutamate from astrocytes. *Biochimica et Biophysica Acta - Molecular Cell Research* **1813**, 984–991 (2011).

35. He, H. *et al.* Ca 2+ waves across gaps in non-excitable cells induced by femtosecond laser exposure. *Appl. Phys. Lett.* (2012). doi:10.1063/1.4707375

36. Nedergaard, M., Ransom, B. & Goldman, S. A. New roles for astrocytes: Redefining the functional architecture of the brain. *Trends Neurosci.* **26**, 523–530 (2003).

37. Wang, G. Y., Lian, K. & Chu, T.-Y. Electrolyte-Gated Field Effect Transistors in Biological Sensing: A Survey of Electrolytes. *IEEE J. Electron Devices Soc.* **9**, 939–950 (2021).

38. Béraud, A. *et al.* Graphene field-effect transistors as bioanalytical sensors: design, operation and performance. *Analyst* **146**, 403–428 (2021).

39. Asgarifar, S. *et al.* Electrochemically Gated Graphene Field-Effect Transistor for Extracellular Cell Signal Recording. in *IFIP Advances in Information and Communication Technology* **470**, 558–564 (2016).

40. Tao, J., Sun, W. & Lu, L. Organic small molecule semiconductor materials for OFET-based biosensors. *Biosens. Bioelectron.* **216**, 114667 (2022).

41. Sun, C., Wang, X., Auwalu, M. A., Cheng, S. & Hu, W. Organic thin film transistors-based biosensors. *EcoMat* **3**, (2021).

42. Ullah, H. *et al.* Recent Advances in Stretchable and Wearable Capacitive Electrophysiological Sensors for Long-Term Health Monitoring. *Biosensors* **12**, 630 (2022).

43. Zhang, A., Lee, J.-H. & Lieber, C. M. Nanowire-enabled bioelectronics. *Nano Today* **38**, 101135 (2021).

44. Bergveld, P. Development of an Ion-Sensitive Solid-State Device for Neurophysiological Measurements. *IEEE Trans. Biomed. Eng.* **BME-17**, 70–71 (1970).

45. Sharma, B. K. & Ahn, J.-H. Graphene based field effect transistors: Efforts made towards flexible electronics. *Solid. State. Electron.* **89**, 177–188 (2013).

46. Spanu, A., Martines, L. & Bonfiglio, A. Interfacing cells with organic transistors: a review of in vitro and in vivo applications. *Lab Chip* **21**, 795–820 (2021).

47. Chen, K.-I., Li, B.-R. & Chen, Y.-T. Silicon nanowire field-effect transistor-based biosensors for biomedical diagnosis and cellular recording investigation. *Nano Today* **6**, 131–154 (2011).

48. Robinson, J. T., Jorgolli, M. & Park, H. Nanowire electrodes for high-density stimulation and measurement of neural circuits. *Front. Neural Circuits* **7**, 38 (2013).

49. Timko, B. P. *et al.* Electrical recording from hearts with flexible nanowire device arrays. *Nano Lett.* **9**, 914–8 (2009).

50. Keefer, E. W., Botterman, B. R., Romero, M. I., Rossi, A. F. & Gross, G. W. Carbon nanotube coating improves neuronal recordings. *Nat. Nanotechnol.* **3**, 434–439 (2008).

51. Mazzatenta, A. *et al.* Interfacing Neurons with Carbon Nanotubes: Electrical Signal Transfer and Synaptic Stimulation in Cultured Brain Circuits. *J. Neurosci.* **27**, 6931–6936 (2007).

52. Shein, M. *et al.* Engineered neuronal circuits shaped and interfaced with carbon nanotube microelectrode arrays. *Biomed. Microdevices* **11**, 495–501 (2009).

53. Sessolo, M. *et al.* Easy-to-fabricate conducting polymer microelectrode arrays. *Adv. Mater.* **25**, 2135–2139 (2013).

54. Richardson-Burns, S. M., Hendricks, J. L. & Martin, D. C. Electrochemical polymerization of conducting polymers in living neural tissue. *J. Neural Eng.* **4**, L6–L13 (2007).

55. Nyberg, T., Shimada, A. & Torimitsu, K. Ion conducting polymer microelectrodes for interfacing with neural networks. *J. Neurosci. Methods* **160**, 16–25 (2007).

56. Leleux, P. *et al.* Conducting polymer electrodes for electroencephalography. *Adv. Healthc. Mater.* **3**, 490–3 (2014).

57. Khodagholy, D. *et al.* In vivo recordings of brain activity using organic transistors. *Nat. Commun.* **4**, 1575 (2013).

58. Hogan, N. C., Talei-Franzesi, G., Abudayyeh, O., Taberner, A. & Hunter, I. Low-cost, flexible polymer arrays for long-term neuronal culture. *Conf. Proc. ... Annu. Int. Conf. IEEE Eng. Med. Biol. Soc. IEEE Eng. Med. Biol. Soc. Annu. Conf.* **2012**, 803–6 (2012).

59. Green, R. A., Lovell, N. H., Wallace, G. G. & Poole-Warren, L. A. Conducting polymers for neural interfaces: Challenges in developing an effective long-term

implant. *Biomaterials* **29**, 3393–3399 (2008).

60. Gerwig, R. *et al.* PEDOT-CNT Composite Microelectrodes for Recording and Electrostimulation Applications: Fabrication, Morphology, and Electrical Properties. *Front. Neuroeng.* **5**, 8 (2012).

61. Aregueta-Robles, U. A., Woolley, A. J., Poole-Warren, L. A., Lovell, N. H. & Green, R. A. Organic electrode coatings for next-generation neural interfaces. *Front. Neuroeng.* **7**, 15 (2014).

62. Fang, Y., Li, X. & Fang, Y. Organic bioelectronics for neural interfaces. *J. Mater. Chem. C* **3**, 6424–6430 (2015).

63. Teixeira, H., Dias, C., Aguiar, P. & Ventura, J. Gold-Mushroom Microelectrode Arrays and the Quest for Intracellular-Like Recordings: Perspectives and Outlooks. *Adv. Mater. Technol.* **6**, 2000770 (2021).

64. Fendyur, A. & Spira, M. E. Toward on-chip, in-cell recordings from cultured cardiomyocytes by arrays of gold mushroom-shaped microelectrodes. *Front. Neuroeng.* **5**, 1–10 (2012).

65. Jeong, H. S., Hwang, S., Min, K. S. & Jun, S. B. Fabrication of Planar Microelectrode Array Using Laser-Patterned ITO and SU-8. *Micromachines* **12**, 1347 (2021).

66. Morales-Carvajal, P. M. *et al.* Makerspace microfabrication of a stainless steel 3D microneedle electrode array (3D MEA) on a glass substrate for simultaneous optical and electrical probing of electrogenic cells. *RSC Adv.* **10**, 41577–41587 (2020).

67. Kim, Y., Alimperti, S., Choi, P. & Noh, M. An Inkjet Printed Flexible Electrocorticography (ECoG) Microelectrode Array on a Thin Parylene-C Film. *Sensors* **22**, 1277 (2022).

68. Ha, Y., Yoo, H.-J., Shin, S. & Jun, S. B. Correction: Ha, Y. et al. Hemispherical Microelectrode Array for Ex Vivo Retinal Neural Recording. Micromachines 2020, 11, 538. *Micromachines* **11**, 720 (2020).

69. Soscia, D. A. *et al.* A flexible 3-dimensional microelectrode array for in vitro brain models. *Lab Chip* **20**, 901–911 (2020).

70. K'Owino, I. O. & Sadik, O. A. Impedance Spectroscopy: A Powerful Tool for Rapid Biomolecular Screening and Cell Culture Monitoring. *Electroanalysis* **17**, 2101–2113 (2005).

71. Helmholtz, H. Studien über electrische Grenzschichten. *Ann. der Phys. und Chemie* **243**, 337–382 (1879).

72. Stern, O. Zur Theorie der Elektrolytischen Doppelschicht. *Zeitschrift fur Elektrochemie* **30**, 508–516 (1924).

73. Xiao, C. & Luong, J. H. T. On-Line Monitoring of Cell Growth and Cytotoxicity Using Electric Cell-Substrate Impedance Sensing (ECIS). *Biotechnol. Prog.* **19**, 1000–1005 (2003).

74. Ramasamy, S., Bennet, D. & Kim, S. Drug and bioactive molecule screening based on a bioelectrical impedance cell culture platform. *International Journal of Nanomedicine* **9**, 5789–5809 (2014).

75. Asphahani, F. *et al.* Single-cell bioelectrical impedance platform for monitoring cellular response to drug treatment. *Phys. Biol.* **8**, 015006 (2011).

76. Opp, D. *et al.* Use of electric cell–substrate impedance sensing to assess in vitro cytotoxicity. *Biosens. Bioelectron.* **24**, 2625–2629 (2009).

77. Rahim, S. & Üren, A. A real-time electrical impedance based technique to measure invasion of endothelial cell monolayer by cancer cells. *J. Vis. Exp.* 10–13 (2011). doi:10.3791/2792

78. D'hahan, N. P.-. Live Cell Analysis: When Electric Detection Interfaces Microfluidics. *J. Biochips Tissue Chips* **01**, 1–9 (2011).

79. Sahl, S. J. & Moerner, W. Super-resolution fluorescence imaging with single molecules. *Curr. Opin. Struct. Biol.* **23**, 778–787 (2013).

80. Etrych, T. *et al.* Fluorescence optical imaging in anticancer drug delivery. *J. Control. Release* **226**, 168–181 (2016).

81. Han, R., Li, Z., Fan, Y. & Jiang, Y. Recent Advances in Super-Resolution Fluorescence Imaging and Its Applications in Biology. *J. Genet. Genomics* **40**, 583–595 (2013).

82. De Matos, L. L., Trufelli, D. C., De Matos, M. G. L. & Da Silva Pinhal, M. A. Immunohistochemistry as an Important Tool in Biomarkers Detection and Clinical Practice. *Biomark. Insights* **5**, BMI.S2185 (2010).

83. Wöll, D. & Flors, C. Super-resolution Fluorescence Imaging for Materials Science. *Small Methods* **1**, 1700191 (2017).

84. Cossart, R., Ikegaya, Y. & Yuste, R. Calcium imaging of cortical networks dynamics. *Cell Calcium* **37**, 451–457 (2005).

85. Varshney, M. & Li, Y. Interdigitated array microelectrodes based impedance biosensors for detection of bacterial cells. *Biosens. Bioelectron.* **24**, 2951–2960 (2009).

86. Taylor, D. M. & Macdonald, A. G. AC admittance of the metal/insulator/electrolyte interface. *J. Phys. D. Appl. Phys.* **20**, 1277–1283 (1987).

87. Barsoukov, E. & Macdonald, J. R. *Impedance Spectroscopy*. *Impedance Spectroscopy: Theory, Experiment, and Applications* (John Wiley & Sons, Inc., 2005). doi:10.1002/0471716243

88. K'Owino, I. O. & Sadik, O. A. Impedance spectroscopy: A powerful tool for rapid biomolecular screening and cell culture monitoring. *Electroanalysis* **17**, 2101–2113 (2005).

89. Leleux, P. *et al.* Organic electrochemical transistors for clinical applications. *Adv. Healthc. Mater.* **4**, 142–147 (2015).

90. Arndt, S., Seebach, J., Psathaki, K., Galla, H.-J. & Wegener, J. Bioelectrical impedance assay to monitor changes in cell shape during apoptosis. *Biosens. Bioelectron.* **19**, 583–594 (2004).

91. Yang, L., Li, Y., Griffis, C. L. & Johnson, M. G. Interdigitated microelectrode (IME) impedance sensor for the detection of viable Salmonella typhimurium. *Biosens. Bioelectron.* **19**, 1139–1147 (2004).

92. Inácio, P. M. C. *et al.* Ultra-low noise PEDOT:PSS electrodes on bacterial cellulose: A sensor to access bioelectrical signals in non-electrogenic cells. *Org. Electron.* **85**, 105882 (2020).

93. Cerquido, M. Fabrication of biocompatible gold mushrooms-shaped microelectrodes for the recording of neuronal signals. (2016).

94. Kaur, G. & Dufour, J. M. Cell lines. *Spermatogenesis* **2**, 1–5 (2012).

95. Mosmann, T. Rapid colorimetric assay for cellular growth and survival: Application to proliferation and cytotoxicity assays. *J. Immunol. Methods* (1983). doi:10.1016/0022-1759(83)90303-4

96. Ghasemi, M., Turnbull, T., Sebastian, S. & Kempson, I. The MTT Assay: Utility, Limitations, Pitfalls, and Interpretation in Bulk and Single-Cell Analysis. *Int. J. Mol. Sci.* **22**, 12827 (2021).

97. Masters, B. R. The Development of Fluorescence Microscopy. in *eLS* (Wiley, 2010). doi:10.1002/9780470015902.a0022093

98. LEUNG, P. S. C. & GERSHWIN, M. E. NATIVE AUTOANTIGENS VERSUS RECOMBINANT AUTOANTIGENS. in *Autoantibodies* 37–45 (Elsevier, 2007). doi:10.1016/B978-044452763-9/50010-X

99. Spira, M. E. & Hai, A. Multi-electrode array technologies for neuroscience and cardiology. *Nat. Nanotechnol.* **8**, 83–94 (2013).

100. Obien, M. E. J., Deligkaris, K., Bullmann, T., Bakkum, D. J. & Frey, U. Revealing neuronal function through microelectrode array recordings. *Front. Neurosci.* **8**, 423 (2015).

101. Hierlemann, A., Frey, U., Hafizovic, S. & Heer, F. Growing cells atop microelectronic chips: Interfacing electrogenic cells in vitro with CMOS-based microelectrode arrays. *Proc. IEEE* **99**, 252–284 (2011).

102. Timko, B. P. *et al.* Electrical recording from hearts with flexible nanowire device arrays. *Nano Lett.* **9**, 914–918 (2009).

103. Richardson-Burns, S. M., Hendricks, J. L. & Martin, D. C. Electrochemical polymerization of conducting polymers in living neural tissue. *J. Neural Eng.* **4**, L6–L13 (2007).

104. Leleux, P. *et al.* Conducting Polymer Electrodes for Electroencephalography. *Adv. Healthc. Mater.* **3**, 490–493 (2014).

105. Khodagholy, D. *et al.* In vivo recordings of brain activity using organic transistors. *Nat. Commun.* **4**, 1575 (2013).

106. Fendyur, A., Mazurski, N., Shappir, J. & Spira, M. E. Formation of Essential Ultrastructural Interface between Cultured Hippocampal Cells and Gold Mushroom-Shaped MEA- Toward ?IN-CELL? Recordings from Vertebrate Neurons. *Front. Neuroeng.* **4**, (2011).

107. Nowak, L., Ascher, P. & Berwald-Netter, Y. Ionic channels in mouse astrocytes in culture. *J. Neurosci.* **7**, 101–9 (1987).

108. Ransom, B., Behar, T. & Nedergaard, M. New roles for astrocytes (stars at last). *Trends Neurosci.* **26**, 520–522 (2003).

109. Shigetomi, E., Patel, S. & Khakh, B. S. Probing the Complexities of Astrocyte Calcium Signaling. *Trends Cell Biol.* **26**, 300–312 (2016).

110. Bazargani, N. & Attwell, D. Astrocyte calcium signaling: the third wave. *Nat. Neurosci.* **19**, 182–189 (2016).

111. Pasti, L., Volterra, A., Pozzan, T. & Carmignoto, G. Intracellular Calcium Oscillations in Astrocytes : A Highly Plastic , Astrocytes In Situ. **17**, 7817–7830 (1997).

112. Wanke, E., Gullo, F., Dossi, E., Valenza, G. & Becchetti, A. Neuron-glia cross talk revealed in reverberating networks by simultaneous extracellular recording of spikes and astrocytes' glutamate transporter and K + currents. *J. Neurophysiol.* **116**, 2706–2719 (2016).

113. Fleischer, W., Theiss, S., Slotta, J., Holland, C. & Schnitzler, A. High-frequency voltage oscillations in cultured astrocytes. *Physiol. Rep.* **3**, e12400 (2015).

114. Rocha, P. R. F. *et al.* Extracellular electrical recording of pH-triggered bursts in C6 glioma cell populations. *Sci. Adv.* **2**, (2016).

115. Rocha, P. R. F. *et al.* Low frequency electric current noise in glioma cell populations. *J. Mater. Chem. B* **3**, 5035–5039 (2015).

116. Paulo R. F. Rocha, Paul Schlett, Ulrike Kintzel, Volker Mailänder, Lode K. J. Vandamme, Gunther Zeck, Henrique L. Gomes, F. B. and D. M. de L. *Electrochemical noise and impedance of Au electrode / electrolyte interfaces*

enabling extracellular detection of glioma cell populations. (2016).

117. Carreira, B. P. *et al.* Nitric oxide from inflammatory origin impairs neural stem cell proliferation by inhibiting epidermal growth factor receptor signaling. *Front. Cell. Neurosci.* **8**, 343 (2014).

118. Guo, J., Yuan, J. & Chan, M. Modeling of the cell-electrode interface noise for microelectrode arrays. *IEEE Trans. Biomed. Circuits Syst.* **6**, 605–613 (2012).

119. Inacio, P. M. C. *et al.* Bioelectrical Signal Detection Using Conducting Polymer Electrodes and the Displacement Current Method. *IEEE Sens. J.* **17**, 3961–3966 (2017).

120. Hassibi, A., Navid, R., Dutton, R. W. & Lee, T. H. Comprehensive study of noise processes in electrode electrolyte interfaces. *J. Appl. Phys.* **96**, 1074–1082 (2004).

121. Yamamoto, E., Akimoto, T., Yasui, M. & Yasuoka, K. Origin of 1/f noise in hydration dynamics on lipid membrane surfaces. *Sci. Rep.* **5**, 8876 (2015).

122. Siwy, Z. & Fuliński, A. Origin of 1/fα Noise in Membrane Channel Currents. *Phys. Rev. Lett.* **89**, 158101 (2002).

123. Franks, W., Schenker, I., Schmutz, P. & Hierlemann, A. Impedance characterization and modeling of electrodes for biomedical applications. *IEEE Trans. Biomed. Eng.* **52**, 1295–1302 (2005).

124. Fatatis, A. & Russell, J. T. Spontaneous Changes in Intracellular Calcium Concentration in Type I Astrocytes From Rat Cerebral Cortex in Primary Culture. **104**, 95–104 (1992).

125. Krug, S. M., Fromm, M. & Günzel, D. Two-Path Impedance Spectroscopy for Measuring Paracellular and Transcellular Epithelial Resistance. *Biophys. J.* **97**, 2202–2211 (2009).

126. Tria, S., Jimison, L. H., Hama, A., Bongo, M. & Owens, R. M. Sensing of EGTA mediated barrier tissue disruption with an organic transistor. *Biosensors* **3**, 44–57 (2013).

127. Rothen-Rutishauser, B., Riesen, F. K., Braun, A., Günthert, M. & Wunderli-Allenspach, H. Dynamics of Tight and Adherens Junctions Under EGTA Treatment. *J. Membr. Biol.* **188**, 151–162 (2002).

128. Savolainen, V. *et al.* Impedance Spectroscopy in Monitoring the Maturation of Stem Cell-Derived Retinal Pigment Epithelium. *Ann. Biomed. Eng.* **39**, 3055 (2011).

129. Giaever, I. & Keese, C. R. Monitoring fibroblast behavior in tissue culture with an applied electric field. *Proc. Natl. Acad. Sci.* **81**, 3761–3764 (1984).

130. Shigetomi, E. *et al.* Imaging calcium microdomains within entire astrocyte territories and endfeet with GCaMPs expressed using adeno-associated viruses. *J. Gen. Physiol.* **141**, 633–647 (2013).

131. Cornell-Bell, A., Finkbeiner, S., Cooper, M. & Smith, S. Glutamate induces calcium waves in cultured astrocytes: long-range glial signaling. *Science (80-.).* **247**, 470–473 (1990).

132. Kuga, N., Sasaki, T., Takahara, Y., Matsuki, N. & Ikegaya, Y. Large-Scale Calcium Waves Traveling through Astrocytic Networks In Vivo. *J. Neurosci.* **31**, 2607–2614 (2011).

133. Zur Nieden, R. & Deitmer, J. W. The Role of Metabotropic Glutamate Receptors for the Generation of Calcium Oscillations in Rat Hippocampal Astrocytes In Situ. *Cereb. Cortex* **16**, 676–687 (2006).

134. Srinivasan, R. *et al.* Ca2+ signaling in astrocytes from Ip3r2−/− mice in brain slices and during startle responses in vivo. *Nat. Neurosci.* **18**, 708–717 (2015).

135. James, L. R. *et al.* High-Throughput Analysis of Calcium Signalling Kinetics in Astrocytes Stimulated with Different Neurotransmitters. *PLoS One* **6**, e26889 (2011).

136. Micali, G., Aquino, G., Richards, D. M. & Endres, R. G. Accurate Encoding and Decoding by Single Cells: Amplitude Versus Frequency Modulation. *PLOS Comput. Biol.* **11**, e1004222 (2015).

137. Balaji, R. *et al.* Calcium spikes, waves and oscillations in a large, patterned epithelial tissue. *Sci. Rep.* **7**, 42786 (2017).

138. Pasti, L., Volterra, A., Pozzan, T. & Carmignoto, G. Intracellular calcium oscillations in astrocytes: A highly plastic, bidirectional form of communication between neurons and astrocytes in situ. *J. Neurosci.* **17**, (1997).

139. Di Capite, J., Ng, S. W. & Parekh, A. B. Decoding of Cytoplasmic Ca2+ Oscillations through the Spatial Signature Drives Gene Expression. *Curr. Biol.* **19**, 853–858 (2009).

140. Dallérac, G., Chever, O. & Rouach, N. How do astrocytes shape synaptic transmission? Insights from electrophysiology. *Front. Cell. Neurosci.* (2013). doi:10.3389/fncel.2013.00159

141. Stobart, J. L. & Anderson, C. M. Multifunctional role of astrocytes as gatekeepers of neuronal energy supply. *Front. Cell. Neurosci.* **7**, (2013).

142. Hassinger, T. D., Guthrie, P. B., Atkinson, P. B., Bennett, M. V & Kater, S. B. An extracellular signaling component in propagation of astrocytic calcium waves. *Proc. Natl. Acad. Sci. U. S. A.* **93**, 13268–13273 (1996).

143. Bordey, a & Sontheimer, H. Electrophysiological properties of human astrocytic tumor cells In situ: enigma of spiking glial cells. *J. Neurophysiol.* **79**, 2782–93 (1998).

144. Parri, H. . & Crunelli, V. The role of Ca2+ in the generation of spontaneous astrocytic Ca2+ oscillations. *Neuroscience* **120**, 979–992 (2003).

145. Cornell-Bell, A., Finkbeiner, S., Cooper, M. & Smith, S. Glutamate induces calcium waves in cultured astrocytes: long-range glial signaling. *Science (80-.).* **247**, 470–473 (1990).

146. Höfer, T., Politi, A. & Heinrich, R. Intercellular Ca2+ Wave Propagation through Gap-Junctional Ca2+ Diffusion: A Theoretical Study. *Biophys. J.* **80**, 75–87 (2001).

147. Sundelacruz, S., Levin, M. & Kaplan, D. L. Role of Membrane Potential in the Regulation of Cell Proliferation and Differentiation. *Stem Cell Rev. Reports* **5**, 231–246 (2009).

148. Friesen, D. E., Craddock, T. J. A., Kalra, A. P. & Tuszynski, J. A. Biological wires, communication systems, and implications for disease. *Biosystems* **127**, 14–27 (2015).

149. Berridge, M. J., Bootman, M. D. & Roderick, H. L. Calcium signalling: dynamics, homeostasis and remodelling. *Nat. Rev. Mol. Cell Biol.* **4**, 517–529 (2003).

150. Asgarifar, S. *et al.* Extracellular electrophysiological based sensor to monitor cancer cells cooperative migration and cell-cell connections. *Biosens. Bioelectron.* **145**, 111708 (2019).

151. Le Roy, C. & Wrana, J. L. Signaling and Endocytosis: A Team Effort for Cell Migration. *Dev. Cell* **9**, 167–168 (2005).

152. Li, D. & Wang, Y. Coordination of cell migration mediated by site-dependent cell–cell contact. *Proc. Natl. Acad. Sci.* **115**, 10678–10683 (2018).

153. Sherratt, M. J. *et al.* Circadian rhythms in skin and other elastic tissues. *Matrix Biol.* **84**, 97–110 (2019).

154. Schwab, A., Fabian, A., Hanley, P. J. & Stock, C. Role of Ion Channels and Transporters in Cell Migration. *Physiol. Rev.* **92**, 1865–1913 (2012).

155. Engeland, C. G., Sabzehei, B. & Marucha, P. T. Sex hormones and mucosal wound healing. *Brain. Behav. Immun.* **23**, 629–635 (2009).

156. Gilliver, S. C. & Ashcroft, G. S. Sex steroids and cutaneous wound healing: the contrasting influences of estrogens and androgens. *Climacteric* **10**, 276–288 (2007).

157. Horng, H. C. *et al.* Estrogen effects on wound healing. *International Journal of Molecular Sciences* (2017). doi:10.3390/ijms18112325

158. Santana, L. C. L. *et al.* Testosterone Increases Fibroblast Proliferation in vitro Through Androgen and Estrogen Receptor Activation. *J. Int. Acad. Periodontol.* **22**, 146–155 (2020).

159. Grin, B. *et al.* Withaferin A Alters Intermediate Filament Organization, Cell Shape and Behavior. *PLoS One* **7**, e39065 (2012).

160. Doillon, C. J., Hembry, R. M., Ehrlich, H. P. & Burke, J. F. Actin filaments in normal dermis and during wound healing. *Am. J. Pathol.* (1987).

161. Carnesecchi, J. *et al.* Estrogens Induce Rapid Cytoskeleton Re-Organization in Human Dermal Fibroblasts via the Non-Classical Receptor GPR30. *PLoS One* **10**, e0120672 (2015).